

**ESD RECORD COPY**RETURN TO  
SCIENTIFIC & TECHNICAL INFORMATION DIVISION  
(ESTI, BUILDING 1211)

COPY NR. \_\_\_\_\_ OF \_\_\_\_\_ COPIES

ESTI PROCESSED☐ DDC TAB ☐ PROJ OFFICER☐ ACCESSION MASTER FILE☐

DATE

**AL 43005**ESTI CONTROL NR. ~~000000~~CY NR. 1OF 1

CYS

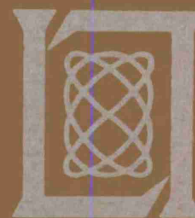
**Technical Report****271****D. A. Cahlander****Echolocation  
with Wide-Band Waveforms:  
Bat Sonar Signals****6 May 1964**

Prepared under Electronic Systems Division Contract AF 19(628)-500 by

**Lincoln Laboratory**

MASSACHUSETTS INSTITUTE OF TECHNOLOGY

Lexington, Massachusetts



AD2605322

The work reported in this document was performed at Lincoln Laboratory, a center for research operated by Massachusetts Institute of Technology, with the support of the U.S. Air Force under Contract AF 19(628)-500.

Non-Lincoln Recipients

**PLEASE DO NOT RETURN**

Permission is given to destroy this document  
when it is no longer needed.

MASSACHUSETTS INSTITUTE OF TECHNOLOGY

LINCOLN LABORATORY

ECHOLOCATION WITH WIDE-BAND WAVEFORMS:  
BAT SONAR SIGNALS

*D. A. CAHLANDER*

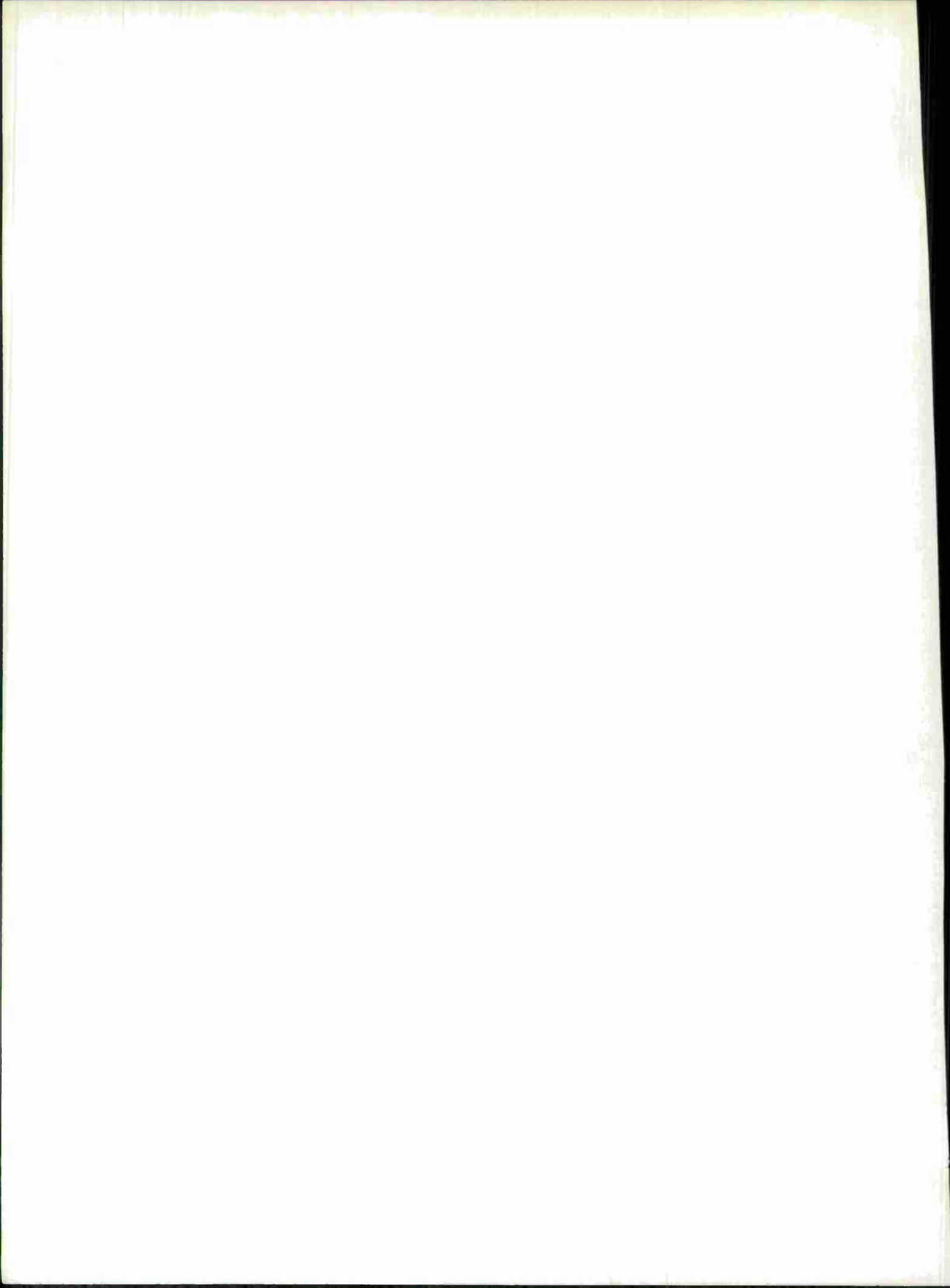
*Group 45*

TECHNICAL REPORT 271

6 MAY 1964

LEXINGTON

MASSACHUSETTS



ECHOLOCATION WITH WIDE-BAND WAVEFORMS:  
BAT SONAR SIGNALS\*

ABSTRACT

The wide-band, echolocating sonar signals of bats are investigated with reference to statistical estimation theory to ascertain the implications of this class of signals. The work is divided into four major sections: (1) The concept of an ideal receiver for the simultaneous measurement of range and velocity of a target is extended to cover wide-band signals; (2) angular localization of a target by means of a fixed, gain-dispersive antenna in the presence of additive Gaussian noise is studied; (3) an ambiguity diagram computer is designed and built which calculates the signal function, defined in Chapter 2, of an arbitrary waveform; and (4) ambiguity diagrams are calculated for several types of bat sonar signals emitted by the bat Myotis lucifugus and one cruising signal emitted by the bat Lasiurus borealis.

Accepted for the Air Force  
Franklin C. Hudson, Deputy Chief  
Air Force Lincoln Laboratory Office

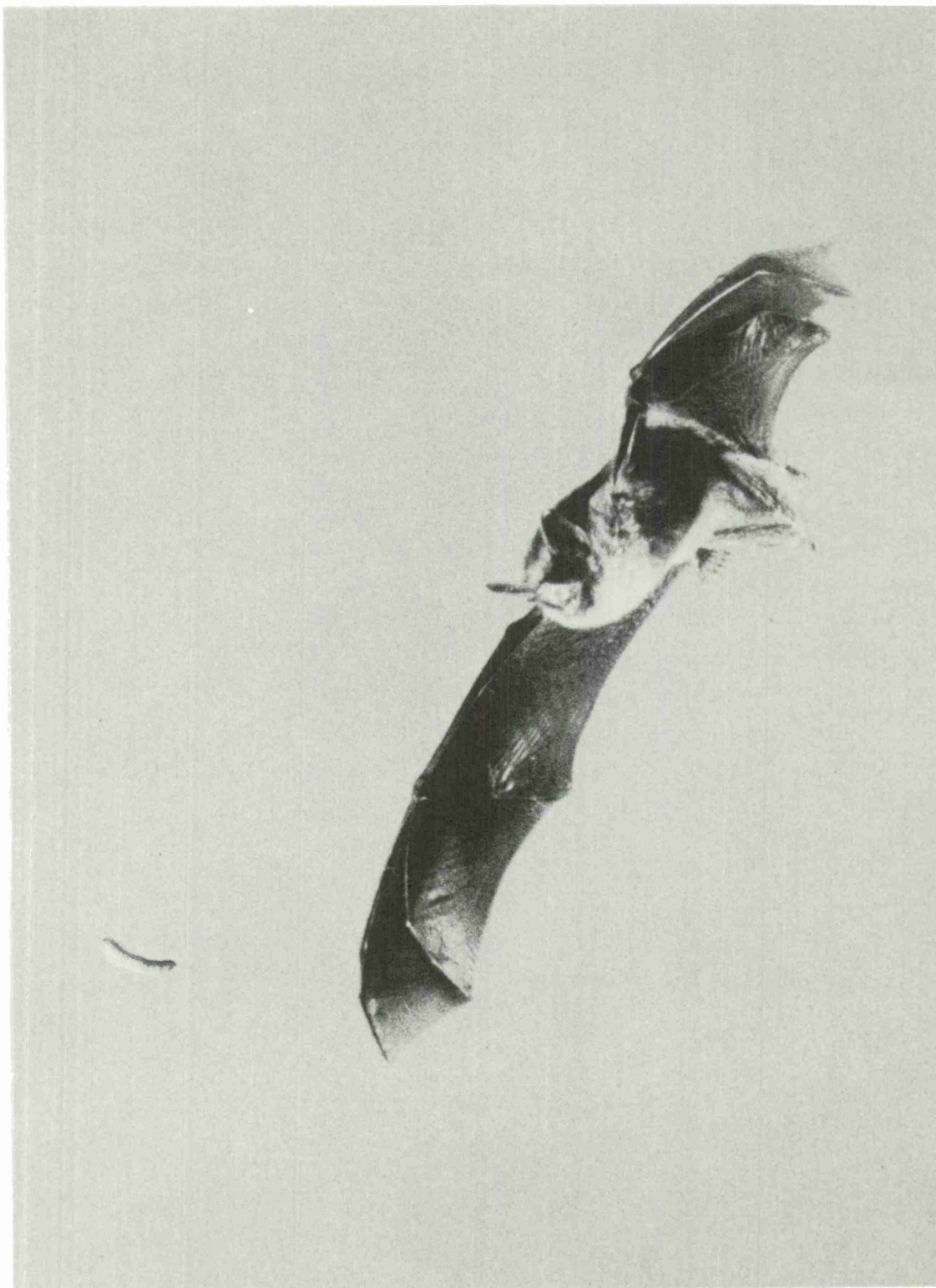
---

\* This report is based on a thesis of the same title submitted in partial fulfillment of the requirements for the degree of Doctor of Philosophy in the Department of Electrical Engineering at the Massachusetts Institute of Technology.

## TABLE OF CONTENTS

Abstract	iii
1. INTRODUCTION	1
1.1 SCOPE OF THE STUDY	1
1.2 BACKGROUND OF THE PROBLEM	1
1.3 OUTLINE OF THE REPORT	4
2. WIDE-BAND ECHOLOCATION THEORY	6
2.1 INTRODUCTION	6
2.2 MODEL AND DERIVATION	6
2.2.1 Ideal Receiver	7
2.2.2 Likelihood Function	7
2.2.3 Receiver Operation	8
2.2.4 Signal Function	9
2.3 RANGE AND RANGE-RATE RESOLUTION LIMITATIONS OF THE <u>A POSTERIORI</u> MODEL	11
2.3.1 Probability Limitation	11
2.3.2 Signal Function Area	11
2.3.3 Ambiguity Diagram of Pulsed FM Signals	14
3. DIRECTIONAL LOCATION WITH GAIN-DISPERSIVE ANTENNAS	17
3.1 INTRODUCTION	17
3.2 MODEL AND DERIVATION	17
3.2.1 Signal Function	18
3.2.2 Noise Function	21
3.3 WINDOW-FUNCTION ANTENNAS	21
3.3.1 Impulse Response of a One-Dimensional Window-Function Antenna	21
3.3.2 Transform Relationship	23
3.4 EXAMPLES OF THE SIGNAL AND LIKELIHOOD FUNCTIONS	23
3.4.1 Antenna With a Square Window Function	23
3.4.2 Antenna With a Cosine Window Function	25
3.5 FINITE BANDWIDTH CONSIDERATIONS	28

4. AMBIGUITY DIAGRAM COMPUTER	31
4.1 INTRODUCTION	31
4.2 RECORD ELECTRONICS	32
4.2.1 Outline and Block Diagram	32
4.2.2 Tape Input	33
4.2.3 Electronic Gating and Switching	34
4.2.4 Drum Delay Unit	35
4.3 REPRODUCE ELECTRONICS	39
4.3.1 Outline and Block Diagram	39
4.3.2 Multiplier	40
4.3.3 Pulse Integration and Control Circuits	41
4.3.4 X-Y Plotter Output and Associated Electronics	42
4.4 ERRORS AND LIMITATIONS IN THE ACCURACY OF THE AMBIGUITY DIAGRAM COMPUTER	43
4.4.1 Function Error	43
4.4.2 Multiplier Error	45
4.4.3 Doppler Error	47
4.4.4 Time Delay Error	47
4.4.5 Integrator and Sample-and-Hold Error	49
4.4.6 Summary of Errors	49
5. AMBIGUITY DIAGRAMS OF BAT SIGNALS	50
5.1 INTRODUCTION	50
5.2 <u>MYOTIS LUCIFUGUS</u>	52
5.2.1 Introduction	52
5.2.2 Ambiguity Diagrams	52
5.2.3 Discussion	56
5.3 <u>LASIURUS BOREALIS</u>	60
5.3.1 Introduction	60
5.3.2 Ambiguity Diagrams	60
6. CONCLUSIONS	63
6.1 SUMMARY	63
6.2 SUGGESTIONS FOR FURTHER INVESTIGATION	64
6.2.1 Equipment Improvements	64
6.2.2 Field Measurements of the Capabilities of Bat Sonar Systems	65
6.2.3 Ambiguity Diagrams of Various Bat Signals	65
ACKNOWLEDGMENTS	67
BIBLIOGRAPHY	68



Little brown bat Myotis lucifugus catching tossed mealworm.

# ECHOLOCATION WITH WIDE-BAND WAVEFORMS: BAT SONAR SIGNALS

## 1. INTRODUCTION

### 1.1 SCOPE OF THE STUDY

In recent years, there has been much speculation about the effectiveness of the sonar system of bats. Most of the work on bats has pertained to measuring the capabilities of the bat in different problem situations such as forcing the bat to avoid wires in a noise field, measuring the bat's abilities to catch flying or thrown targets, and measuring evoked responses in the bat's auditory nervous system. Some attempts have been made to measure and to understand the significance of the various echolocating signals used by various species of bats.

This research investigates the way in which the characteristics of the narrow-band ideal receiver theory, worked out by Woodward<sup>27</sup> and others, apply to the case of octave-wide-band bat signals. A wide-band signal function that characterizes the operation of an ideal receiver is defined and the properties of this signal function are studied. The problem of elevation estimation with a wide-band signal is studied from an ideal receiver point of view and two simple examples are worked out to show the capabilities of this type of system.

An analog computer is developed to calculate the ambiguity diagrams of several, typical, bat echolocating signals. Signals of bats are obtained and the measurement capabilities of these signals are deduced.

### 1.2 BACKGROUND OF THE PROBLEM

In the 18th century, Lazaro Spallanzani demonstrated that bats need both their ears and mouths unimpaired to fly without bumping into things, while removal of a bat's eye does not affect his agility in avoiding obstacles. At that time this curious behavior "contradicted common sense and reasonableness based on normal experience." In 1809, Montagu wrote, "... it might fairly be asked, 'Since bats see with their ears, do they hear with their eyes?' " (see Ref. 3, pp. 62-64).

In 1938, Donald R. Griffin, who is now Professor of Zoology at Harvard University but was then an undergraduate there, entered the physics laboratory of George W. Pierce carrying a cage of bats. Pierce had just perfected a microphone sensitive to ultrasound. When they turned it toward the cage of bats, Pierce's loudspeaker emitted clicks, demonstrating that bats produce ultrasound (see Ref. 3, p. 67).

Later experiments, conducted by Griffin and Robert Galambos, demonstrated that the bat was indeed using a sonar similar in principle to the radars and sonars that were being developed by man (see Ref. 3, p. 69).

In 1958, Griffin reported some of his work in Scientific American,<sup>5</sup> claiming unusually high "efficiencies" for bats compared to man-made radars. Although there were some basic errors made in interpreting the data, the bat still seemed to do very well.

M.I.T. Lincoln Laboratory became interested in studying the bat's ability to avoid wires in the presence of loud, Gaussian jamming noise. Improved experiments by Griffin, McCue, and Grinnell<sup>8</sup> and more comprehensive theory demonstrate that the bat's ability to avoid wires is very good but does not violate the limits imposed by information theory.

There are many different species of bats using echolocating sonar systems. It is presumed that since the bats have had literally millions of years (see Ref. 3, p. 6) in which to evolve their sonar that they would have developed some sort of an optimum system. The numerous and widely distributed Vespertilionidae use a type of pulsed FM system; the Rhinolophidae, the "horseshoe bats" of Europe, have developed a pulsed CW system. While the Vespertilionidae keep their ears stationary during flight, the Rhinolophidae move their ears at rates up to 30 cps.<sup>7</sup>

Each individual species has its own distinguishing characteristics and individual diet. The vampire bat (family Desmodontidae), found only in tropical South and Central America, exists on a diet consisting entirely of blood obtained from large and relatively stationary prey. The Vespertilionidae, however, have the problem of detecting and pursuing the small and elusive insects on which they feed. For the purposes of this study, the little brown bat (Myotis lucifugus) has been trained to catch thrown mealworms. A photograph showing the Myotis catching a mealworm appears as the frontispiece. The Rhinolophidae also pursue and catch small insects and moths. A photograph taken by F.A. Webster and D.R. Griffin of a greater horseshoe bat (Rhinolophus ferrum-equinum) in the act of catching a moth is shown in Fig. 1. There are bats that feed on the nectar of flowers and bats that feed on fruit. One of the most unusual diets for a bat is that of the fishing bat, Noctilio leporinus. The Noctilio makes his living by catching

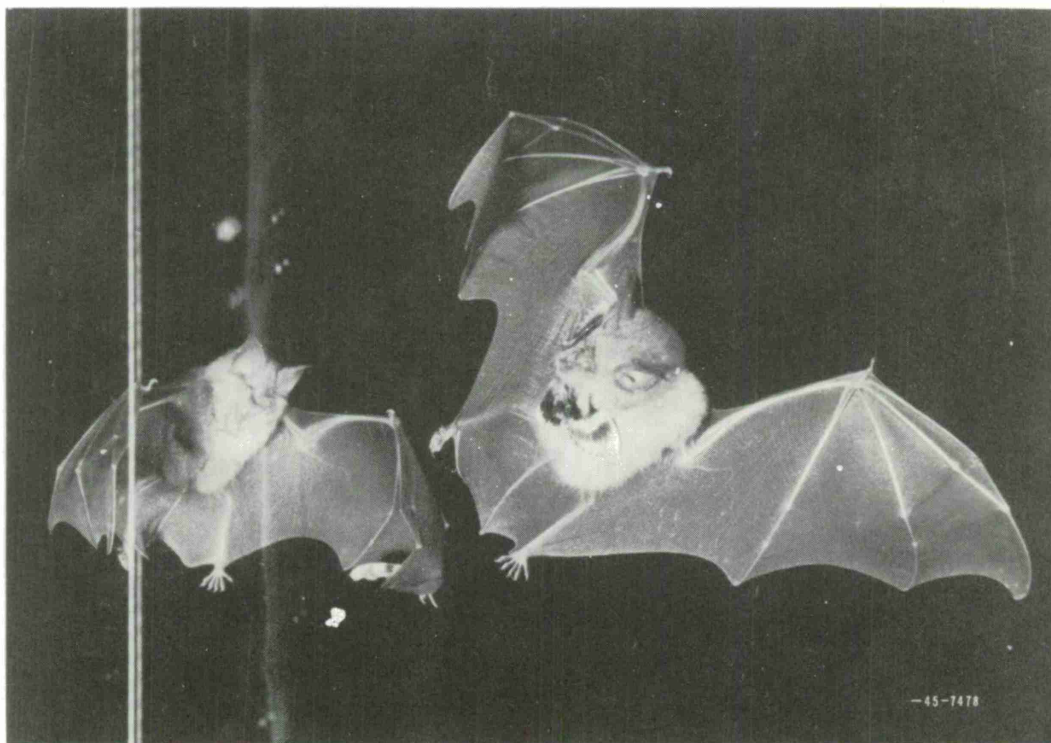


Fig. 1. Horseshoe bat (Rhinolophus ferrum-equinum) capturing moth thrown by D.R. Griffin. (Photograph is reproduced with permission of F.A. Webster.)

small fish that are swimming near the surface of the ocean. A photograph of a Noctilio in the act of catching a piece of fish is shown in Fig. 2.

It is supposed that the sonar system of each species of bat has developed to some sort of an optimum for the particular task which that species performs. Since the echolocation problems facing a vampire bat are much simpler than the problems facing an insectivorous bat, the sonar system of the latter is expected to be more complex than that of the former.

P. M. Woodward<sup>27</sup> and others have shown that the best that an echolocation system can do in the way of detection of a signal in additive Gaussian noise is to pass the received signal through a matched filter. The time-delay and velocity measurement capabilities of such an "ideal receiver" are represented by the signal function which is derived from the transmitted signal.

The signal function of the bat's sonar pulse contains the relevant information about the range and range-rate resolution of his signal when it is used in an additive background of white Gaussian noise. When it is clear what type of signals are used by the different species of bats for the different operations that they perform, some clues as to the way in which we can improve our modern radar systems may appear.

The bat has a more difficult problem than that of determining the range of his target. He must simultaneously determine the range, the azimuth and the elevation as well as determine the type of target. Very little is known about the process involved in determining the elevation of the target. Although it is hypothesized that the bat determines range from the target-echo delay and that he determines azimuth by the same methods that are used by humans to determine azimuth, it is not clear how the bat or the human determines elevation of a sound source. Some believe that very small movements of the head are used to obtain two base lines for interaural

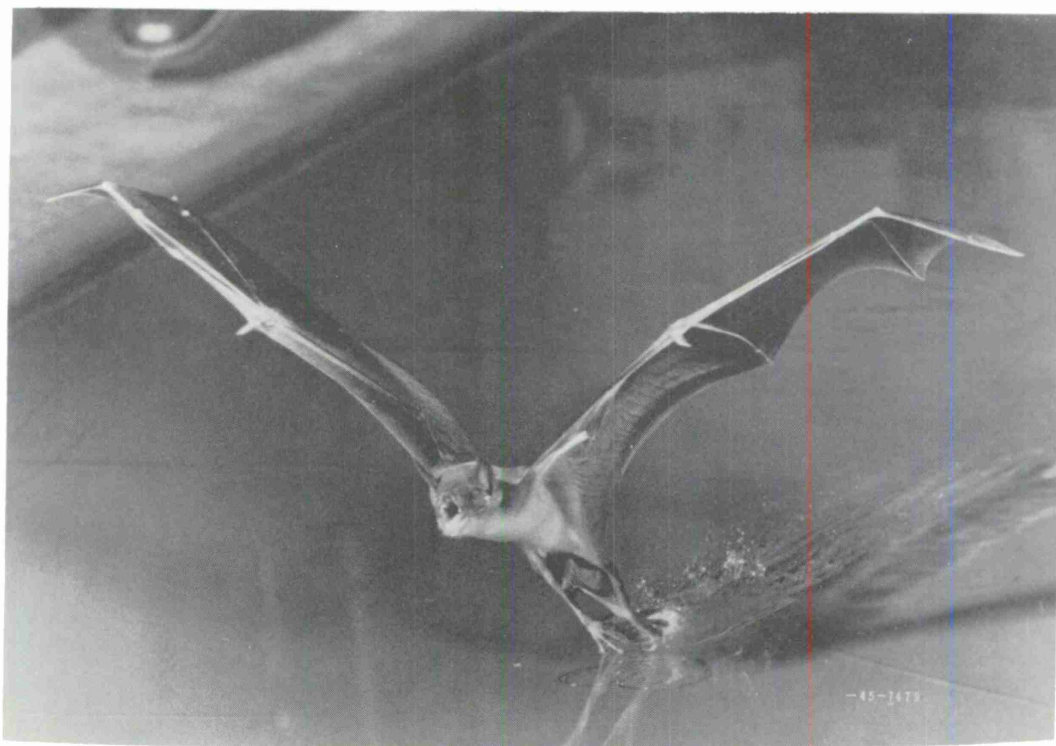


Fig. 2. Fishing bat (Noctilio leporinus) catching piece of fish from indoor pool of water.

time delay measurements. From these two interaural delay measurements, the elevation of the source is supposed to be predicted. This does not seem reasonable for humans or for bats. A human can determine the elevation of a transient noise with his head stationary and a vesperilionid bat does not wiggle his head during the pursuit of a target.

Azimuthal angular location by humans has been reported by Jongkees and von der Veer,<sup>32</sup> Pierce,<sup>35</sup> and Mills.<sup>33</sup> Mills has shown that humans can resolve, under rather ideal conditions, interaural time differences on the order of 1  $\mu$ sec. Very little work has been reported on the abilities of humans to locate the elevation of a sound source. In the work reported by Jongkees, *et al.*, angular location by unilaterally deaf subjects was investigated. Although he does not actually mention the possibility that gain-dispersive transducers are the mechanism of the angular location scheme, he reported that distortion of the shape of the outer ear affected the ability of the subject to locate objects. It is reasonable to assume that the gain pattern of a person's ear changes greatly with frequency. It is therefore plausible that a person could use this variation in gain pattern to determine the angular elevation of a sound source. It is also plausible that a bat would use this type of system to determine the elevation of his targets. An ideal model of this type of system is investigated in this report.

### 1.3 OUTLINE OF THE REPORT

The report is divided into three parts: theoretical derivations (Chapters 2 and 3), description of the electronic equipment and techniques that were used (Chapter 4), and the results of the study (Chapter 5).

Chapter 2 contains the theoretical basis of the ambiguity diagram concept. The Woodward concept of the ideal receiver for range and range-rate detection is extended to treat wide-band signals. The signal function for a wide-band bat signal is developed and the resolution limitations of the system are discussed. A different way of looking at the ambiguity diagram of a pulsed FM signal is derived and then related to the bat sonar problem.

A derivation of the ideal-receiver concept as related to angular location by means of a gain-dispersive antenna is made in Chapter 3. A gain-dispersive antenna is an antenna with an angular gain pattern that changes as a function of frequency. A signal function for the angle-locating system is defined which relates the uncertainties in time-delay (range) measurements to the uncertainties in angular measurements. The special case of "window-function antennas" is treated. A window-function antenna is an antenna whose impulse response at a particular angle is related to the "window function" of the antenna by a proportionality factor and a compression or expansion of the time axis. The relationship between the window function of the antenna and the signal function is derived and two special examples are treated. It is presumed that bats might use this type of system for angular determination, but no definite proof has been established.

An analog ambiguity diagram computer, which was designed to calculate the wide-band signal function developed in Chapter 2, is described in Chapter 4. This computer calculates the ambiguity diagram of an arbitrary signal that is recorded on magnetic tape. The signal is re-recorded from the magnetic tape onto a magnetic drum that has two signal tracks, one for the direct signal and one for the Doppler-shifted signal. The two signals are shifted with respect to each other by means of a movable playback head on the magnetic drum. The signals are multiplied and integrated; then the output is displayed.

The results obtained by analyzing several different bat signals with the ambiguity diagram computer are presented in Chapter 5. Photographs of the actual bat signals as well as the ambiguity diagrams are presented. The range and the range-rate resolution of the different bat signals are presented as a result of the ambiguity diagrams. The results and conclusions of this research are summarized in Chapter 6.

## 2. WIDE-BAND ECHOLOCATION THEORY

### 2.1 INTRODUCTION

If a suitable (and simple) model is made of the sonar system of the bat, one can ask what is the best that an "ideal receiver" can do with the bat's signals. Some of the interesting characteristics of ideal receivers that have been developed in the radar literature were developed by assuming that the signals are the narrow-band signals usually encountered in radar systems. Clearly there is some doubt as to whether or not these characteristics apply for octave-wide-band bat signals. Most of the basic derivations in the literature are general in nature and apply to all types of signals, or require only slight interpretation for application to wide-band signals. In particular, for narrow-band signals, a Doppler shift is considered only as a change in center frequency. For wide-band signals a Doppler shift must be considered as an expansion or compression of the time axis of the transmitted signal.

A complete derivation is given in the following section to introduce a wide-band signal function and investigate its characteristics.

### 2.2 MODEL AND DERIVATION

The model chosen for this analysis consists of a moving target at some distance from the receiver, as shown in Fig. 3. The signal at the receiver input is

$$y(t) = \sqrt{\alpha} s[\alpha(t - \tau)] + n(t) \quad (2-1)$$

where

$y(t)$  = received signal

$s(t)$  = transmitted or expected signal

$n(t)$  = additive Gaussian noise

$\tau$  = time delay associated with the range of the target

$$\alpha = \left[ \frac{1 - \frac{v}{c}}{1 + \frac{v}{c}} \right] = \text{Doppler factor}$$

$v$  = target velocity or range rate

$c$  = speed of propagation

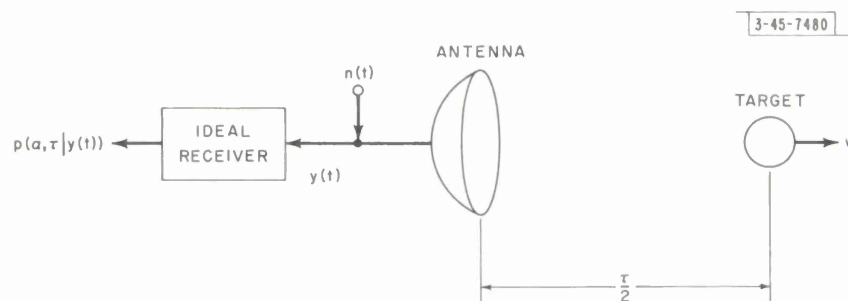


Fig. 3. Model of echolocation system for determination of time delay and Doppler shift.

The  $\sqrt{\alpha}$  term multiplying the signal in Eq. (2-1) makes the signal term have an energy that is independent of the velocity of the target. This is, in effect, an assumption that the target cross section is independent of the velocity of the target.

There are many factors omitted from this model: amplitude variation of the received signal, target cross section, antenna pattern, etc. These factors, although present in any real echo-location system, do not add to the clarity of the ideal receiver derivation and are therefore omitted.

### 2.2.1 Ideal Receiver

An ideal receiver is defined as a system that destroys all unwanted information in a received signal and retains all wanted information. In the system described, the wanted information is the range ( $c\tau/2$ ) and the Doppler factor ( $\alpha$ ) of the target, all other information is unwanted. Since the additive Gaussian noise is statistical in nature, the output of the ideal receiver is also of a statistical nature. All the information contained in  $y(t)$  concerning  $\tau$  and  $\alpha$  is expressed as the joint conditional probability density function for  $\tau$  and  $\alpha$  given  $y(t)$ :

$$p(\tau, \alpha | y(t)) \quad . \quad (2-2)$$

No additional amount of processing of the received signal can extract any more information concerning the values of  $\tau$  and  $\alpha$ . Also, in obtaining this probability function, there has been no information about  $\tau$  and  $\alpha$  that has been destroyed. Therefore, a receiver that computes  $p(\tau, \alpha | y(t))$ , or something monotonically related to this, is the ideal receiver for this problem.

The computation of  $p(\tau, \alpha | y(t))$  is performed by using a probability theory identity

$$p(a, b | c) p(c) = p(a, b, c) = p(c | a, b) p(a, b) \quad (2-3)$$

$$p(a, b | c) = \frac{p(a, b)}{p(c)} p(c | a, b) \quad . \quad (2-4)$$

By substitution,

$$p(\tau, \alpha | y(t)) = \frac{p(\tau, \alpha)}{p(y(t))} p(y(t) | \tau, \alpha) \quad , \quad (2-5)$$

where  $p(\tau, \alpha)$  is the probability density function for  $\tau$  and  $\alpha$  before the reception of the received signal. It is called the a priori probability density function. The probability density function  $p(y(t))$  is a strange function. To be mathematically rigorous,  $y(t)$  would be confined to a finite bandwidth, the sampling theorem would be applied, and the samples of  $y(t)$  would be used to form a vector in waveform space. The function  $p(y(t))$  is therefore the probability per unit volume of waveform space that a particular  $y(t)$  is received. It is a scalar function with a vector argument. Likewise,  $p(y(t) | \tau, \alpha)$ , the likelihood function, is the probability per unit volume of waveform space that a particular  $y(t)$  is received given that the actual target was at  $\tau$  moving with a Doppler factor  $\alpha$ .

### 2.2.2 Likelihood Function

Since the noise is added to the received signal, and the form of the signal is known exactly, the likelihood function is equal to the probability density for the corresponding noise signal

$$p(y(t) | \tau, \alpha) = p(n(t)) \quad . \quad (2-6)$$

The notation used here is slightly ambiguous since the probability function notation is used to denote two different functions. What is implied by this notation is that the probability density (probability per unit volume of waveform space) for a particular received signal  $y(t)$  is equal to the probability density for the particular noise signal  $n(t)$  that was received. As developed by Woodward (see Ref. 27, p. 38), the probability density function for a particular white Gaussian noise waveform with mean energy  $N_0$  watts/cps (single-sided spectrum) is given by

$$p(n(t)) = k \exp \left[ -\frac{1}{N_0} \int n^2(t) dt \right] \quad (2-7)$$

The value of the constant  $k$  depends on the limits of the integration. From Eq. (2-1),

$$n(t) = y(t) - \sqrt{\alpha} s[\alpha(t - \tau)] \quad (2-8)$$

Combining this with Eqs. (2-5), (2-6), and (2-7),

$$\begin{aligned} p(\tau, \alpha | y(t)) &= \frac{p(\tau, \alpha)}{p(y(t))} k \exp \left[ -\frac{1}{N_0} \int y^2(t) dt \right] \\ &\times \exp \left[ \frac{2\sqrt{\alpha}}{N_0} \int y(t) s[\alpha(t - \tau)] dt \right] \exp \left[ -\frac{\alpha}{N_0} \int s^2[\alpha(t - \tau)] dt \right] \quad (2-9) \end{aligned}$$

All the factors not containing  $\tau$  and  $\alpha$  can be lumped together in one common constant  $k$ . The signal is normalized by setting

$$u(t) = \frac{1}{\sqrt{E}} s(t) \quad (2-10)$$

where  $E$  is the energy of the signal, given by

$$E = \int s^2(t) dt \quad (2-11)$$

Combining (2-9), (2-10), and (2-11),

$$p(\tau, \alpha | y(t)) = kp(\tau, \alpha) \exp \left[ -\frac{E}{N_0} \right] \exp \left[ \frac{2\sqrt{E\alpha}}{N_0} \int y(t) u[\alpha(t - \tau)] dt \right] \quad (2-12)$$

### 2.2.3 Receiver Operation

The operation of the receiver on the received signal is contained in the exponent of the last factor of Eq. (2-12). This exponent is called

$$q(\tau, \alpha) = \frac{2\sqrt{E\alpha}}{N_0} \int y(t) u[\alpha(t - \tau)] dt \quad (2-13)$$

From Eq. (2-1),  $y(t)$  is the sum of two terms, the signal term and the noise term. Assuming that the target was actually at  $\tau_0$  with a Doppler factor of  $\alpha_0$ ,

$$q(\tau, \alpha) = h(\tau, \alpha) + g(\tau, \alpha) \quad (2-14)$$

$$h(\tau, \alpha) = \frac{2\sqrt{E\alpha}}{N_0} \int n(t) u[\alpha(t - \tau)] dt \quad (2-15)$$

$$g(\tau, \alpha) = \frac{2E\sqrt{\alpha\alpha_0}}{N_0} \int u[\alpha_0(t - \tau_0)] u[\alpha(t - \tau)] dt \quad (2-16)$$

Since, in Eq. (2-15),  $n(t)$  is white Gaussian noise,  $h(\tau, \alpha)$  is a Gaussian variable where the mean = 0 and

$$\text{variance} = \sigma_h^2 = E[h^2(\tau, \alpha)] \quad (2-17)$$

$$\sigma_h^2 = \frac{4E\alpha}{N_0^2} \iint E[n(t) n(t + \eta)] u[\alpha(t - \tau)] u[\alpha(t + \eta - \tau)] dt d\eta \quad (2-18)$$

The noise process is stationary so that the ensemble average is equal to the autocovariance function  $\varphi(\eta)$ . In Helstrom (see Ref. 21, p. 50), the autocovariance function for white Gaussian noise is given as

$$\varphi(\eta) = E[n(t) n(t + \eta)] = \frac{N_0}{2} \delta(\eta) \quad (2-19)$$

where  $\delta(\eta)$  is the Dirac  $\delta$ -function. When the  $\eta$  integration is performed on Eq. (2-18) this yields

$$\sigma_h^2 = \frac{2E\alpha}{N_0} \int u[\alpha(t - \tau)] u[\alpha(t - \tau)] dt \quad (2-20)$$

$$\sigma_h^2 = \frac{2E}{N_0} \quad (2-21)$$

The ratio  $2E/N_0$  keeps showing up in these equations. This is the signal-energy-to-noise-power-density ratio and occurs often enough to be given the special name

$$R \equiv \frac{2E}{N_0} \quad (2-22)$$

Summarizing the previous results:

$$q(\tau, \alpha) = h(\tau, \alpha) + g(\tau, \alpha) \quad [(2-14)]$$

$$h(\tau, \alpha) = \text{Gaussian random variable (mean} = 0, \sigma_h^2 = R) \quad (2-23)$$

$$g(\tau, \alpha) = R \int u[\alpha_0(t - \tau_0)] u[\alpha(t - \tau)] \sqrt{\alpha\alpha_0} dt \quad (2-24)$$

#### 2.2.4 Signal Function

The integral of Eq. (2-24) can be simplified by setting

$$t' = \alpha_0(t - \tau_0)$$

$$\tau' = \alpha_0(\tau - \tau_0)$$

$$\alpha' = \frac{\alpha}{\alpha_0} \quad (2-25)$$

then

$$g(\tau', \alpha') = R \int u(t') u[\alpha'(t' - \tau')] \sqrt{\alpha'} dt' \quad (2-26)$$

This integral contains the interesting characteristics of the detection processes that are a function of the transmitted signal. The primes are removed from the variables in Eq. (2-26) to simplify the notation and the integral is called the signal function

$$\chi(\tau, \alpha) = \int u(t) u[\alpha(t - \tau)] \sqrt{\alpha} dt \quad (2-27)$$

The significance of  $\chi(\tau, \alpha)$  can be seen by substituting back into the probability expression (2-12)

$$p(\tau, \alpha | y(t)) = kp(\tau, \alpha) e^{h(\tau, \alpha)} e^{R\chi(\tau, \alpha)} \quad (2-28)$$

If the a priori probability density function  $p(\tau, \alpha)$  is flat and for a given  $R$ , the signal function  $\chi(\tau, \alpha)$  is proportional to the logarithm of  $p(\tau, \alpha | y(t))$ , except for the amount contributed by the function  $h(\tau, \alpha)$ . Since the average value of  $h(\tau, \alpha)$  is zero, the greater  $\chi(\tau, \alpha)$  is, the more probable that particular  $\tau$  and  $\alpha$  are.  $\chi(\tau, \alpha)$  is a cross-correlation function between two signals with unit energy. Therefore,

$$\chi(0, 1) = 1 \geq \chi(\tau, \alpha) \quad (2-29)$$

The proportionality factor between  $\chi(\tau, \alpha)$  and  $\ln[p(\tau, \alpha | y(t))]$  is  $R$ . This means that at very high signal-to-noise ratios ( $R \gg 1$ ) very good  $\tau$  and  $\alpha$  estimation is possible.

An alternate method of determining the signal function can be derived by substituting the Fourier transform

$$u(t) = \int U(\omega) e^{j\omega t} \frac{d\omega}{2\pi} \quad (2-30)$$

for the signal in Eq. (2-27),

$$\chi(\tau, \alpha) = \iint U(\omega') e^{j\omega' t} \frac{d\omega'}{2\pi} \int U(\omega) e^{j\omega \alpha(t-\tau)} \frac{d\omega}{2\pi} \sqrt{\alpha} dt \quad (2-31)$$

$$= \iiint U(\omega') U(\omega) e^{j(\omega' + \alpha\omega)t} e^{-j\omega\alpha\tau} \frac{d\omega'}{2\pi} \frac{d\omega}{2\pi} \sqrt{\alpha} dt \quad (2-32)$$

but

$$\int e^{j(\omega' + \alpha\omega)t} dt = 2\pi\delta(\omega' + \alpha\omega) \quad (2-33)$$

so that

$$\chi(\tau, \alpha) = \int U(-\alpha\omega) U(\omega) e^{-j\omega\alpha\tau} \sqrt{\alpha} \frac{d\omega}{2\pi} \quad (2-34)$$

but since  $u(t)$  is real:

$$U(-\alpha\omega) = U^*(\alpha\omega) \quad (2-35)$$

Combining (2-34) and (2-35), the alternate form for  $\chi(\tau, \alpha)$  is obtained:

$$\chi(\tau, \alpha) = \int U^*(\alpha\omega) U(\omega) e^{-j\alpha\omega\tau} \sqrt{\alpha} \frac{d\omega}{2\pi} \quad (2-36)$$

## 2.3 RANGE AND RANGE-RATE RESOLUTION LIMITATIONS OF THE A POSTERIORI MODEL

There are several conditions which limit the type of function that  $\chi(\tau, \alpha)$  can be. Since this function in fact characterizes the range and range rate resolution limitations of an echolocation system, the more that can be said about the function the better the designer's position is when selecting a transmitted signal waveform.

### 2.3.1 Probability Limitation

Since  $p(\alpha, \tau|y(t))$  is a probability density function, the volume of this function must integrate to one. That is,

$$\iint p(\alpha, \tau|y(t)) d\alpha d\tau = 1 \quad (2-37)$$

Referring to Eq. (2-28) it is seen that this condition tells us nothing about the a posteriori model but is merely a way of evaluating the constant  $k$ .

### 2.3.2 Signal Function Area

As was noted in Eq. (2-29), the signal function for  $\tau = 0$  and  $\alpha = 1$  is equal to one. Since the height of the signal function is related to the likelihood that the target is at some range traveling at some velocity, if the signal function is equal to one at some point other than  $(0, 1)$ , this point in range and range rate space is as likely as the point  $(0, 1)$ . In other words, over the region that the signal function has a value close to one, the values of range and range rate are indistinguishable or ambiguous. Therefore, the most desirable echolocation signal would be one for which the signal function takes on a value of one at  $(0, 1)$ , and zero or a negative value elsewhere. Such a signal is not possible because of the restrictions on the form of  $\chi(\tau, \alpha)$ .

An estimate of the spread of the signal function in frequency and time can be made by calculating

$$\iint_{-\infty}^{\infty} |\chi(\tau, \alpha)|^2 \frac{\omega_0 d\alpha}{2\pi} d\tau \quad (2-38)$$

In order to calculate this function, several constants are defined. If we assume that our echolocation signal does not contain any DC component,

$$\int u(t) dt = 0 \quad (2-39)$$

and has unit energy

$$\int_{-\infty}^{\infty} u^2(t) dt = 1 = \int_{-\infty}^{\infty} U^*(\omega) U(\omega) \frac{d\omega}{2\pi} \quad (2-40)$$

a center frequency  $\omega_0$  can be defined as the average frequency of the signal

$$\omega_o = \int_{-\infty}^{\infty} |\omega| U^*(\omega) U(\omega) \frac{d\omega}{2\pi} \quad (2-41)$$

A bandwidth  $\beta$  is then defined as twice the second moment of the signal transform around the center frequency

$$\left(\frac{\beta}{2}\right)^2 = r^2 = \int_{-\infty}^{\infty} (|\omega| - \omega_o)^2 U^*(\omega) U(\omega) \frac{d\omega}{2\pi} \quad (2-42)$$

The absolute value signs on the  $\omega$  are needed to take care of the negative half of the signal transform.

The expression (2-38) can be rewritten by substituting, from Eq. (2-36),

$$\begin{aligned} & \int_{-\infty}^{\infty} \left[ \int_{-\infty}^{\infty} U(\alpha\omega) U^*(\omega) e^{j\alpha\omega\tau} \sqrt{\alpha} \frac{d\omega}{2\pi} \right] \\ & \times \left[ \int_{-\infty}^{\infty} U^*(\alpha\omega') U(\omega') e^{-j\alpha\omega'\tau} \sqrt{\alpha} \frac{d\omega'}{2\pi} \right] \frac{\omega_o d\alpha}{2\pi} d\tau \quad (2-43) \end{aligned}$$

Performing the  $\tau$  integration,

$$\int_{-\infty}^{\infty} e^{j\alpha(\omega - \omega')\tau} \alpha d\tau = 2\pi\delta(\omega - \omega') \quad (2-44)$$

The  $\omega'$  integration can also be performed, reducing (2-43) to

$$\int_{-\infty}^{\infty} U(\alpha\omega) U^*(\omega) U^*(\alpha\omega) U(\omega) \frac{d\omega}{2\pi} \frac{\omega_o d\alpha}{2\pi} \quad (2-45)$$

Let

$$\nu = \omega\alpha \quad (2-46)$$

then

$$d\nu = \omega d\alpha \quad (2-47)$$

The integration limits on  $\nu$  are the same as on  $\alpha$ , if  $\omega > 0$ . If  $\omega < 0$ , the integration limits in Eq. (2-45) are reversed. Changing the limits back, Eq. (2-47) is written

$$d\nu = -\omega d\alpha \quad (\omega < 0) \quad (2-48)$$

Equivalently,

$$d\nu = |\omega| d\alpha \quad (2-49)$$

Equation (2-45) then becomes

$$\int_{-\infty}^{\infty} U^*(\omega) U(\omega) \int_{-\infty}^{\infty} U^*(\nu) U(\nu) \frac{d\nu}{2\pi} \frac{\omega_o}{|\omega|} \frac{d\omega}{2\pi} \quad (2-50)$$

If  $U(\omega)$  is nonzero only near  $\omega = \pm\omega_o$ ,  $\omega_o/|\omega|$  can be expanded in a Taylor series around both  $+\omega_o$  and  $-\omega_o$

$$\frac{\omega_o}{|\omega|} = \begin{cases} 1 - \frac{1}{\omega_o} (\omega - \omega_o) + \frac{1}{\omega_o^2} (\omega - \omega_o)^2 - \dots & (\omega > 0) \\ 1 + \frac{1}{\omega_o} (\omega + \omega_o) + \frac{1}{\omega_o^2} (\omega + \omega_o)^2 + \dots & (\omega < 0) \end{cases} \quad (2-51)$$

Reducing this to a simpler form,

$$\frac{\omega_o}{|\omega|} = 1 - \frac{1}{\omega_o} (|\omega| - \omega_o) + \frac{1}{\omega_o^2} (|\omega| - \omega_o)^2 - \dots \quad (2-52)$$

substituting this into Eq. (2-50) and applying Eq. (2-40) on the  $\nu$  integration,

$$\int_{-\infty}^{\infty} U^*(\omega) U(\omega) \left[ 1 - \frac{1}{\omega_o} (|\omega| - \omega_o) + \frac{1}{\omega_o^2} (|\omega| - \omega_o)^2 - \dots \right] \frac{d\omega}{2\pi} \quad (2-53)$$

By substituting Eqs. (2-40), (2-41), and (2-42) into (2-53), the result is

$$\int_{-\infty}^{\infty} |\chi(\tau, \alpha)|^2 \frac{\omega_o d\alpha}{2\pi} d\tau = 1 + \left[ \frac{\beta}{2\omega_o} \right]^2 - \dots \quad (2-54)$$

This equation has been derived by integrating  $\alpha$  from  $-\infty$  to  $+\infty$ . For  $\alpha$  less than zero, the target is moving toward the transmitter at a velocity greater than the velocity of propagation in the medium. For sonar, the target would be moving toward the transmitter at a velocity greater than the velocity of sound. For radar, the target would be moving toward the transmitter at a velocity greater than the speed of light!

Clearly the  $\alpha$  integration should be performed only over, at most, the region where  $\alpha$  lies between 0 and  $\infty$ . This restriction is easy to include by referring to Eqs. (2-50), (2-40), and (2-46). Since  $u(t)$  is a real function,

$$U^*(\nu) U(\nu) = U(-\nu) U^*(-\nu) \quad (2-55)$$

The argument of the  $\nu$  integration in Eq. (2-50) is therefore symmetrical around  $\nu = 0$ . The integral on  $\alpha$  between 0 and  $\infty$  is therefore equal to one-half the integral on  $\alpha$  between  $-\infty$  and  $+\infty$ . The result as stated in Eq. (2-54) is then changed to

$$\int_{-\infty}^{\infty} \int_0^{\infty} |\chi(\tau, \alpha)|^2 \frac{\omega_o d\alpha}{2\pi} d\tau = \frac{1}{2} \left[ 1 + \left( \frac{\beta}{2\omega_o} \right)^2 - \dots \right] \quad (2-56)$$

This is an important result and requires some comment. Equation (2-56) implies roughly that the volume under the signal function is a constant. Roughly speaking, different transmitted signals just change the position of the fixed amount of volume contained by the signal function. This is almost analogous to moving around a fixed amount of sand in a box. The analogy is not perfect because Eq. (2-56) is actually a statement about the volume under the square of the signal function, rather than the actual volume under the signal function. Negative values of the signal function are therefore treated the same as the positive values. In the actual measurement, the negative values of the signal function signify a lower likelihood than would a value of zero and should not be treated the same as positive values of the signal function. With narrow-band signals, the peaks and the valleys of the signal function are very close together and because of other limitations of the transmitter and receiver are often indistinguishable.

One method that is very useful in getting rid of ambiguous area in the  $\alpha, \tau$  plane is to use a system for which the ambiguous area is located outside the limits imposed by the a priori probability conditions. For example, the operation of a system that has a priori constraints on the velocity of its targets can be improved by locating an ambiguous area outside these maximum velocity limits.

### 2.3.3 Ambiguity Diagram of Pulsed FM Signals

The general form of the ambiguity diagram can be predicted from the general form of some transmitted signals. A long-duration constant-frequency pulse has an area of ambiguity that lies along the time delay axis of the ambiguity diagram, whereas a short-duration constant-frequency pulse has an area of ambiguity that lies along the Doppler axis of the ambiguity diagram. This means that with the former pulse, good Doppler resolution is achieved at the expense of time resolution and with the latter pulse, good time resolution is achieved at the expense of Doppler resolution. With a pulse that is long in duration, with the frequency varying linearly as a function of time, the area of ambiguity lies along a line that makes an angle with the time-delay axis of the ambiguity diagram. As stated previously, if a priori constraints on the echolocation situation eliminate the possibility that the target is moving at a greater velocity than some fixed amount, the area of ambiguity can sometimes be reduced by substantial factors. Even after the a priori constraints have been applied, some improvement in the apparent time-delay measurement accuracy of the system can be obtained. Suppose that an echolocation system that uses a pulsed FM signal has the ambiguity diagram shown in Fig. 4 with the a priori constraints also shown in the figure. The basic uncertainty  $\Delta\tau$  of the time delay estimation of this system is given by the distance between the two dotted lines. This deterioration in the time resolution of the system over the resolution that is obtained when the target velocity is known exactly is caused by asking the wrong question of the system. If the question were asked "Where will the target be in  $t$  seconds?" rather than "Where is the target now?", an improvement in the apparent time resolution of the system can be obtained.

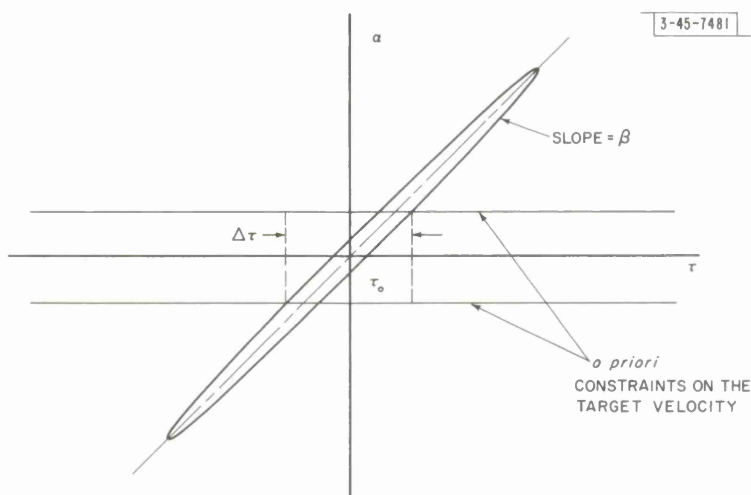


Fig. 4. Ambiguity diagram of pulsed FM signal with a priori velocity constraints.

Let the slope of the line that goes through the center of the area of ambiguity in Fig. 4 be  $\beta$ . The equation for this line is then given by

$$\alpha - 1 = \beta(\tau - \tau_0) \quad (2-57)$$

Using the approximate form for the relation between the target velocity  $v$  and the Doppler factor

$$\alpha = 1 - \frac{2v}{c} \quad (2-58)$$

Eq. (2-57) can be reduced to an expression for the time delay associated with the range of the target

$$\tau = \tau_0 - \frac{2v}{\beta c} \quad (2-59)$$

The equation of motion for the range  $x$  of the target is

$$x = x_0 + vt \quad (2-60)$$

where  $x_0$  is the position of the target at time  $t = 0$ . The position of the target at time  $t = 0$  as determined by the echolocation system from Eq. (2-59) is

$$x_0 = \frac{c\tau}{2} = \frac{c\tau_0}{2} - \frac{v}{\beta} \quad (2-61)$$

Combining Eqs. (2-60) and (2-61),

$$x = \frac{c\tau_0}{2} - \frac{v}{\beta} + vt \quad (2-62)$$

which, at time

$$t = \frac{1}{\beta} \quad (2-63)$$

yields for the position of the target:

$$x = \frac{c\tau_0}{2} \quad (2-64)$$

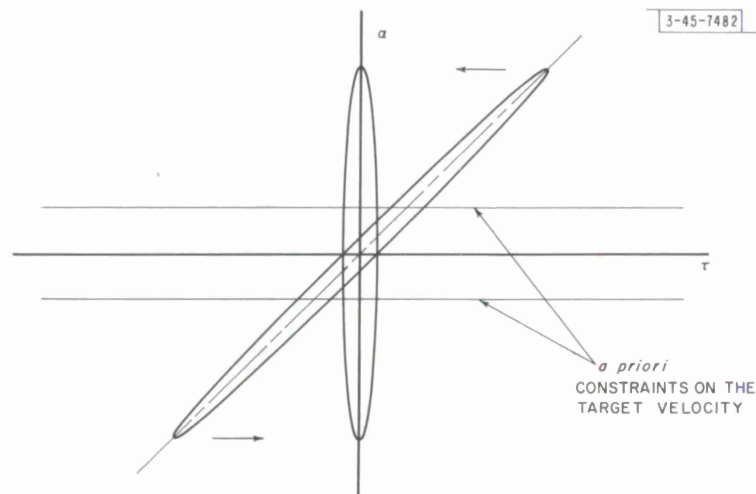


Fig. 5. Ambiguity diagram of pulsed FM signal modified to show ambiguity diagram for position of target at later time ( $t = 1/\beta$ ).

independent of the velocity of the target. Therefore, the position of the target can be determined as accurately as if the velocity of the target were known exactly. The time for which the position of the target is known is a little later or a little earlier than the time that the signal bounces off the target, depending, respectively, on whether  $\beta$  is positive or negative.

The modified ambiguity diagram for the range and the velocity of the target at the earlier time is shown in Fig. 5. As an example, a radar is tracking a missile. The waveform is pulsed FM, sweeping up in frequency:

Center frequency	1 Gcps
Frequency sweep	10 Mcps
Pulse duration	10 $\mu$ sec

Under these conditions, a 1-msec delay will cause the axis of the ambiguous area to rotate enough to coincide with the  $\tau = \tau$  zero line.

### 3. DIRECTIONAL LOCATION WITH GAIN-DISPERSIVE ANTENNAS

#### 3.1 INTRODUCTION

A bat that is catching a target needs three coordinates of information about his target: range, azimuth, and elevation. He can obtain range information from the target echo delay. He can obtain azimuth information from the interaural delay of the echo. The problem remains as to how the bat obtains elevation information.

One theory is that the bat wiggles his head back and forth to obtain several interaural delay measurements with different baselines. Although the bats of one family, the Rhinolophidae, are known to wiggle their ears at a high rate, they use very narrow-band signals which would give them poor time resolution. High-speed photography of vespertilionid bats, in particular, the little brown bats (Myotis lucifugus) in pursuit of thrown targets, shows no such head wiggling, while it clearly shows that the bats have excellent elevation aim.

Another possible explanation is that the bat is using the gain pattern of his ears to determine the elevation of his target. The bat's ears have a different Fourier system function for different elevation angles. In other words, the gain pattern of the bat's ears varies as a function of frequency. The bat must determine from what angle his echo is returning by determining which system function it is more probable that his signal was passed through.

The problem reduces to one of determining the impulse response of a linear system from the noisy output of the system, given the form of the input signal and the class of functions to which the impulse response belongs. By assuming additive Gaussian noise in the reception system that is independent of the position of the target, the problem can be treated in the same framework as the problem in Chapter 2. The best that an ideal filter can do is to compute the a posteriori probability distribution for the elevation angle and the time delay of the target, given the received signal. An antenna function is defined which is the complex Fourier system function for the antenna at the angle  $\theta$ . A signal function is then defined which describes the operation of the time delay and elevation measurement system. This signal function is similar to the signal function described in Chapter 2, except that this signal function depends on the form of the antenna as well as on the form of the transmitted signal.

The special case of a window-function antenna is examined. A window-function antenna is an antenna which has a sensitive area that lies on a plane and has a local sensitivity that can be defined as a function of the position on the plane of the antenna. Any one point on the antenna is assumed to be equally sensitive to a signal from any direction.

Two window-function antennas are used as examples to demonstrate the concept of the antenna function, the signal function and the operation of the echolocation system.

#### 3.2 MODEL AND DERIVATION

The model used for this analysis is shown in Fig. 6. The echo signal comes into the receiving antenna at an angle  $\theta$ . After the signal is received by the antenna, white Gaussian noise is added. Therefore, the received signal  $y(t)$  consists of two parts: the transmitted signal  $s(t)$  passed through a linear filter (the antenna), and the additive, white Gaussian noise

$$y(t) = n(t) + \int_{-\infty}^{\infty} s(\eta - \tau) h(\theta, t - \eta) d\eta \quad , \quad (3-1)$$

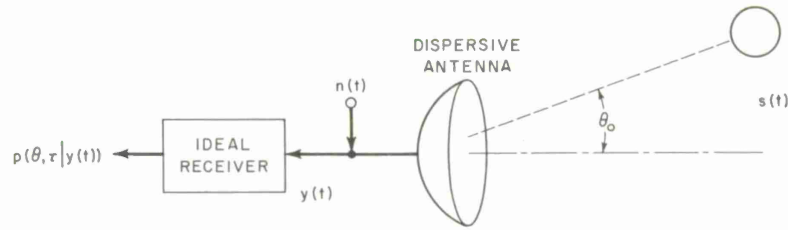


Fig. 6. Gain-dispersive antenna model.

where

$s(t)$  = transmitted signal

$n(t)$  = additive Gaussian noise

$\tau$  = time delay associated with the range

$h(\Theta, t)$  = impulse response of antenna at angle  $\Theta$

$y(t)$  = received signal

If the Fourier transform of  $s(t)$  and  $h(\Theta, t)$  are used,

$$s(t) = \int S(\omega) e^{j\omega t} \frac{d\omega}{2\pi} \quad (3-2)$$

$$h(\Theta, t) = \int H(\Theta, \omega) e^{j\omega t} \frac{d\omega}{2\pi} \quad (3-3)$$

Eq. (3-1) can be written in the form

$$y(t) = n(t) + \iint S(\omega) e^{j\omega(\eta-\tau)} \int H(\Theta, \omega') e^{j\omega'(t-\eta)} \frac{d\omega}{2\pi} \frac{d\omega'}{2\pi} d\eta \quad (3-4)$$

By noting that

$$\int_{-\infty}^{\infty} e^{j(\omega-\omega')\eta} d\eta = 2\pi\delta(\omega-\omega') \quad (3-5)$$

and performing the  $\omega'$  integration, Eq. (3-4) reduces to

$$y(t) = n(t) + \int S(\omega) H(\Theta, \omega) e^{j\omega(t-\tau)} \frac{d\omega}{2\pi} \quad (3-6)$$

### 3.2.1 Signal Function

The a posteriori probability density function for  $\Theta$  and  $\tau$  is given by

$$p(\Theta, \tau | y(t)) = \frac{p(\Theta, \tau)}{p(y(t))} p(y(t) | \Theta, \tau) \quad (3-7)$$

where, since the convolution integral in Eq. (3-1) is entirely deterministic when the parameters  $\Theta$  and  $\tau$  are given, the probability density function for the likelihood function is given by

$$p(y(t) | \Theta, \tau) = p(n(t)) = k \exp \left[ -\frac{1}{N_0} \int n^2(t) dt \right] \quad (3-8)$$

where with the use of Eq. (3-6) the exponent of Eq. (3-8) can be rewritten

$$-\frac{1}{N_0} \int n^2(t) dt = -\frac{1}{N_0} \int \left[ y(t) - \int S(\omega) H(\Theta, \omega) e^{j\omega(t-\tau)} \frac{d\omega}{2\pi} \right]^2 dt \quad (3-9)$$

$$= -\frac{1}{N_0} \int y^2(t) dt + \frac{2}{N_0} \int y(t) \left[ \int S(\omega) H(\Theta, \omega) e^{j\omega(t-\tau)} \frac{d\omega}{2\pi} \right] dt \quad (3-10)$$

$$- \frac{1}{N_0} \iiint S(\omega) H(\Theta, \omega) S(\omega') H(\Theta, \omega') e^{j(\omega+\omega')(t-\tau)} \frac{d\omega}{2\pi} \frac{d\omega'}{2\pi} dt$$

The first term in Eq. (3-10) concerns only  $y(t)$  and can therefore be lumped with  $p(y(t))$  in Eq. (3-7) and  $k$  in Eq. (3-8). The third term is related to the energy of the signal from the antenna that is expected at a particular angle. Letting this term be called  $\xi(\Theta, \tau)$  and after performing the integration

$$\int_{-\infty}^{\infty} e^{j(\omega+\omega')t} dt = 2\pi\delta(\omega + \omega') \quad , \quad (3-11)$$

the integration on  $\omega'$  can be performed leaving

$$\xi(\Theta, \tau) = -\frac{1}{N_0} \int S(\omega) H(\Theta, \omega) S(-\omega) H(\Theta, -\omega) \frac{d\omega}{2\pi} \quad . \quad (3-12)$$

Since both  $s(t)$  and  $h(\Theta, t)$  are real

$$S(-\omega) = S^*(\omega) \quad (3-13)$$

$$H(\Theta, -\omega) = H^*(\Theta, \omega) \quad , \quad (3-14)$$

Eq. (3-12) reduces to

$$\xi(\Theta, \tau) = -\frac{1}{N_0} \int S^*(\omega) S(\omega) H^*(\Theta, \omega) H(\Theta, \omega) \frac{d\omega}{2\pi} \quad . \quad (3-15)$$

Assuming that the actual target is at the angle  $\Theta_0$  and at the range corresponding to the time delay  $\tau_0$ , the second term of Eq. (3-10) can be written in two parts: the part due to the signal  $\psi(\Theta, \tau)$ , and the part due to the noise  $\nu(\Theta, \tau)$

$$\begin{aligned} \psi(\Theta, \tau) &\equiv \frac{2}{N_0} \int \left[ \int H(\Theta_0, \omega) S(\omega) e^{j\omega(t-\tau_0)} \frac{d\omega}{2\pi} \right] \\ &\quad \times \left[ \int H(\Theta, \omega') S(\omega') e^{j\omega'(t-\tau)} \frac{d\omega'}{2\pi} \right] dt \end{aligned} \quad (3-16)$$

$$\nu(\Theta, \tau) \equiv \frac{2}{N_0} \int n(t) \left[ \int H(\Theta, \omega) S(\omega) e^{j\omega(t-\tau)} \frac{d\omega}{2\pi} \right] dt \quad . \quad (3-17)$$

The  $t$  integration in Eq. (3-16) is

$$\int_{-\infty}^{\infty} e^{j(\omega'+\omega)t} dt = 2\pi\delta(\omega' + \omega) \quad . \quad (3-18)$$

Performing the  $\omega'$  integration and using Eqs. (3-13) and (3-14), Eq. (3-16) becomes

$$\psi(\Theta, \tau) = \frac{2}{N_0} \int H^*(\Theta, \omega) H(\Theta_0, \omega) |S(\omega)|^2 e^{j\omega(\tau-\tau_0)} \frac{d\omega}{2\pi} \quad (3-19)$$

Since, unlike the problem of Chapter 2, the expected energy of the received signal can depend on the parameter that is being measured ( $\Theta$ ), the function which describes the operation of the ideal receiver on the signal, the signal function ( $q(\Theta, \tau)$ ), consists of the sum of the operations described by Eqs. (3-15) and (3-19),

$$q(\Theta, \tau) = \xi(\Theta, \tau) + \psi(\Theta, \tau) \quad (3-20)$$

$$q(\Theta, \tau) = \frac{2}{N_0} \int \left[ H^*(\Theta, \omega) H(\Theta_0, \omega) |S(\omega)|^2 e^{j\omega(\tau-\tau_0)} - \frac{1}{2} |H(\Theta, \omega)|^2 |S(\omega)|^2 \right] \frac{d\omega}{2\pi} \quad (3-21)$$

Normalizing the signal

$$\int s^2(t) dt = E \quad (3-22)$$

$$u(t) = \frac{1}{\sqrt{E}} s(t) \quad (3-23)$$

$$U(\omega) = \frac{1}{\sqrt{E}} S(\omega) \quad (3-24)$$

$$R = \frac{2E}{N_0} \quad (3-25)$$

Eq. (3-21) reduces to

$$q(\Theta, \tau) = R \int \left[ H^*(\Theta, \omega) H(\Theta_0, \omega) |U(\omega)|^2 e^{j\omega(\tau-\tau_0)} - \frac{1}{2} |H(\Theta, \omega)|^2 |U(\omega)|^2 \right] \frac{d\omega}{2\pi} \quad (3-26)$$

This  $q(\Theta, \tau)$  function is similar in several ways to the  $\chi(\alpha, \tau)$  function of Chapter 2. The meaning of this function can be seen by substituting Eq. (3-26) back into Eq. (3-7) by using Eqs. (3-8), (3-10), (3-15), (3-16), (3-17), and (3-20)

$$p(\Theta, \tau | y(t)) = k p(\Theta, \tau) e^{\nu(\Theta, \tau)} e^{q(\Theta, \tau)} \quad (3-27)$$

This signal function  $q(\Theta, \tau)$  is proportional to the logarithm of the a posteriori probability density function for  $\Theta$  and  $\tau$ . Since the logarithm is a monotonically increasing function, the probability density that the target is located at a particular  $\Theta$  and  $\tau$  is monotonically related to the signal function. This means that the greater the value of the signal function, the greater the corresponding probability density function will be.

The form of the signal function is determined by the antenna function and the transmitted signal. Since the normalized transmitted signals spectrum ( $U(\omega)$ ) appears in Eq. (3-26) only as the absolute magnitude, signals with identical magnitude of signal spectrum will produce identical

signal functions. Therefore, an impulse, white noise, and swept FM signals would give identical signal functions. This is not to say that if the receiver is set for use with an impulse as the transmitted signal, white noise could be used. The receiver has to be set up for the exact form of the transmitted signal. Under these conditions, the above signals will give identical signal functions.

### 3.2.2 Noise Function

The noise function  $\nu(\Theta, \tau)$ , defined by Eq. (3-17), is a Gaussian random variable. Since  $n(t)$  has zero mean,  $\nu(\Theta, \tau)$  also has zero mean. The variance of the noise function is

$$\sigma_n^2 = E [\nu^2(\Theta, \tau)] = \frac{4}{N_0^2} \iint E [n(t) n(t')] \times \left[ \iint H(\Theta, \omega) H(\Theta, \omega') S(\omega) S(\omega') e^{j\omega(t-\tau)} e^{j\omega'(t'-\tau)} \frac{d\omega}{2\pi} \frac{d\omega'}{2\pi} \right] dt dt' \quad (3-28)$$

but

$$E [n(t) n(t')] = \frac{N_0}{2} \delta(t - t') \quad , \quad (3-29)$$

performing the  $t'$  integration and then the integration on  $\omega'$

$$\int e^{j(\omega+\omega')t} dt = 2\pi\delta(\omega + \omega') \quad (3-30)$$

and substituting from Eqs. (3-24) and (3-25), Eq. (3-28) reduces to

$$\sigma_n^2 = R \int |H(\Theta, \omega)|^2 |U(\omega)|^2 \frac{d\omega}{2\pi} \quad . \quad (3-31)$$

## 3.3 WINDOW-FUNCTION ANTENNAS

The class of antennas that can be described by window functions allows some simplification of the signal function. A window-function antenna is an antenna whose sensitive area lies on a plane, no energy storage takes place, and the sensitivity at any point can be either positive or negative. An acoustical example of this type of antenna is the piston-in-a-wall transducer.

### 3.3.1 Impulse Response of a One-Dimensional Window-Function Antenna

The point sensitivity of the antenna is  $g(x/c)$ . Each point on the antenna is acting independently of all other points on the antenna and is independent of frequency. The impulse response of this antenna at an angle  $\Theta$  can be calculated by inspection from Fig. 7(a-b).

The relationship between a point of time on the impulse response and the coordinate of the window function is

$$t = \frac{x}{c} \sin \Theta \quad . \quad (3-32)$$

Since each point on the antenna is considered separately, the area under the impulse response is a constant, equal except for a sensitivity constant to the area under the window function. Choosing the scale for  $g(x/c)$  in such a way that the sensitivity constant is unity,

$$h(\Theta, t) dt = g\left(\frac{x}{c}\right) d\left(\frac{x}{c}\right) \quad . \quad (3-33)$$

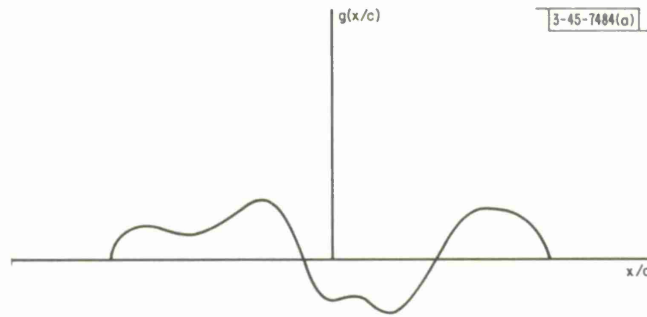


Fig. 7(a). Window function for antenna.

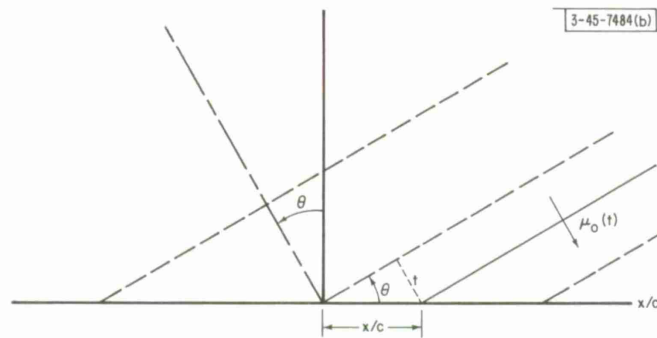


Fig. 7(b). Construction showing timing of impulse coming from angle  $\theta$  on window-function antenna.

By differentiating Eq. (3-32)

$$dt = \sin \theta d\left(\frac{x}{c}\right) \quad (3-34)$$

and substituting into Eq. (3-33)

$$h(\theta, t) = \frac{1}{\sin \theta} g\left(\frac{t}{\sin \theta}\right) \quad (3-35)$$

which is the relationship between the impulse response of a window-function antenna at a particular angle and the window function. Under the normalizing condition on the window function

$$\int g^2(\mu) d\mu = 1 \quad (3-36)$$

the energy of the impulse response is

$$\int h^2(\theta, t) dt = \frac{1}{\sin^2 \theta} \int g^2\left(\frac{t}{\sin \theta}\right) dt \quad (3-37)$$

$$\int h^2(\theta, t) dt = \frac{1}{\sin^2 \theta} \quad (3-38)$$

Notice that as  $\theta \rightarrow 0$ , the energy of the impulse response  $\rightarrow \infty$ . This is normal and expected, since the energy in a unit impulse is infinite.

### 3.3.2 Transform Relationship

The Fourier transforms for the impulse response and the window function are

$$H(\Theta, \omega) = \int_{-\infty}^{\infty} h(\Theta, t) e^{-j\omega t} dt \quad (3-39)$$

$$G(\eta) = \int_{-\infty}^{\infty} g(\mu) e^{-j\eta\mu} d\mu \quad (3-40)$$

Combining Eqs. (3-35) and (3-39)

$$H(\Theta, \omega) = \int \frac{1}{\sin \Theta} g\left(\frac{t}{\sin \Theta}\right) e^{-j\omega t} dt \quad (3-41)$$

by substituting  $\mu$  for  $t/\sin \Theta$  this becomes

$$H(\Theta, \omega) = \int g(\mu) e^{-j\omega \sin \Theta \mu} d\mu \quad (3-42)$$

which, with Eq. (3-40), reduces to

$$H(\Theta, \omega) = G(\omega \sin \Theta) \quad (3-43)$$

### 3.4 EXAMPLES OF THE SIGNAL AND LIKELIHOOD FUNCTIONS

Two examples are worked out to show graphically the possibilities of this angular measurement scheme. To simplify the arithmetic, the transmitted signal spectrum is assumed to be flat:

$$|S(\omega)|^2 = 1 \quad (3-44)$$

This assumption gives infinite bandwidth to the transmitted signal, obviously not the case in any real echolocation system. Because of the nature of the two window-function antennas described below, the infinite bandwidth assumption affects the signal function radically only when  $\Theta_0$  is near zero.

#### 3.4.1 Antenna With a Square Window Function

The window function of this example is shown in Fig. 8. The equation for the function is

$$g\left(\frac{x}{c}\right) = \begin{cases} \frac{1}{\sqrt{\alpha}} & , \quad \left|\frac{x}{c}\right| < \frac{\alpha}{2} \\ 0 & , \quad \left|\frac{x}{c}\right| > \frac{\alpha}{2} \end{cases} \quad (3-45)$$

The Fourier transform of the window function is

$$G(\eta) = \sqrt{\alpha} \frac{\sin\left(\frac{\eta\alpha}{2}\right)}{\left(\frac{\eta\alpha}{2}\right)} \quad (3-46)$$

From Eq. (3-43),

$$H(\Theta, \omega) = G(\omega \sin \Theta) \quad [(3-43)]$$

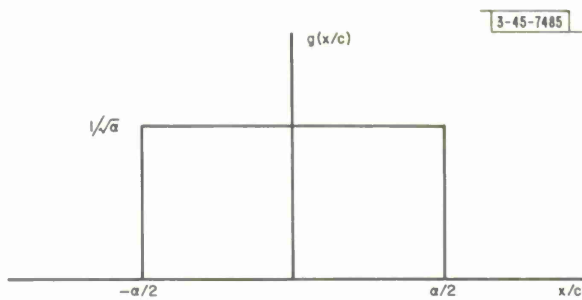


Fig. 8. Window function for square-window-function antenna.

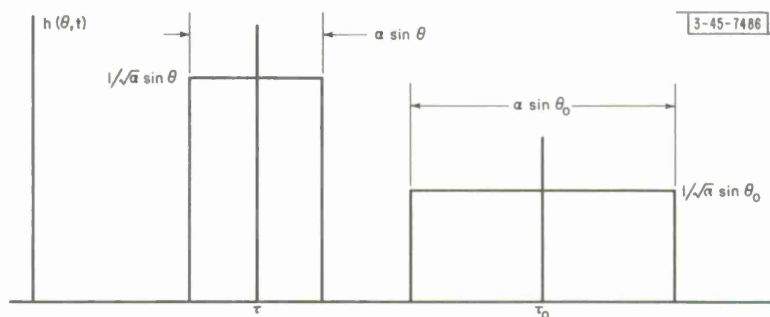
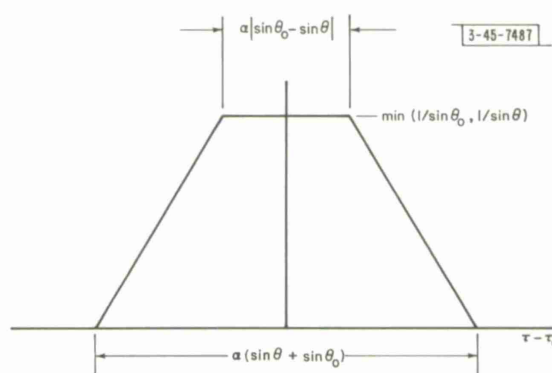


Fig. 9. Square-window-function antenna: impulse response for target at  $\theta_0, \tau_0$  and for target at  $\theta, \tau$ .

Fig. 10. Convolution integral for impulse responses of square-window-function antenna.



the transform of the impulse response is

$$H(\Theta, \omega) = \sqrt{\alpha} \frac{\sin(\frac{\alpha}{2} \omega \sin \Theta)}{(\frac{\alpha}{2} \omega \sin \Theta)} \quad (3-47)$$

and from Eq. (3-35),

$$h(\Theta, t) = \frac{1}{\sin \Theta} g\left(\frac{t}{\sin \Theta}\right) \quad [(3-35)]$$

the impulse response is

$$h(\Theta, t) = \begin{cases} \frac{1}{\sqrt{\alpha} \sin \Theta} & , \quad \left| \frac{t}{\sin \Theta} \right| < \frac{\alpha}{2} \\ 0 & , \quad \left| \frac{t}{\sin \Theta} \right| > \frac{\alpha}{2} \end{cases} \quad (3-48)$$

Since multiplication in the frequency domain is equivalent to convolution in the time domain, under the conditions of Eq. (3-44), Eq. (3-24) can be rewritten as

$$q(\Theta, \tau) = \frac{2}{N_o} \left[ h(\Theta_o, \mu) * h(\Theta, \mu - (\tau - \tau_o)) - \frac{1}{2} \int h^2(\Theta, t) dt \right] \quad (3-49)$$

From Eq. (3-38) the second term of the above integral is

$$-\frac{1}{2} \int h^2(\Theta, t) dt = -\frac{1}{2 \sin \Theta} \quad (3-50)$$

The antenna impulse responses, as shown in Fig. 9, when convolved yield the function shown in Fig. 10. A three-dimensional graph of the signal function with  $\Theta_o = 30^\circ$  is shown in Fig. 11.

Sectioning through the signal function with the plane  $\tau = 0$ , the equation for the signal function becomes

$$q(\Theta, 0) = \frac{2}{N_o} \left[ \min\left(\frac{1}{\sin \Theta_o}, \frac{1}{\sin \Theta}\right) - \frac{1}{2 \sin \Theta} \right] \quad (3-51)$$

which is shown graphically in Figs. 12 and 13 for two values of  $\Theta_o$  along with the corresponding likelihood functions for various signal-to-noise ratios.

### 3.4.2 Antenna With a Cosine Window Function

The window function for this example is shown in Fig. 14. The equation for the function is

$$g\left(\frac{x}{c}\right) = \begin{cases} \sqrt{\frac{2}{\alpha}} \cos \frac{10\pi}{\alpha} \left(\frac{x}{c}\right) & , \quad \left|\frac{x}{c}\right| < \frac{\alpha}{2} \\ 0 & , \quad \left|\frac{x}{c}\right| > \frac{\alpha}{2} \end{cases} \quad (3-52)$$

and from Eq. (3-35) the impulse response of the antenna at an angle  $\Theta$  is

$$h(\Theta, t) = \begin{cases} \sqrt{\frac{2}{\alpha}} \frac{1}{\sin \Theta} \cos 10\pi \frac{t}{\alpha \sin \Theta} & , \quad |t| < \frac{\alpha \sin \Theta}{2} \\ 0 & , \quad |t| > \frac{\alpha \sin \Theta}{2} \end{cases} \quad (3-53)$$

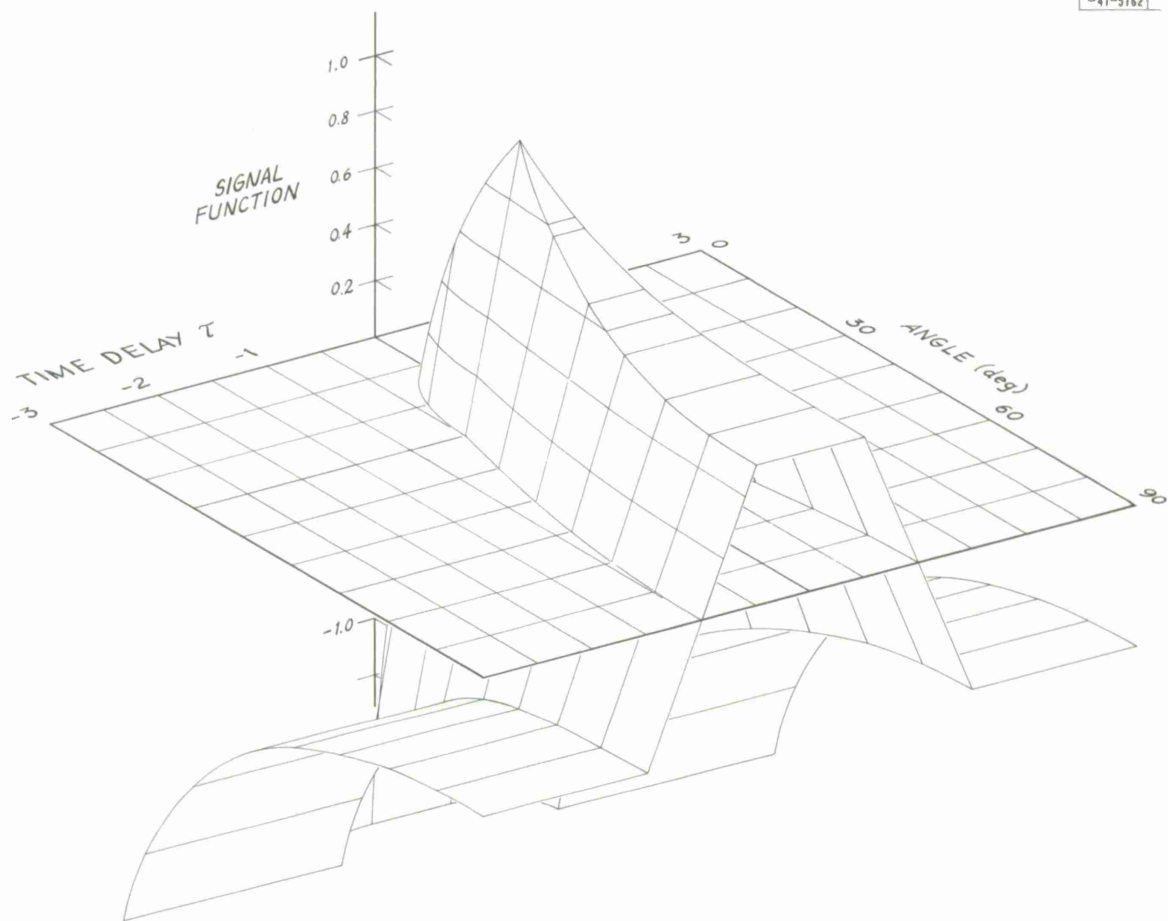


Fig. 11. Three-dimensional graph of signal function of square-window-function antenna.

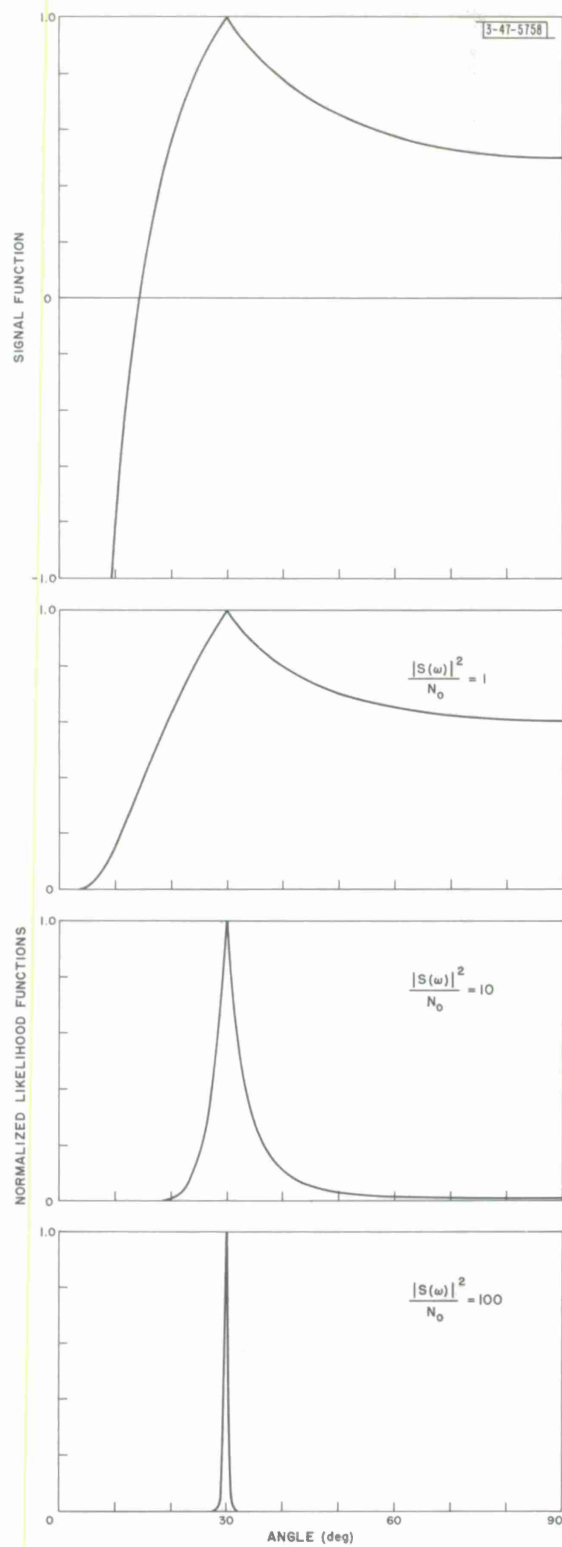


Fig. 12. Signal and likelihood functions for square-window-function antenna ( $\tau = 0$ ,  $\theta_0 = 30^\circ$ ).

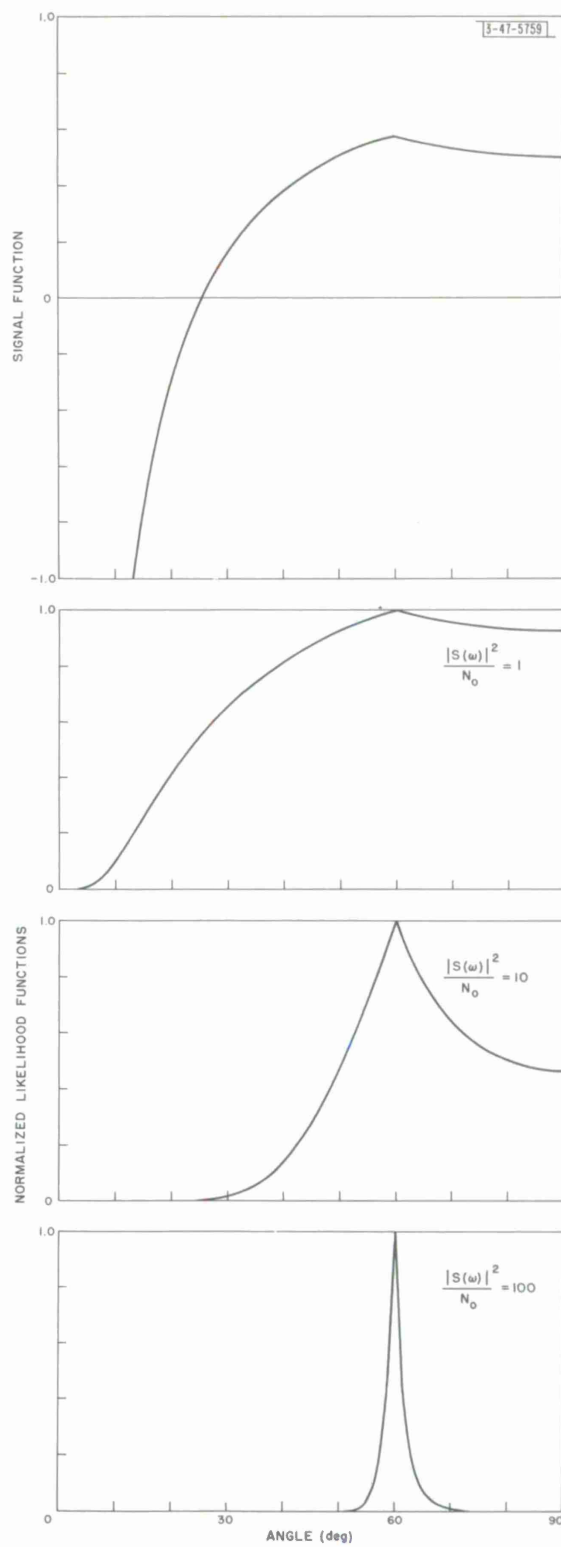


Fig. 13. Signal and likelihood functions for square-window-function antenna ( $\tau = 0$ ,  $\theta_0 = 60^\circ$ ).

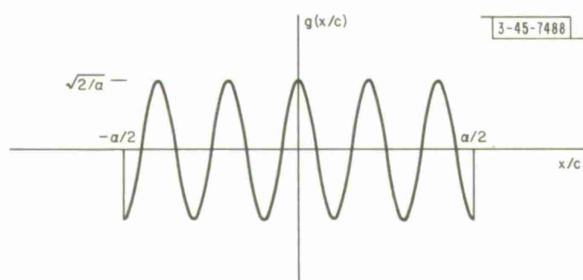


Fig. 14. Window function for 5-cycle-cosine window-function antenna.

Let

$$a = \max\left(\frac{1}{\sin \Theta}, \frac{1}{\sin \Theta_0}\right) \quad (3-54)$$

$$b = \min\left(\frac{1}{\sin \Theta}, \frac{1}{\sin \Theta_0}\right) \quad (3-55)$$

Sectioning through the signal function with the plane  $\tau = 0$  the equation for the signal function becomes

$$q(\Theta, 0) = \frac{2}{N_0} \left[ \frac{2ab^2}{5\pi(a^2 - b^2)} \sin 5\pi \frac{b}{a} - \frac{1}{2 \sin \Theta} \right] \quad (3-56)$$

which is shown graphically in Figs. 15 and 16 for two values of  $\Theta_0$  along with the corresponding likelihood functions for various signal-to-noise ratios.

### 3.5 FINITE BANDWIDTH CONSIDERATIONS

The two previous examples (Secs. 3.4.1 and 3.4.2) were worked out under the assumption that the transmitted signal had an infinite bandwidth. This can obviously never be the case in an actual echolocation system. Equation (3-49) was derived from Eq. (3-26) under the infinite bandwidth assumption. For a finite bandwidth, the first term of Eq. (3-49), the cross-correlation function of the antenna impulse response, should be cross correlated with the normalized, signal autocorrelation function. The second term can be written as it appears in Eq. (3-26). The effect of the cross correlation with the autocorrelation function can be seen intuitively. Suppose, for instance, that the signal autocorrelation function is very narrow, and has the general form of a Gauss error function. Cross correlating the narrow Gauss error function with the function represented by the first term of Eq. (3-49) has the effect of rounding the corners, in the  $\tau$ -direction, and generally smoothing the shape of this function. This rounding of the sharp corners in the  $\tau$ -direction will usually round sharp corners in the  $\Theta$ -direction also. The flat regions are not affected, since the Gauss error function integrates to some constant value over these regions.

A signal that has a wider autocorrelation function, and therefore a narrower bandwidth, will cause a greater rounding of the corners of the first term of the signal function. In the region where this autocorrelation function of the antenna impulse response is narrow, near  $\Theta_0 = 0$ , the signal autocorrelation function will affect the signal function radically. The signal function takes on the rough shape of the signal autocorrelation function rather than the shape of the autocorrelation function of the antenna impulse response.

In any real echolocation system, limitations on the lower frequency cutoff must be imposed as well as the upper frequency limitations. In particular, it is unreasonable to assume that the

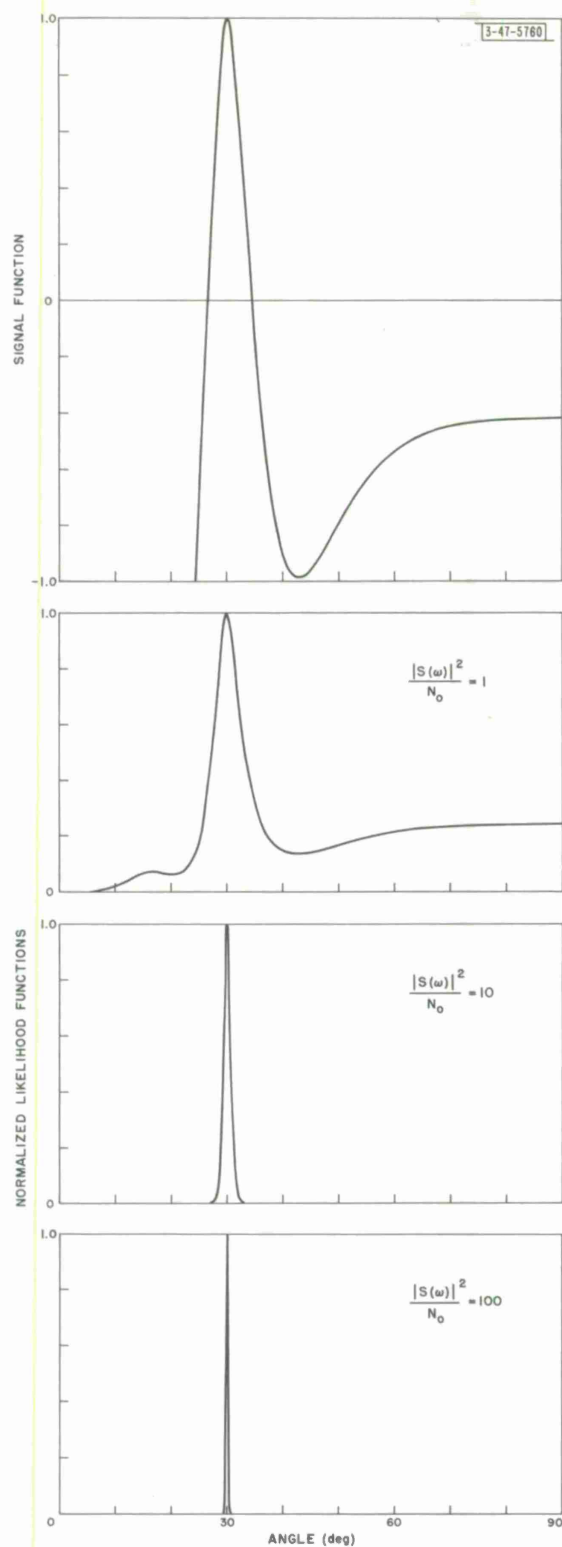


Fig. 15. Signal and likelihood functions for 5-cycle-cosine window-function antenna ( $\tau = 0$ ,  $\theta_0 = 30^\circ$ ).

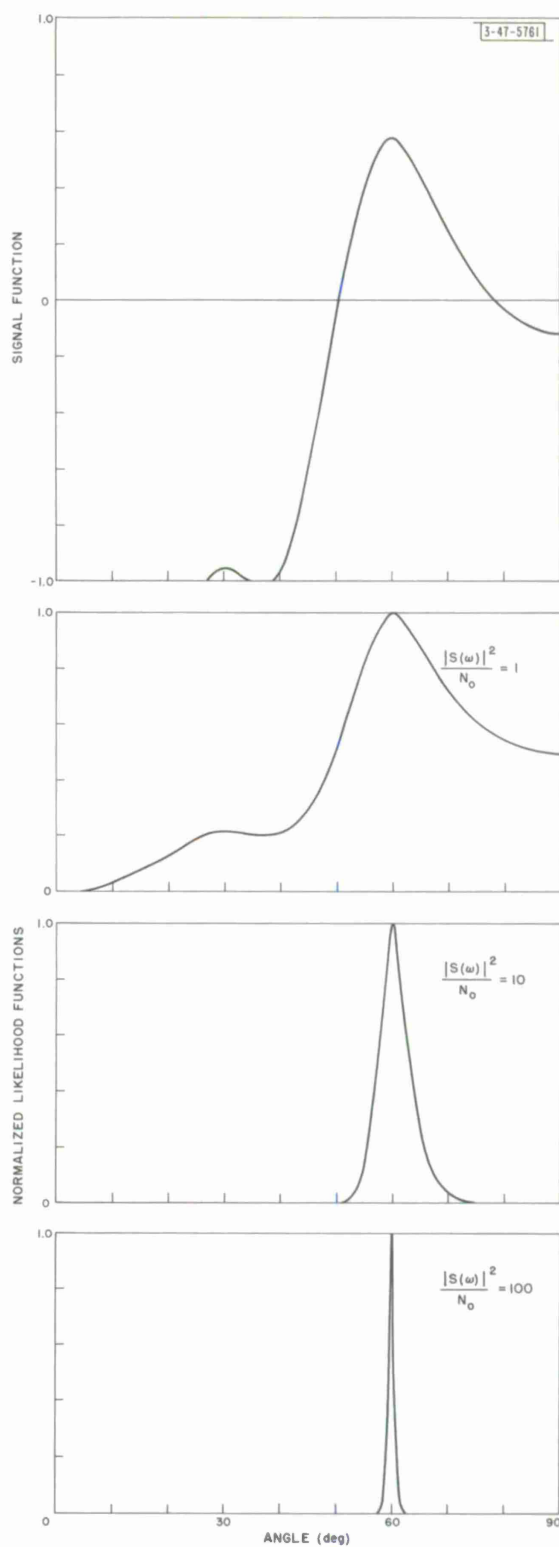


Fig. 16. Signal and likelihood functions for 5-cycle-cosine window-function antenna ( $\tau = 0$ ,  $\theta_0 = 60^\circ$ ).

echolocation signal has a DC component. If the signal does not have a DC component, the signal autocorrelation function does not have a DC component. The effect of this restriction can be observed by referring to Fig. 11. Slices parallel to the  $\Theta = 0$  plane are, in effect, passed through a band-pass filter whose impulse response is the autocorrelation function of the transmitted signal. (Since the autocorrelation function is nonzero for negative time as well as positive time, this hypothetical band-pass filter is physically unrealizable.) The DC level for these signals, or slices, can be determined by referring to Eq. (3-26). The second term of this equation is the one that controls the DC level of the slices. Changing the equation from the frequency domain to the time domain and using correlation notation, the second term of Eq. (3-26) can be written as

$$-\frac{R}{2} h(\Theta, t - \eta) * h(\Theta, \mu - \eta) * u(\mu - \beta) * u(-\beta) \quad , \quad \text{for } t = 0 \quad , \quad (3-57)$$

where  $\eta$ ,  $\mu$ , and  $\beta$  are dummy variables. The DC level of the output of the hypothetical band-pass filter for each of these slices is therefore equal to minus one-half the output of this filter at  $\tau = 0$  with the autocorrelation function of the antenna impulse response on the input.

The graph in Fig. 11 is changed by the finite bandwidth restriction in the following ways:

- (1) The level of the graph goes below the DC level as well as above it.
- (2) The flat region in the vicinity of  $60^\circ$  to  $90^\circ$  sags slightly.
- (3) The sharp edges are rounded and the central spike is smoothed.
- (4) The DC level of the graph is modified to equal the level given by Eq. (3-57).

## 4. AMBIGUITY DIAGRAM COMPUTER

### 4.1 INTRODUCTION

An ambiguity diagram computer is a device that computes the signal function expressed by Eq. (2-27)

$$\chi(\tau, \alpha) \equiv \int u(t) u[\alpha(t - \tau)] \sqrt{\alpha} dt \quad . \quad [(2-27)]$$

The terms "ambiguity diagram" and "signal function" are used almost interchangeably in the radar literature. P. M. Woodward first used the term signal function to describe the narrow-band approximation to the function mentioned above. Since this function describes the area of ambiguity of a received signal waveform, it has also been called an ambiguity function. To avoid ambiguities, the above function will be called the signal function while the graph of this function will be called the ambiguity diagram.

The basic requirements of an ambiguity diagram computer are:

- (a) A device to simulate and/or repeat the signal  $u(t)$ ,
- (b) A method of producing a variable time delay,
- (c) A method of producing a Doppler shift,
- (d) A multiplier,
- (e) A pulsed integrator,
- (f) A method of displaying the output.

There are many ways to obtain each of the above operations. One rather obvious solution would be to compute the signal function on a digital or an analog computer. Several years ago, a student in the M.I.T. acoustics laboratory, Kenneth Goff, built an analog, magnetic drum, time delay unit.<sup>16</sup> This unit records one or two signals on two tracks of a magnetic drum. One of the record heads is movable so that the signal being recorded on one track can be advanced or retarded with respect to the signal being recorded on the other track. Because this time delay unit was available, it was decided that a special-purpose, analog ambiguity diagram computer would be constructed to analyze the echolocation signals of bats.

The Goff delay drum was originally built to continuously record, reproduce, and erase on the two signal tracks. With only minor modifications, the unit was redesigned to accept a pulse signal. The pulse signal is recorded on the drum and remains there. Since the drum is rotating, the pulse signal is repeated over and over again. The signals on the two tracks are advanced or retarded with respect to each other by advancing or retarding a movable playback head. When the correlation function has been plotted, the signals are erased and the drum is ready to accept the next pair of pulse signals.

The signals of the bats are recorded on a high-speed, instrumentation tape recorder. By reproducing the tape at  $1/32$  of the recorded speed, the 20- to 120-kcps frequency of the bat signals is reduced to a frequency range of 600 to 4000 cps, which is audible to human ears. It thus falls well within the frequency band for which the Goff time-delay unit is designed to work.

Doppler shift is introduced by changing the speed of the tape reproducer by incremental amounts. This Doppler shift is a compression or expansion of the time axis of the signal, thus simulating an actual Doppler shift.

A vacuum-tube quarter-square multiplier is used for the multiplication of the two signals. The multiplier was originally designed and built as a Master's thesis project by the author.<sup>29</sup> The pulsed integrator was built out of Philbrick operational amplifiers with the gating, sampling, and resetting operations performed by electronically driven relay circuitry.

The output of the computer is displayed on a Variplotter X-Y recorder. When a three-dimensional graph output is desired,  $\tan 30^\circ$  times the X deflection of the recorder is subtracted from the Y deflection of the recorder. The zero line of the output of the computer is, therefore, plotted at a  $30^\circ$  angle with respect to the horizontal. A tri-metric drawing is then traced from a composite of these slanted graphs to obtain a two-dimensional representation of these three-dimensional graphs.

## 4.2 RECORD ELECTRONICS

### 4.2.1 Outline and Block Diagram

When a bat pulse is transferred to the magnetic drum delay unit from the magnetic tape reproducer, several timing and gating operations take place. Figure 17 is a block diagram of the arrangement used to gate a bat signal onto the magnetic drum. On the second channel of the tape reproducer a pulse marker signal has been placed 0.1 to 0.2 sec before the start of the bat signal. This signal is used to trigger the B sweep of a Tektronix 535A oscilloscope. The oscilloscope is used as a signal generator to provide the gating signals needed to gate the bat signal onto the time delay drum. The A sweep on the oscilloscope is triggered by the internal delay pickoff on the B sweep. The A sweep gate signal is used to drive a relay that connects the output of the record amplifiers of the Goff delay drum to the record heads. The A sawtooth signal is fed into a trigger pickoff unit that triggers an electronic switch on and then off, electronically gating the bat signal into the record amplifier.

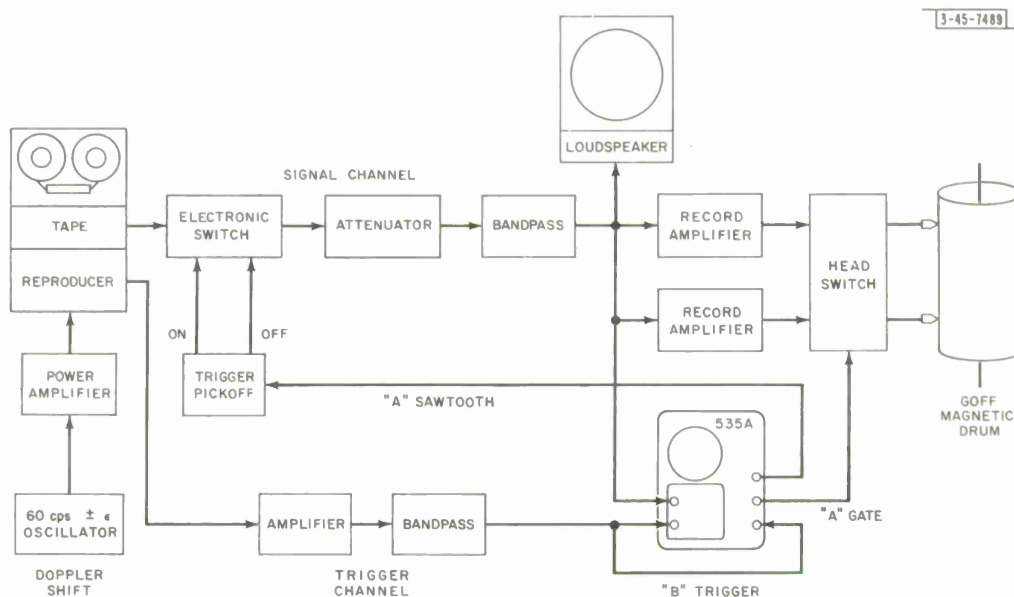


Fig. 17. Electronics used to record signal onto magnetic drum.

During this operation of the record electronics, the bat signal to be analyzed is played by the tape reproducer. The gating circuitry gates the bat signal onto track 1 of the drum. The playing speed of the tape reproducer is changed by the incremental amount corresponding to the desired amount of Doppler shift; then the tape is replayed and the Doppler-shifted bat signal is gated onto track 2 of the drum.

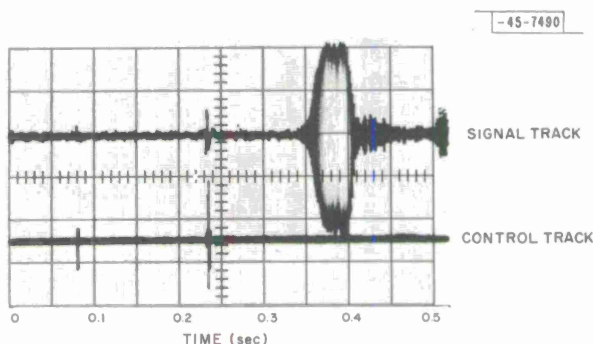
#### 4.2.2 Tape Input

The slowed-down bat-signal sound track is recorded on  $\frac{1}{4}$ -inch magnetic tape at  $7\frac{1}{2}$  inches/sec on a conventional stereo tape recorder, an Ampex 601-2. After locating the physical position of the desired bat pulse on the tape, the tape is magnetically marked as follows:

- (a) The bat pulse is manually positioned approximately 1 inch ahead of the record head, with the tape disengaged from the capstan drive mechanism.
- (b) The recorder control is turned to RECORD position and then off.

This procedure magnetically marks both tracks of the magnetic tape at the points where the record head and the erase head are in contact with the tape. When the tape is played, two short pulses are reproduced on both tracks 0.1 to 0.3 sec before the bat signal is reproduced on the signal track as is shown in Fig. 18.

Fig. 18. Synchronizing marker timing on typical  $\frac{1}{4}$ -inch magnetic tape record (bat pulse 4).



The first marker signal on the control track, the record head signal, is used to trigger the gating circuitry that gates the bat signal onto the magnetic drum.

Doppler shift is introduced into the tape-recorded bat signal by changing the speed of the tape reproducer. The Ampex 601-2 tape recorder has a synchronous motor capstan drive so that, if the frequency of the motor drive power is changed, the speed of the motor, and hence the tape speed, will be changed by a proportional amount. The motor of the Ampex is driven by a variable frequency oscillator followed by a high-power amplifier. A very stable and accurately calibrated oscillator is needed, since the change in frequency due to the Doppler shift is usually very small. A Krohn-Hite model 310-AB push-button oscillator was found to be suitable. It has an accuracy of 1 percent and a drift of less than 0.05 percent/hr. The power amplifier is a Vectron VS-250 that was modified to accept the external oscillator input.

The oscillator setting for each particular Doppler shift was calculated by using the approximate formula for the oscillator setting:

$$f = 60 \left( 1 - \frac{2v}{c} \right) \quad (4-1)$$

A list of the oscillator settings for various target velocities is given in Table I.

TABLE I DOPPLER FACTOR AND MOTOR-DRIVE OSCILLATOR SETTINGS FOR GIVEN TARGET VELOCITIES		
Target Velocity (m/sec)	Doppler Factor (dimensionless)	Oscillator Frequency (cps)
-10	1.0579	63.47
-8	1.0463	62.78
-6	1.0347	62.09
-4	1.0232	61.39
-2	1.0116	60.70
0	1.0000	60.00
2	0.9885	59.31
4	0.9769	58.62
6	0.9654	57.92
8	0.9538	57.23
10	0.9422	56.54

#### 4.2.3 Electronic Gating and Switching

Two types of gating must be provided to record a chosen bat signal onto the magnetic drum. The signal is electronically switched to provide the desired bat pulse to the record amplifiers. The currents to the recording heads of the tape drum are switched so that recording takes place only during one revolution of the magnetic drum. The electronic switching is done by a Grason-Stadler (Model E3382) modulating switch and the head-current switching is done with a relay. Timing signals for the switching processes are obtained from the Tektronix oscilloscope. The signal from the second track of the tape reproducer, after being amplified and filtered, is used to trigger the B sweep of the Tektronix. The A sweep of the oscilloscope is triggered internally after a fixed time delay. The timing of this operation is shown for a typical bat pulse in Fig. 19. The A sweep gate output of the oscillator is used to drive a relay-driver circuit which, in turn, connects the record amplifiers to the record heads during the time that the A sweep gate is

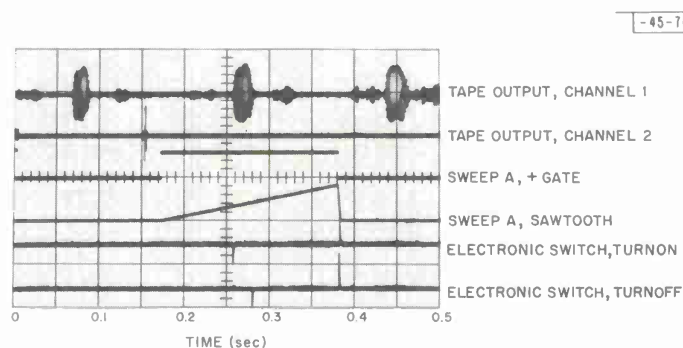


Fig. 19. Timing sequence for gating signals which are derived from oscilloscope that is triggered by channel 2 signal of input tape.

positive. The A sweep sawtooth is used to drive a trigger pickoff circuit which turns the electronic switch on and off at times that correspond to voltage levels on the sawtooth.

The relay-driver circuit provides power to the relay when the oscilloscope gate is positive, that is when the gate is at +20 volts. This gate is usually set for a duration of between 0.2 to 0.25 sec because the drum makes one revolution in 0.25 sec. The schematic for the relay driver is shown in Fig. 20. The relay ungrounds the output of the record amplifiers and connects the amplifiers' outputs to their respective record heads or to ground depending on whether the record switch is on or off. In Goff's design of the magnetic drum circuitry, the movable head is a record head. After the pulse signals have been recorded on the drum, it is one of the playback heads that must be moved. Fortunately, the movable head works satisfactorily as a playback head and its connections have therefore been modified so that it can be used as the playback head as well as the record head. A switch has been installed on the input of the number 2 playback amplifier to facilitate the use of either the normal record or the normal playback head.

The high-frequency bias signal to the erase heads is also switched. Before recording a pulse on the drum, the entire drum is erased by turning on the erase switch. If this switch is turned off, a large spike will be recorded on the magnetic drum. To avoid this, the bias to the erase heads is turned off slowly by disconnecting B+ from the bias oscillator. This is accomplished by turning off the microswitch that provides power to a relay in the record amplifier unit which, in turn, switches the power to the drum drive motor as well as switching the B+ to the bias oscillator. After turning off the bias in this way, the erase switch is turned off and then the microswitch is turned back on. The entire drum is now erased.

The A sweep sawtooth from the oscilloscope is a positive-going ramp starting at ground potential and climbing to about +150 volts. Pulses to turn the electronic switch on and off are obtained from a trigger pickoff circuit which operates from the A sweep sawtooth. The schematic diagram for the trigger pickoff circuit is given in Fig. 21. The 50-volt negative pulses needed to switch the electronic switch are obtained from the sawtooth with Philbrick operational amplifiers (type K-2W). The transition time on the output of these amplifiers is decreased by the use of positive feedback around the amplifiers. The triggering levels for turnon and turnoff are set by the potentiometers on the positive input of the operational amplifiers. Figure 19 shows the timing of the turnon and turnoff signals for a typical bat pulse. When the voltage on the negative input to the amplifier increases to equal the voltage on the positive input, the output goes through a fast negative transition. This negative step is capacitor-coupled to the triggering input of the Grason-Stadler switch. The diode in parallel with the output is necessary because of the peculiarities of the Grason-Stadler switch. If the trigger signal to this switch is allowed to go negative, the unit will not turn off properly.

#### 4.2.4 Drum Delay Unit

The drum delay unit was originally designed to operate by continuously recording and reproducing signals on two separate tracks. It has been modified to accept pulse signals that are recorded once and reproduced many times.

The drum is 8 inches in diameter and rotates 4 revolutions/sec, giving a linear speed of 100 inches/sec at the rim of the drum. The record and reproduce heads are located a nominal 0.001 inch from the surface of the drum. For an input signal of constant amplitude, the recording current is constant to about 1 kcps and gradually increases to a maximum of pre-emphasis of 7 db at 10 kcps. The reproduce amplifiers have several filters that can be switched to give the frequency

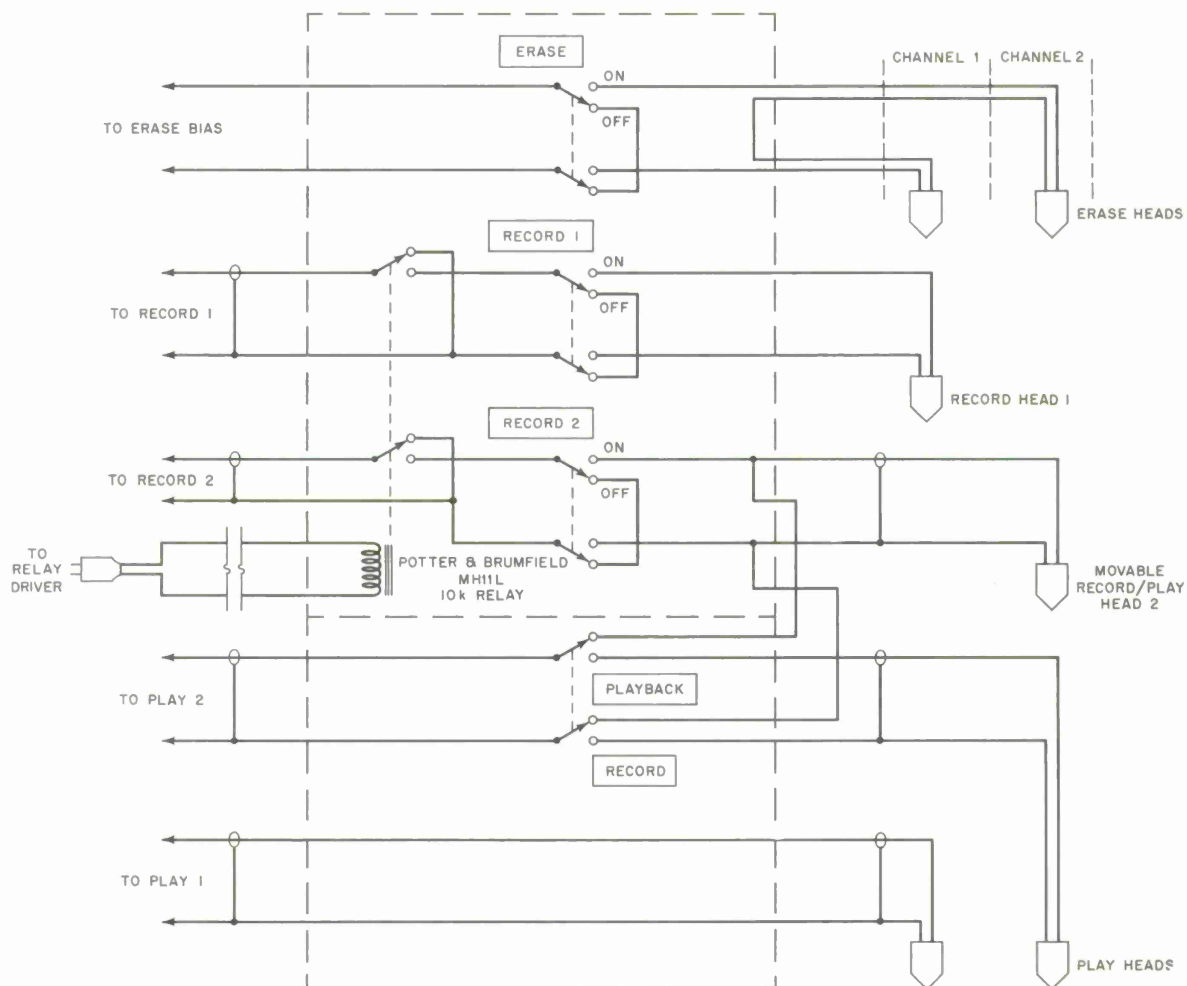
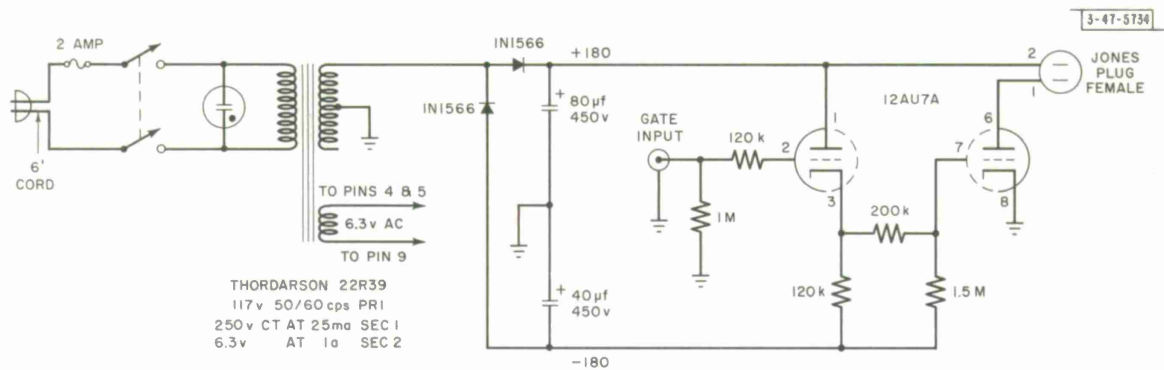


Fig. 20. Relay driver and head switching.

characteristics that are shown in Fig. 22. For the work with the bat signals, position three was normally used on the reproduce amplifiers to help eliminate the small amount of 60-cps hum that is introduced by the drum delay unit.

The drum surface is magnetically very smooth and there do not seem to be any dropouts in signals that are recorded on the drum. Because of a very slight eccentricity in the bearings that hold the movable head, the drum output varies as a function of the position of the movable head. The gains of the drum amplifiers are not stabilized so a slow variation in the output of the drum is also encountered. The addition of attenuators on the output of the reproduce electronics helps to compensate for these variations. After the pulse signals are recorded on the drum, these attenuators are set so that the output is within 0.2 db of the nominal output, 3 volts peak to peak.

A small amount of noise is introduced into the system by a permanently recorded signal on the drum. This signal is probably due to variations in the magnetization of the magnetic layer in the vicinity of the recorded track that is too far out to be erased by the erase head. Goff mentions in his instruction manual (see Ref. 17, p. 41) that such a problem exists with this equipment and says that this signal can be erased with a hand-held erase head, an oscillator, and a power amplifier. Since this signal is about 40 db below the level of the recorded signal, the process of hand erasing was not deemed necessary.

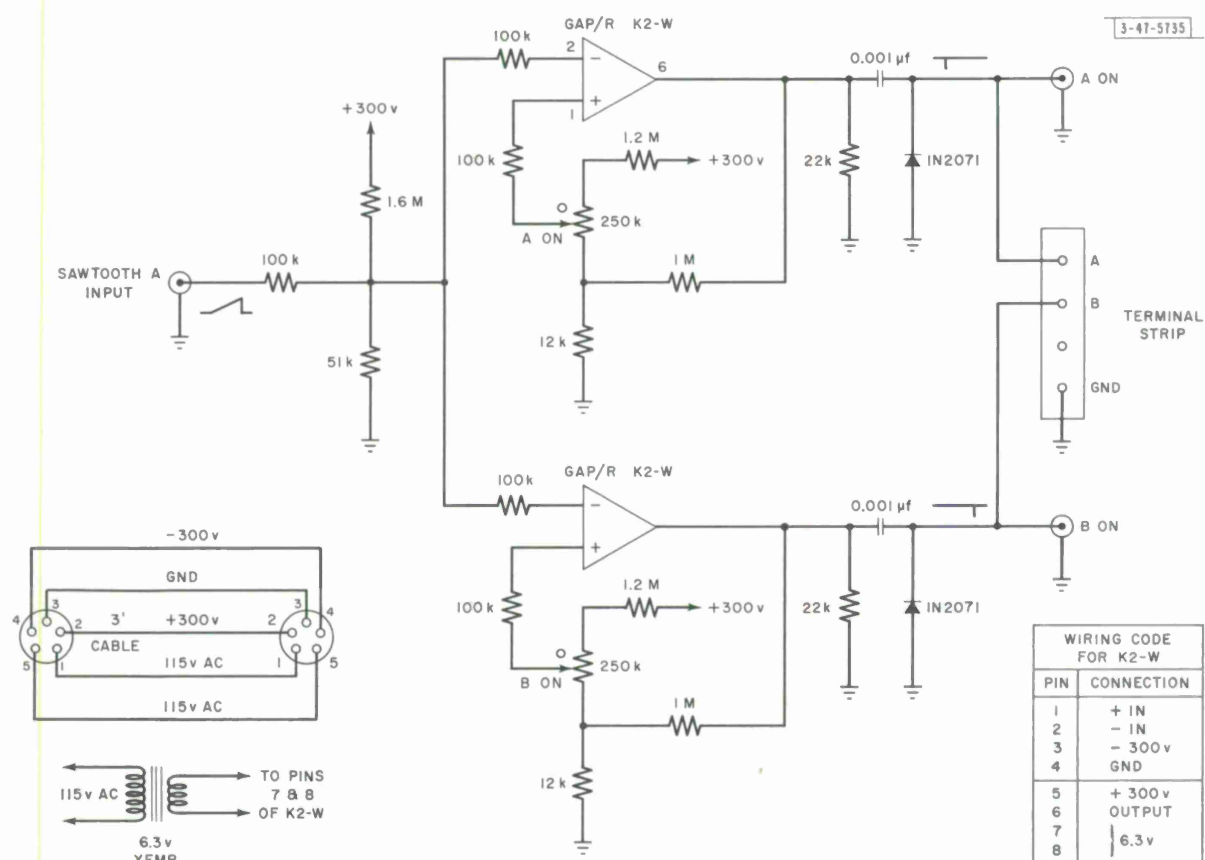


Fig. 21. Trigger pickoff circuit.

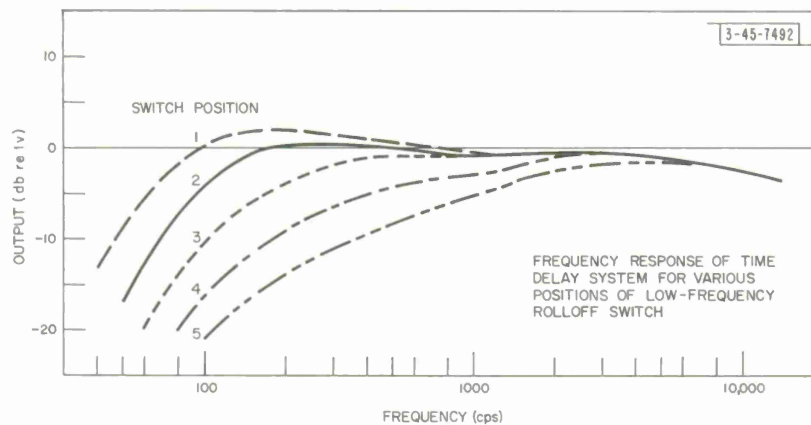


Fig. 22. Goff time delay drum: frequency response for various positions of low-frequency rolloff switch. (Reproduced from Goff's "Instruction Manual for Analog Correlator," 1954, with permission from John A. Kessler, former Executive Officer of the M.I.T. Acoustics Laboratory.)

The drum unit has a mechanical filter to help reduce flutter in the reproduced signal. The flutter of the unit is below 0.02 percent. The drum is driven by a synchronous motor that is, in turn, driven by a precision-fork frequency standard through a power amplifier.

The movable head can be moved manually or driven at various rates by a synchronous motor-and-gear arrangement. The head has access to 205 msec of the 250-msec-long surface of the drum. There is a mechanical revolution counter on a shaft that is geared to the head drive shaft. This counter displays the drum delay in tenths of a millisecond. Since the signals are put on at random, this counter can indicate only a relative position of the movable head.

A potentiometer with a slip-clutch drive was added to the drum delay unit to give an electrical output that is proportional to the position of the movable head. Figure 23 shows how the ten-turn potentiometer is mounted on the drum. The potentiometer shaft is gear-driven from the motor that drives the movable head. A pair of gears can be changed to give various ratios between the drum delay time and the potentiometer rotation, as shown in Table II. The electrical circuitry and the performance characteristics of the potentiometer position indication are discussed in Sec. 4.3.4.

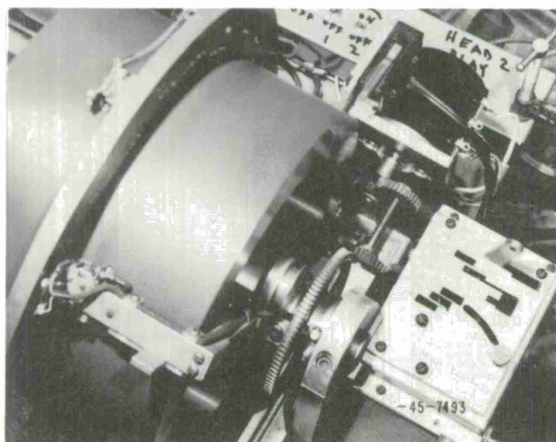


Fig. 23. Mounting of ten-turn helipot that is used to drive X-axis of X-Y recorder.

TABLE II		
DRUM DELAY TIME/POTENTIOMETER-ROTATION CALIBRATION		
Gear Ratio Motor Gear/Potentiometer Gear		Calibration Drum Delay Time/Potentiometer Rotation (msec/revolution)
1:4		0.625
1:2		1.25
1:1		2.5
2:1		5.0
4:1		10.0

### 4.3 REPRODUCE ELECTRONICS

#### 4.3.1 Outline and Block Diagram

Once the signal is on the magnetic drum, the problem becomes that of multiplying and integrating the function given by Eq. (2-27):

$$\chi(\tau, \alpha) = \int u(t) u[\alpha(t - \tau)] \sqrt{\alpha} dt \quad [(2-27)]$$

After taking care of the time delay and the Doppler shift, the only operations left to perform are the multiplication and the integration. Multiplication by  $\sqrt{\alpha}$  is omitted, since the error introduced by omitting this multiplication is less than 3 percent. A block diagram of the reproduce electronics is given in Fig. 24. The multiplication operation is performed with a tube-characteristic quarter-square multiplier. The product signal is gated and then integrated by

3-45-7494

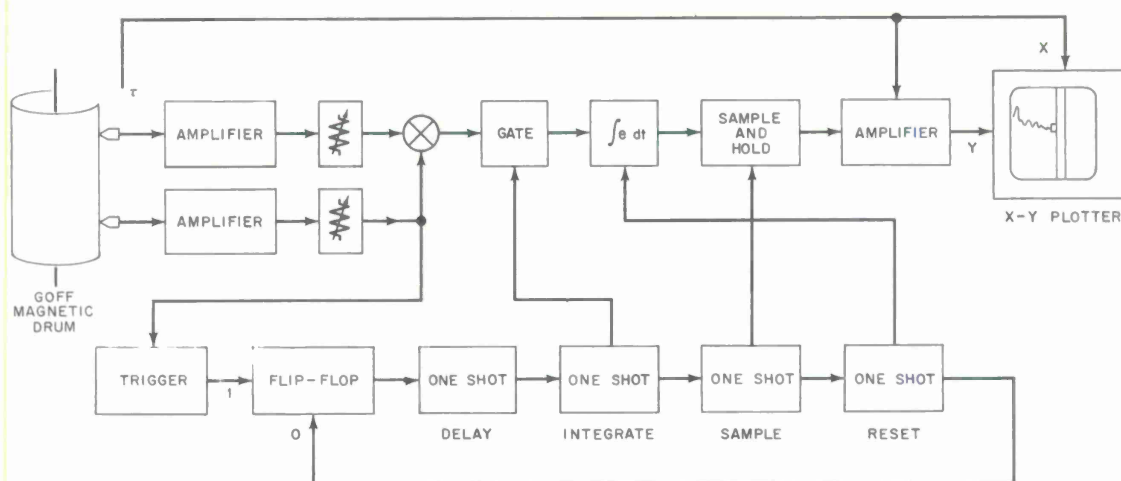


Fig. 24. Electronics used for multiplication and integration of signals on magnetic drum.

using relays and Philbrick operational amplifiers. The output of the integrator is sampled at the end of the integration and is electrically held on a capacitor in a sample-and-hold circuit. The output of the sample-and-hold circuit is connected to an amplifier that drives the Y input of an X-Y recorder.

The X drive of the X-Y recorder is driven from either a 12-minute sawtooth generator or from the output of an amplifier connected to the potentiometer that is mounted on the drum delay unit. Since the temporal stability and the linearity of the potentiometer drive are much better than that of the sawtooth generator, the sawtooth generator is no longer used.

When three-dimensional drawings are to be made from the output of the computer, it is desirable to plot the slices of the ambiguity diagram on a 30° angle with respect to the horizontal. This is accomplished by algebraically subtracting  $\tan 30^\circ$  times the X input to the X-Y recorder from the output of the sample-and-hold circuit and applying this to the Y input of the X-Y recorder.

#### 4.3.2 Multiplier

The multiplier is a direct-coupled multiplier that uses the nearly parabolic plate-current-grid-voltage characteristics of back-to-back 6AS6/5725 pentodes with the control and suppressor grids tied together in a quarter-square arrangement. The output of the multiplier is ideally given by

$$xy = \frac{1}{4} [(x + y)^2 - (x - y)^2] \quad . \quad (4-2)$$

The multiplier consists of a pair of difference amplifiers on the two inputs, a resistive summing network, four 6AS6/5725 squaring tubes, and a difference amplifier on the output. All amplifiers are direct coupled, giving the multiplier a DC to better than 100 kcps frequency response. Since the multiplier is written up in some detail in the Master's thesis report,<sup>29</sup> only the changes and the shortcomings will be mentioned here.

A very serious amount of DC drift was encountered in the output of the original multiplier. Therefore, a new power supply was designed and built into the multiplier which made all the power supply voltages dependent on one accurate gas-tube standard. This modification decreased the DC drift by about a factor of two, not nearly enough. It was found that a variation in the voltage of the power line caused a sizeable change in the output level. This effect is probably due to the fact that the heaters in the tubes are not run from a regulated supply. With the addition of a Sola constant-voltage transformer on the power input of the multiplier, thus regulating the heaters, the output drift due to changes in the line voltage decreased by more than an order of magnitude.

Normally the multiplier operates with 1-volt rms signals on the input. The output for this input, with different frequency sine waves on the two inputs, is about 2 volts rms. After the above changes were made to the multiplier, the output drift was on the order of 0.01 volt.

The resistors in the voltage dividers that feed the output difference amplifier change value slightly with a change in temperature. Blowing cold air on one of these resistors changes the output level by about 0.1 volt. Wire-wound, deposited film, and common carbon resistors were tried in this location without causing a significant change in the amount of drift. Since the resistors are one-watt resistors with only 1/8 watt of power dissipated, it did not seem that an increase in the wattage would give a substantial decrease in the amount of drift encountered.

Since the 0.01-volt drift is still greater than the resolution capabilities of the output recorder, a circuit for effectively resetting the output level of the multiplier, before multiplication

of each pulse, was devised. This system ties the two inputs of the integrator circuit together before the pulse comes through the multiplier. The integral is then the integral of the difference between the multiplier outputs with the pulse on the inputs and with zero on the inputs. This system satisfactorily solves the DC drift problem and is described in more detail in Sec. 4.3.3.

#### 4.3.3 Pulse Integration and Control Circuits

Gating, integration, and sampling are done with Philbrick K-2W operational amplifiers controlled by relays. The problem is one of integrating a portion of the signal from the multiplier, holding the value of the integral for display, and resetting the integrator to prepare for the next pulse from the multiplier.

The product signal from the multiplier is amplified by a factor of ten before gating operations take place so that its amplitude is in the optimum range for the operational amplifiers. This is done with suitable feedback to give the gain of minus ten. Before the arrival of the product pulse, the plus and minus inputs to the integrator are tied together. Just before the pulse arrives, the positive input to the integrator is disconnected from the output of the amplifier. There is a 1- $\mu$ f capacitor holding the potential on the positive input of the integrator. When the pulse signal arrives, the difference between the signal and the potential stored on the capacitor is integrated. Since the capacitor was set when the multiplier was multiplying zero by zero, the output of the integrator is the integral of the difference between the product signal from the multiplier and the zero level of the product signal.

After integration, the output of the integrator is sampled by the sample-and-hold circuit. This sample-and-hold circuit is similar to the one described by Brubaker.<sup>28</sup> It consists of an operational amplifier with feedback for a gain of plus one followed by an integrator, connected through a sampling switch, with over-all feedback on the circuit to give a gain of minus one when the sampling switch is closed. At the end of the integration by the integrator circuit, the sampling relay is closed for about 10 msec. The contacts on the sampling relay bounce for about 2 msec after they first close. The output of the sampling circuit rises (or falls) in a linear fashion, while the contacts are closed, until it is within about 2 volts of the negative of the input voltage. The output then exponentially approaches the negative of the input voltage with approximately a 0.25-msec time constant.

When the echolocation pulse is recorded on the magnetic drum, the record head current is switched on and then off. This switching of the head current causes two large pulses to be recorded on the magnetic drum. One of these pulses is used to trigger a string of one-shot multivibrators that control the timing of relay operations in the pulse integrator. The signal from channel one of the magnetic drum is fed into a Schmidt trigger circuit that shapes this trigger pulse. This shaped trigger pulse sets a flip-flop which, in turn, triggers the delay one-shot multivibrator. The timing of the operations of this circuit is shown in Fig. 25. When the delay one-shot turns off, the integrate one-shot is triggered, operating the integrate relay which disconnects the positive input of the integrator from the output of the gain-of-ten amplifier. The integrator circuit is now integrating the output of the multiplier. When the integrate one-shot turns off, the sample one-shot is triggered, the sample relay closes, and the integrate relay opens. The capacitor in the sample-and-hold circuit is charged to the proper value and then, after 10 msec, the sample one-shot turns off. The reset one-shot is triggered and the sample relay drops out; then the reset relay closes, discharging the integration capacitor in the integrator, and remains closed until the reset one-shot turns off. When the reset one-shot turns on,

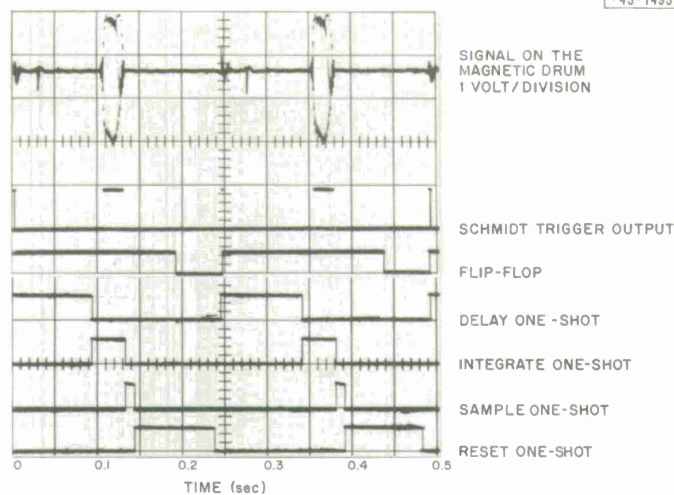


Fig. 25. Timing of the sequence of operations performed by the pulse integrator timing circuitry.

the flip-flop is reset. Until this flip-flop is reset and the reset one-shot turns off, the delay one-shot cannot be triggered. This prevents the echolocation signal from triggering the string of one-shot multivibrators.

Therefore, one trigger signal is propagated down the string of one-shot multivibrators and then returns to enable the flip-flop. If, while setting the delays of the one-shot multivibrators, the trigger signal is lost (this can and does happen under certain circumstances when the one-shot capacitors are being switched), the flip-flop can be reset manually by pressing the reset push button.

#### 4.3.4 X-Y Plotter Output and Associated Electronics

A Variplotter, Model 1100E, X-Y pen-and-ink recorder is used to plot the output of the pulsed integrator as a function of the delay time. Since the movable head on the delay drum can be driven at a constant rate by a synchronous motor, it was decided that the easiest way to drive the X input of the X-Y recorder was from a sawtooth generator that could be started at the same time that the synchronous motor was started. A 12-minute sawtooth generator was designed and constructed. This generator uses a 100-megohm resistor and five 1- $\mu$ f capacitors in an integrator circuit. The integrator is a standard integrator built around a Philbrick K-2W operational amplifier. A relay is used to reset the sawtooth generator by shorting out the integrating capacitor. The output sawtooth sweeps from -40 volts up to +35 volts. This is enough to give the required 15 inches of deflection on the recorder when the recorder sensitivity is set at 5 volts/inch.

After a considerable amount of computer operation, it was decided that the 12-minute sawtooth generator could stand some improvement. Although this generator was accurate to better than one percent, it had the wrong type of accuracy. Since a plot is made from a minus time delay through zero up to a plus time delay, even though the minus time delay is set exactly, the position of the zero might vary back and forth 1 percent of the full-scale time delay. If errors are to be introduced, it is much better that they are introduced at the two extremes of the time delay rather than have the zero displaced.

A method of marking the zero of the graph was used. When a monitor oscilloscope registered that the zero point had been reached, a button was pressed, causing a 1/2- to 1-inch jump in the pen position. The accuracy of pressing the button at the point of zero time delay was approximately 1/4 to 1/2 sec, corresponding to 0.005 to 0.010 inch on the output graph. The only trouble encountered in pressing the button was caused by the fact that the button was pressed 6 minutes after the start of the plotting, halfway through the 12-minute plot. Operator fatigue caused the marking point to be missed several times. A photographic timer was used very successfully in alerting the operator. This eliminated the marking being missed due to operator fatigue.

Another solution of the problem of marking the zero point is to use a potentiometer to obtain the X deflection of the X-Y recorder.

The potentiometer is mounted on the drum unit, gear driven from a shaft that is driven by the synchronous motor that drives the movable head. A mechanical description of the mounting and gearing of this potentiometer is given in Sec. 4.2.4. The resistors in parallel with the potentiometer that go to ground help to reduce the effect of possible power supply variations on the nulled output of the potentiometer. This circuit keeps the zero of the delay scale of the output within an ink-line width, 0.02 inch, of the correct position, which is more than an order of magnitude better than the sawtooth generator. Not only does the potentiometer drive improve the accuracy of the location of the zero position of the graph, but it also improves the linearity of the sweep and the temporal stability of the delay scale calibration. The linearity of the sawtooth generator and of the potentiometer circuit is illustrated in Fig. 26(a-b). The error from linearity is given as a function of the desired X position of the pen on the X-Y recorder. This error from linearity is plotted for four consecutive sweeps by each sweep system. It may be readily observed that use of the potentiometer circuit has greatly improved the temporal stability.

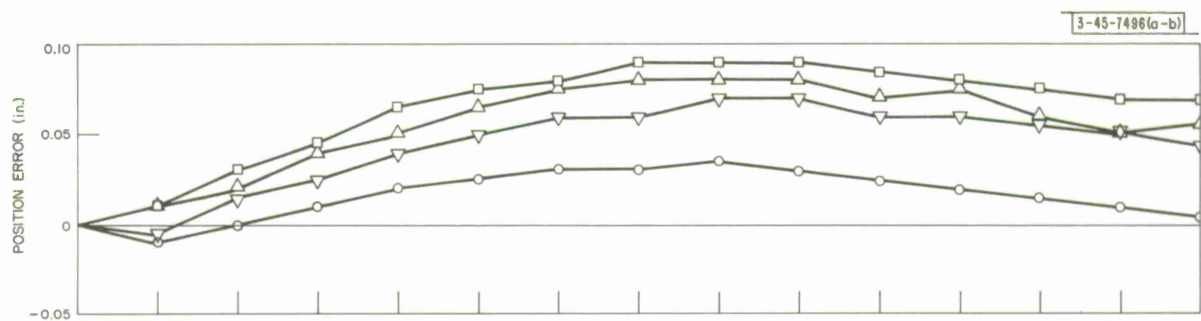
When a three-dimensional drawing is to be made from the computer output, it is desirable to plot the slices of the ambiguity surface on a slant. A typical slice is shown in Fig. 27. A trimetric representation was chosen where one axis is plotted on a 30° slope with respect to the horizontal and the other axis is plotted on a 10° slope with respect to the horizontal. These slices are easily obtained by simply subtracting  $\tan 30^\circ$  times the X deflection of the recorder from the Y deflection of the recorder. The circuit that does this is included on the X-Y recorder-drive chassis. The signal from the sample-and-hold circuit is the negative of the cross-correlation function, so that when the X deflection signal is added to it at the summing point of the operational amplifier with the appropriate multiplicative constant, the output of the operational amplifier is equal to the cross-correlation function minus  $\tan 30^\circ$  times the X deflection. An attenuator is inserted between the sample-and-hold circuit and the summing operational amplifier to adjust the gain of the system so that the maximum amplitude of the autocorrelation function can be normalized to one.

#### 4.4 ERRORS AND LIMITATIONS IN THE ACCURACY OF THE AMBIGUITY DIAGRAM COMPUTER

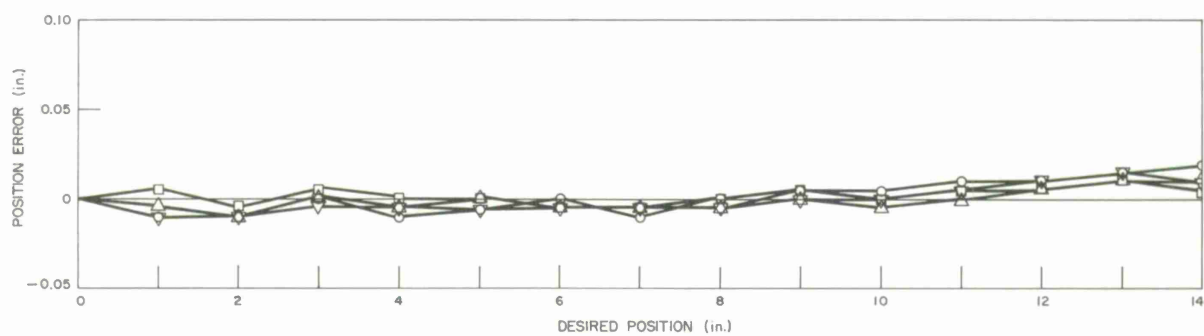
This section pertains to an investigation of the errors introduced by the ambiguity diagram computer. Each significant error is discussed in an attempt to place some meaningful bounds on the accuracy of the computer output.

##### 4.4.1 Function Error

An error in the functions  $u(t)$  and  $u(\alpha(t - \tau))$  can be introduced in several places. The process of recording the bat signal onto tape is probably the place where the largest amount of error



(a) 12-minute sawtooth generator.



(b) Potentiometer drive.

Fig. 26. Linearity of sweep output.

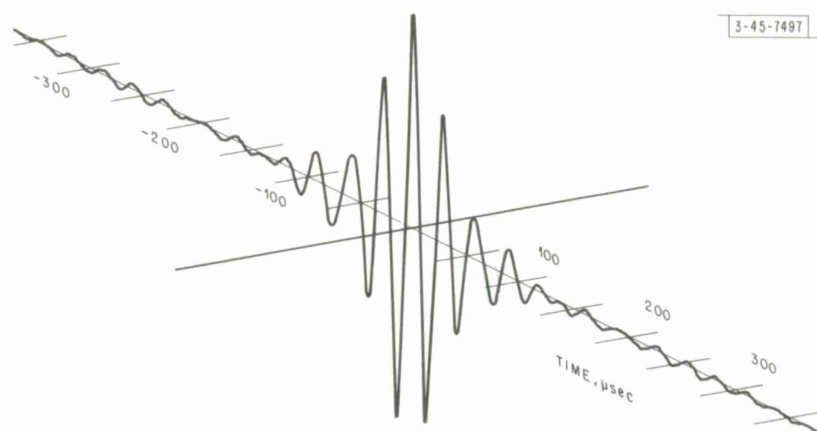


Fig. 27. Slice of typical ambiguity surface plotted on  $30^\circ$  slope for use in making trimetric representation of surface (bat pulse 4,  $\alpha = 1$ ).

is introduced. The microphones that are used to pick up the bat signal are not perfect and have a frequency-dependent gain pattern. Echoes from the surroundings and noise from the microphone amplifiers add a level of hash to the signals. It is difficult to estimate in some cases which is the white noise introduced by the microphone amplifiers and which is the noise introduced by room echoes. This hash level can be as low as -35 db, and is usually not higher than -20 db. The signal that is recorded on the magnetic tape will therefore be assumed to be the signal for which the ambiguity diagram is to be calculated.

When the tape is played, a variation in the amplitude of the signal might occur. With the Ampex 601-2 tape recorder, using type  $\frac{1}{4}$ -200-24 Minnesota Mining and Manufacturing magnetic tape, the amplitude variation appeared to be less than 1 percent.

When the signal is put onto the magnetic drum, the drum noise is added to the signal. The level of the noise on the magnetic drum is about 40 db below the level of the recorded signal. This corresponds to a signal error of 1 percent.

#### 4.4.2 Multiplier Error

The error introduced by the multiplier is probably the most difficult to estimate. There can be several types of errors introduced by the multiplier. Most of these do not affect the results of the correlation integral. If, for example, there is a drift in the DC balance of the input difference amplifiers, the output of the multiplier would be given by

$$e_o = (e_1 + a)(e_2 + b) \quad (4-3)$$

where  $e_1$  and  $e_2$  are the input voltages to the multiplier and  $a$  and  $b$  are the unbalance levels. Equation (4-3) can be rewritten as

$$e_o = e_1 e_2 + b e_1 + a e_2 + ab \quad (4-4)$$

The last term of this equation does not affect the output since this corresponds to a steady DC level on the output of the multiplier. This steady level is canceled out by the pulsed integrator circuit described in Sec. 4.3.3. The two middle terms in Eq. (4-4) do not affect the output of the integrator, since neither the  $e_1$  nor the  $e_2$  signal has any DC component in its energy density spectrum.

With two sine waves on the input to an ideal multiplier, the output contains only the sum and difference frequencies. With the multiplier used for these experiments, the output contains not only the sum and difference frequencies, but also components of the two input frequencies and cross-modulation terms between the output and the sum frequencies. The level of these spurious modulation products was usually at least 20 db below the level of the sum and difference frequency components.

Since the only term that appears on the output of the integrator is the zero frequency component, the testing of the multiplier accuracy is done only on the difference component of the output. A block diagram of the testing arrangement is shown in Fig. 28. Two oscillators feed the two inputs of the multiplier through attenuators. The output of the multiplier is low-passed and its level is measured with a true-rms voltmeter. The reading on the voltmeter is plotted as a function of the signal level on the X input to the multiplier for three different Y input levels and is shown in Fig. 29. The maximum deviation from the correct output for a 50-db operating range is less than 0.5 db. This corresponds to an error of less than 0.4 percent.

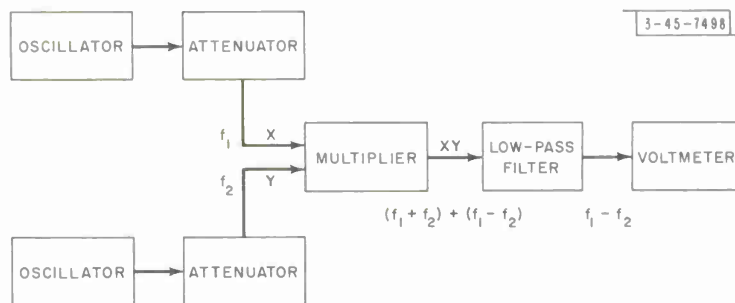


Fig. 28. Setup used to test accuracy of multiplier.

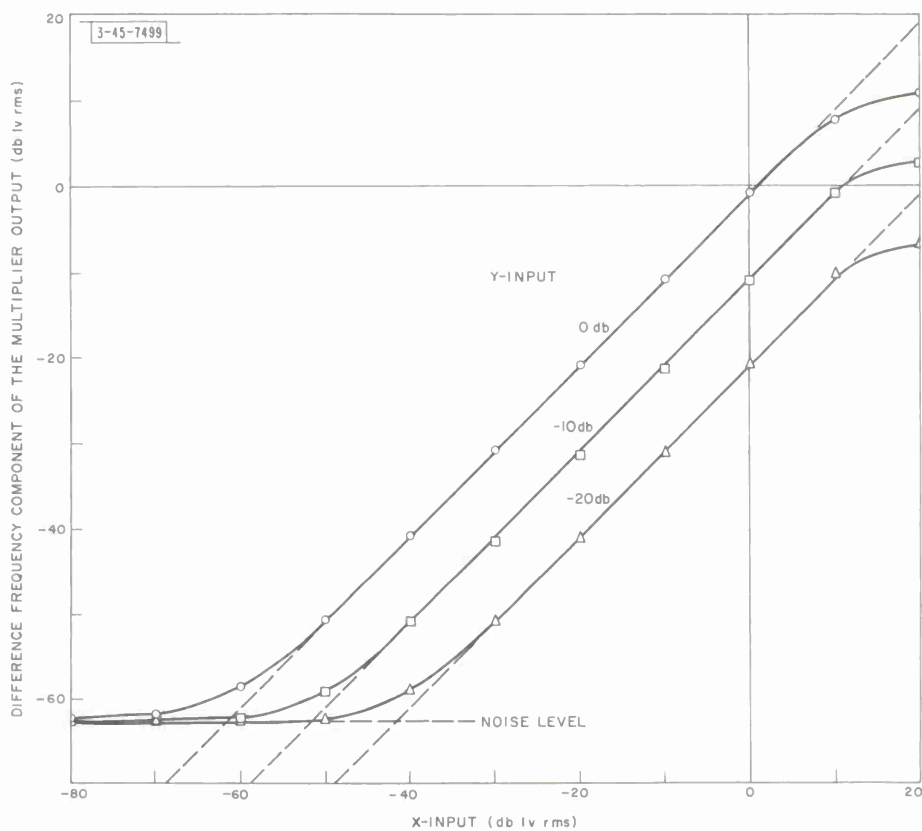


Fig. 29. Multiplier accuracy test. Three straight lines indicate correct output for multiplier; circles show actual output of multiplier.

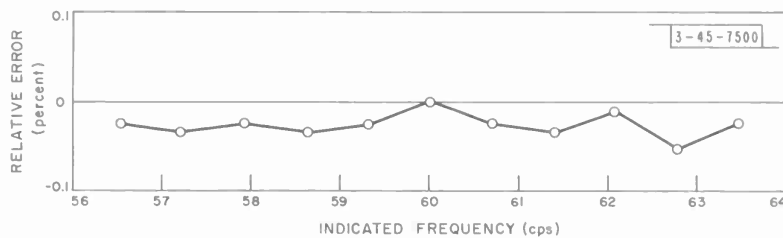


Fig. 30. Error in frequency of Doppler shift oscillator, normalized relative to frequency at setting of 60 cps.

#### 4.4.3 Doppler Error

The error in the accuracy of the Doppler shift puts a serious limitation on the accuracy of the ambiguity diagrams. The largest Doppler shift that was plotted in this project was 10 m/sec. This corresponds to a Doppler factor of 1.06, or in other words is only a 6-percent change in the frequency of the bat signal. Additional changes in the frequency of the bat signal can be introduced in the following three ways.

- (a) Oscillator Error:- The Doppler shift oscillator that drives the tape reproducer can introduce errors in the Doppler shift of the signal, if it is not operating at the correct frequency. The specifications for the oscillator given by the manufacturer state that the oscillator has an accuracy of 1 percent and a drift of less than 0.05 percent/hr. The absolute accuracy of the oscillator is of no real importance for this work, since it is the relative accuracy of the oscillator that affects the accuracy of the Doppler shift. That is to say, if the oscillator were operating at a frequency 1 percent above the desired frequency for all the oscillator settings, no change in the output of the computer would result. If, however, the oscillator operates at 1 percent above the desired frequency for one setting and at 0.96 percent above the desired frequency for another setting, a 0.04-percent error in the position of the Doppler slice would result.

Figure 30 illustrates the relative amount of error in the oscillator frequency for the various settings of the oscillator. This graph has been normalized in such a way that the error in the oscillator frequency is measured relative to the oscillator frequency that occurs when the oscillator is set on 60 cps. It is obvious from this graph that the relative error in the position of the Doppler slices due to the oscillator is less than 0.05 percent.

- (b) Tape Reproducer Flutter:- The tape reproducer can introduce errors of two types. It can operate at a speed lower or higher than the correct speed or it can actually change speed during the time that the bat signal is being played. The manufacturer specifies that the flutter (error around the operating speed) is less than 0.17 percent. The tape reproducer was analyzed by the method described by Cox<sup>30</sup> and was found to have a peak flutter of 0.36 percent. If flutter components above 10 cps are ignored, the flutter is less than the 0.17 percent that is specified by the manufacturer. The time displacement error accumulated, in the 1/4 sec that it takes the drum to make one revolution, is 0.2 msec. Along with the flutter, the tape reproducer introduces an operating speed error. This error is 0.075 percent.
- (c) Drum Flutter:- According to Goff (see Ref. 15, p. 19), the amount of flutter introduced by the magnetic drum is less than 0.02 percent. This has been measured and confirmed.

The total error in the position of a Doppler slice is the sum of the individual frequency errors divided by the percentage change in frequency that corresponds to the largest Doppler shift. Another way of calculating this is to determine, from the frequency errors, the actual amount of velocity that can be expected. The maximum frequency error due to the flutter of the tape reproducer and the magnetic drum is 0.38 percent. The maximum frequency error due to oscillator drift and the operating speed error of the tape reproducer is 0.125 percent. Adding these two errors, the maximum frequency error is 0.5 percent. If the velocity of sound in air is taken as 346 m/sec, this frequency error corresponds to a target velocity error of 0.9 m/sec. If the ambiguity diagram extends from a target velocity of -10 m/sec to a target velocity of +10 m/sec, the 0.9 m/sec is a position error of the Doppler slice equal to 4.4 percent.

#### 4.4.4 Time Delay Error

The time delay error caused by the potentiometer drive system and the X-Y plotter can be estimated from Fig. 26(b). Since the maximum error indicated is 0.02 inch and the full-scale

TABLE III  
SUMMARY OF THE ERRORS INTRODUCED BY THE AMBIGUITY  
DIAGRAM COMPUTER

Error	Change (percent)	Total Error of Full Scale (percent)
<u>Height</u>		
Function error		4.0
Tape dropout (channel 1)	1.0	
Tape dropout (channel 2)	1.0	
Drum noise (channel 1)	1.0	
Drum noise (channel 2)	1.0	
Multiplier		0.4
Integrator		1.0
Sample and hold		<u>0.00025</u>
		5.4
<u>Time delay</u>		
Potentiometer drive		0.14
Goff drum		0.2
Zero setting		<u>0.2</u>
		0.54
<u>Doppler shift</u>		
Oscillator	0.05	0.43
Tape reproducer		
Flutter	0.36	3.1
Drift	0.075	0.65
Drum flutter	0.02	<u>0.17</u>
		4.4

width of the X-Y plotter is 15 inches, the maximum error in the time delay is estimated at 0.14 percent.

The error in the calibration of the time delay on the Goff drum is given by Goff (see Ref. 15, p. 20) as less than 0.2 percent. The error in setting the zero time delay for the ambiguity diagrams is about 50  $\mu$ sec. The total delay is 24 msec, so the error introduced by setting the zero is about 0.2 percent.

#### 4.4.5 Integrator and Sample-and-Hold Error

The way that the integrator is connected, to cancel out the DC drift of the multiplier, introduces some error in the output. A small amount of 60-cps noise is introduced into the signal by the Goff preamplifiers. This noise is squared by the multiplier and results in a small amount of 120-cps ripple on the output of the multiplier. This 120-cps ripple offsets the zero of the integrator slightly. The amount of error in the output due to this offset is estimated at about 1 percent.

In the sample-and-hold circuit, with the sampling relay open, a slight change in output is encountered as the grid current of the operational amplifier very slowly charges or discharges the sampling capacitor. Since the grid current is on the order of  $10^{-10}$  amp and the holding capacitor is a 0.1- $\mu$ f capacitor, the output voltage changes at a rate of about 1 mv/sec. The output range of the sample-and-hold circuit is  $\pm 50$  volts and the hold time is usually 1/4 sec. This drift rate corresponds to an error in reading of 0.00025 percent, far less than the readability of the computer's output plotter.

#### 4.4.6 Summary of Errors

The errors are grouped into three classes: errors producing changes in the height of the ambiguity diagram, errors producing changes in the position of a point along the time delay axis, and errors producing changes in the position of a particular Doppler shift slice. The errors are summarized in Table III, which lists the maximum errors that occur. Since the contributions to the function error occur on both channels, the individual errors are counted twice. The total estimated error in the height of the ambiguity diagram is 5.4 percent of the maximum value; the total error in the time delay is 0.54 percent of the full-scale value; the total error in the position of a particular Doppler shift slice is 4.4 percent of the full-scale value.

## 5. AMBIGUITY DIAGRAMS OF BAT SIGNALS

### 5.1 INTRODUCTION

Signals of two species of vespertilionid bats, Myotis lucifugus and Lasiurus borealis, were obtained while they were in pursuit of thrown targets. The signals of the Myotis were obtained in the laboratory of F. A. Webster; the signals of the Lasiurus were obtained in the field. The Myotis was an animal that had been in captivity for several months and had been trained to catch mealworms thrown into the air. He was very expert at catching the mealworms and missed less than 10 percent of the mealworms thrown. The Lasiurus was an animal that had been trained by Dr. A. E. Treat and his family to come close to their house to receive moths that were thrown into the bat's approximate path. Since some of the moths are able to detect the ultrasonic cries of the bats and subsequently to avoid the bat,<sup>12</sup> the Lasiurus had a much more difficult pursuit problem than the Myotis. The Lasiurus, however, was still able to catch more than 50 percent of the moths that were thrown to him.

In connection with certain research projects, attempts were being made to obtain photographs of the bats in the act of pursuing and catching targets. In early attempts, a room was flooded with fruit flies and bats were allowed to fly about and catch as many flies as they could. Since a bat is small and travels at a comparatively high speed, most of the pictures that were obtained were either blank (the bat was out of the field) or were out of focus. Even when a sharp photograph of the bat was obtained, the bat was most likely just flying around and was nowhere near a fruit fly. Because of the limitations imposed by the size of the photographic field and the depth of field of photographic equipment, drastic measures had to be taken to obtain any pictures of bats in the act of catching targets.

Since the bat ate mealworms (the larvae of the mealworm beetle) out of a dish to supplement what was caught on the wing, it was decided that an attempt would be made to teach the bat to catch thrown mealworms, which could be more easily controlled than the fruit flies. About one bat in 25 finally learned to catch mealworms that were tossed to him while he was flying. After learning to catch these targets, the bat would assume a regular flight pattern around the area of the room where the mealworms were thrown. Cameras could be set up to photograph the bat since his exact position could be predicted from the trajectory of the thrown mealworm. Finally, a "mealworm mortar" was designed and built which fired a mealworm to an exact location at an exact time. This mortar made possible high-quality photographs of the bats catching targets. Subsequently, high-speed motion pictures with synchronized sound tracks were obtained.<sup>38</sup>

Thrown moths, however, are not as cooperative as thrown mealworms. When the moths are thrown into the air, they try to evade the bat rather than going to the position in the photographic field for which they were intended. This makes photography of bats catching moths very difficult. The bat, however, is still forced to fly into a particular area in order to catch the thrown moth; consequently, it is a simple matter to obtain tape recordings of his ultrasonic cries.

The bat's echolocating cries were picked up with a special ultrasonic microphone that was built by Dr. L. P. Granath of Worcester Polytechnic Institute. The microphone is similar in design to the solid-dielectric condenser microphones described by Kuhl, Schodder, and Schröder.<sup>36</sup> The particular microphones used have a frequency response that extends up to 200 kcps. The signals from the microphone are recorded on a high-speed instrumentation tape recorder (Ampex FR-1100) running at 60 ips. The tape recorder has a frequency response that is fairly flat out to 100 kcps and then drops very rapidly.

Since the microphone that is used is not perfect, it will change the nature of the bat signal slightly. Off the main axis of the microphone, the microphone has zeros in its frequency response. The general response of the microphone is roughly given by

$$S(\omega) = \frac{2J_1(a\omega \sin \Theta)}{a\omega \sin \Theta} \quad (5-1)$$

where  $J_1(x)$  is the first-order Bessel function. Since the position of the bat during pursuit of the target is known, the microphone is aimed in such a way that the bat flies on the axis of the microphone most of the time. This is not too difficult, since the beamwidth of the microphone at the highest frequency that the bat uses is on the order of  $30^\circ$ .

## 5.2 MYOTIS LUCIFUGUS

### 5.2.1 Introduction

The bat Myotis lucifugus is the little brown bat common to the New England area. The full-grown adult has a maximum wing spread of about 10 inches, and weighs between 5 and 12 grams. The bat's diet consists largely of insects that are caught in flight. He has some eyesight but this is barely more than a discrimination between light and no light. If he is placed in a dish containing food, too close for him to make use of his sonar, he moves around in a random fashion until his nose actually bumps into some of the food before he realizes where it is in the dish.

The particular Myotis whose signals appear in this thesis is a bat that was caught in the wild and then trained to catch thrown targets in the laboratory. The laboratory is a quonset hut that was converted by F. A. Webster into a place to study bats. The bat was trained to catch thrown targets by repeatedly throwing mealworms into his flight path. When he had learned that the targets were edible, he learned to fly in a particular flight pattern that brought him over the area of the room where the targets were thrown. He would continue to fly over this area until his food was thrown to him.

One or two microphones, placed in the path of his flight, were used to obtain tape recordings of his sonar signals while he was in pursuit of a target. Figure 31 illustrates the wide variation in the type of signal used in pursuit of his target. It is an oscillographic record made from tape recordings. The upper trace is the sound pressure on one microphone, the lower trace is the sound pressure on a second microphone, simultaneously recorded. The distortions of the amplitude waveform are partially due to the gain pattern of the bat's emitted signal, the gain pattern of the microphones, and inclusion of additive multipath echoes. The position of the bat can be determined relative to the positions of the two microphones by measuring the relative time delay between a particular pulse on the two signal tracks.

Five representative pulses were chosen from this sequence, on the basis of being "typical" and having a high signal-to-noise ratio. These pulses, assigned the numbers 2, 3, 4, 5, and 6, as indicated in Fig. 35, were analyzed in detail by means of the ambiguity diagram computer.

### 5.2.2 Ambiguity Diagrams

The first signal to be analyzed is designated as pulse 2 in Fig. 31. A more detailed photograph of the pulse is shown in Fig. 32 along with a plot of the instantaneous period of the pulse. This "instantaneous period" is the time between positive-going zero crossings of the sound pressure waveform. It can be thought of as the inverse of the instantaneous frequency of the

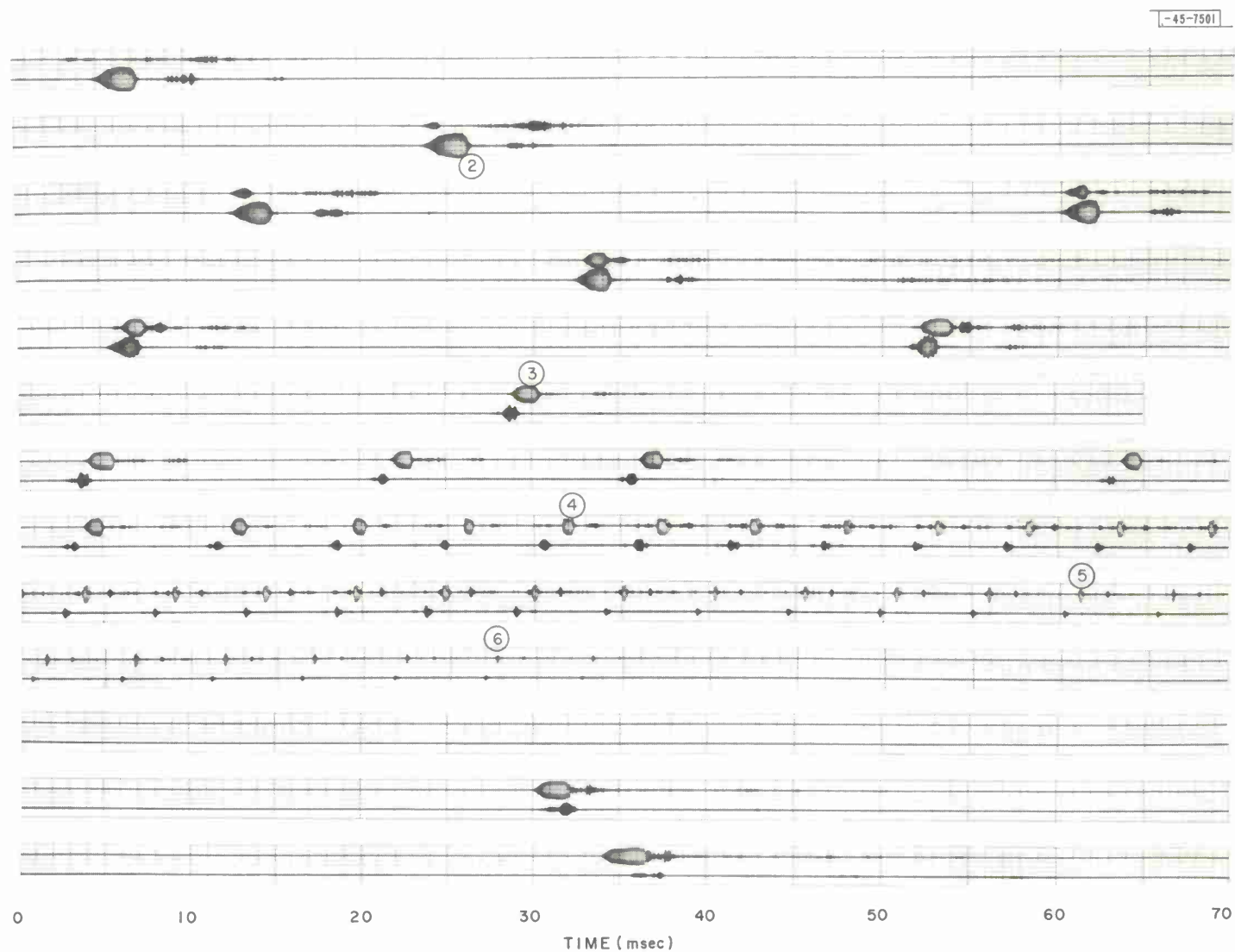


Fig. 31. Sounds emitted by *Myotis lucifugus* while cruising in laboratory room, then in pursuit of target, as picked up by two microphones and recorded on continuous oscillographic record. Vertical lines are time markers, spaced 1 msec apart. Length of each strip is 70 msec, except one that was cut short to avoid splitting pulse.

signal. The snow effect that is seen in this display when a pulse is not present is due to the fact that the period meter is being triggered by noise with random zero crossings.

Pulse 2 is almost sinusoidal with a period that is steadily increasing in a slightly nonlinear fashion. This pulse is designated as a cruising pulse. The bat uses a pulse like this when he is cruising in search of food, but has not yet located any targets. The starting frequency of this pulse is 100 kcps, the final frequency is 40 kcps, and the duration is 3.2 msec.

A three-dimensional drawing of the ambiguity diagram for this pulse is shown in Fig. 33. The width of the area of ambiguity, if the velocity of the target is known to be zero, is about  $85\mu\text{sec}$ . One of the interesting things about this ambiguity diagram is that the fine structure of the ambiguity surface is on approximately the same scale as the coarse structure. If the signal-to-noise ratio were high enough, and the velocity of the target were known, the measurement accuracy of the target range would be limited only by the width, in the time-delay direction, of the central spike of this surface. If the same modulation were used on a much higher frequency carrier, the area of ambiguity would be determined by roughly the upper envelope of this surface of ambiguity. The upper envelope of this surface can be visualized as the surface that would result if a silk scarf were laid over the entire surface. The ratio of the width of the envelope to the width of the central spike for this particular ambiguity diagram is approximately 7:1.

The quantity  $1/\beta$  is equal to  $-5.3\text{ msec}$ . This means that if the acceleration of the target is small, the position that the target had 5.3 msec before the echo hit it is known as accurately as if the target were stationary. This is not quite true, because the signal function exhibits a curious spreading behavior when the target velocity is on the order of 10 m/sec. The 3-db width of the signal function envelope for a target velocity of 10 m/sec is about  $110\mu\text{sec}$ . This width corresponds to a range accuracy of 1.9 cm.

The second signal that is analyzed is shown in Fig. 34 and is designated as pulse 3. The position of this signal in the over-all pulse train can be seen in Fig. 31. This pulse occurs either just before or just after the bat detects the target. Detection of the target is followed by the decrease in the interpulse period that can be seen in Fig. 31 and is plotted in Fig. 35. The interpulse period varies during cruising between 20 and 100 msec. When the target is detected, the interpulse period drops, the duration of the bat's signal decreases, and the rate of change of frequency increases. In this particular plot, the interpulse period is relatively constant and then decreases sharply. The constant interpulse period before detection of the target is not typical of the general case. Usually, the interpulse period varies up and down in a rather irregular fashion until the target is detected; the interpulse period then decreases as is shown in Fig. 35. The jump in the interpulse period just before the long sequence of closely spaced pulses is present in many cases. It has been hypothesized that this is due to the bat's taking in a breath of air so that he can emit the entire sequence of closely spaced pulses with one breath. In this case, the relatively constant amount of interpulse period before detection might be due to the fact that the bat knew that a mealworm was being thrown and was searching a known area for the target.

A three-dimensional drawing of the ambiguity diagram for pulse 3 is shown in Fig. 36. The over-all nature of this surface is very similar to the ambiguity diagram for pulse 2. This is interesting since the shape, the duration, and the frequency modulation of pulse 3 are somewhat different from those of pulse 2. A close examination of the structure of the ambiguity diagram for pulse 3 reveals that the parameters of this surface are different. The width of the  $v = 0$  slice of the surface is  $70\mu\text{sec}$ ; the width of the  $v = 10\text{ m/sec}$  slice is  $100\mu\text{sec}$ ; the quantity  $1/\beta$  is equal to  $-3.5\text{ msec}$ .

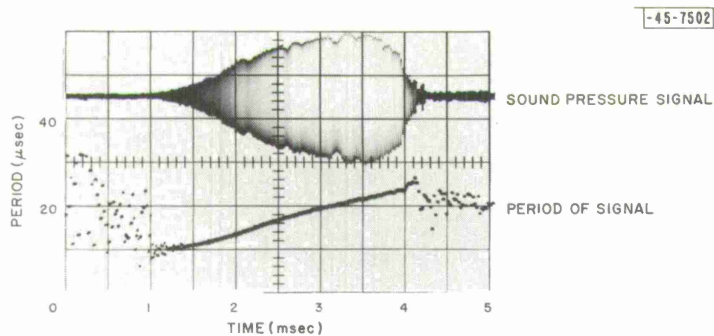


Fig. 32. Myotis lucifugus cruising pulse (pulse 2).

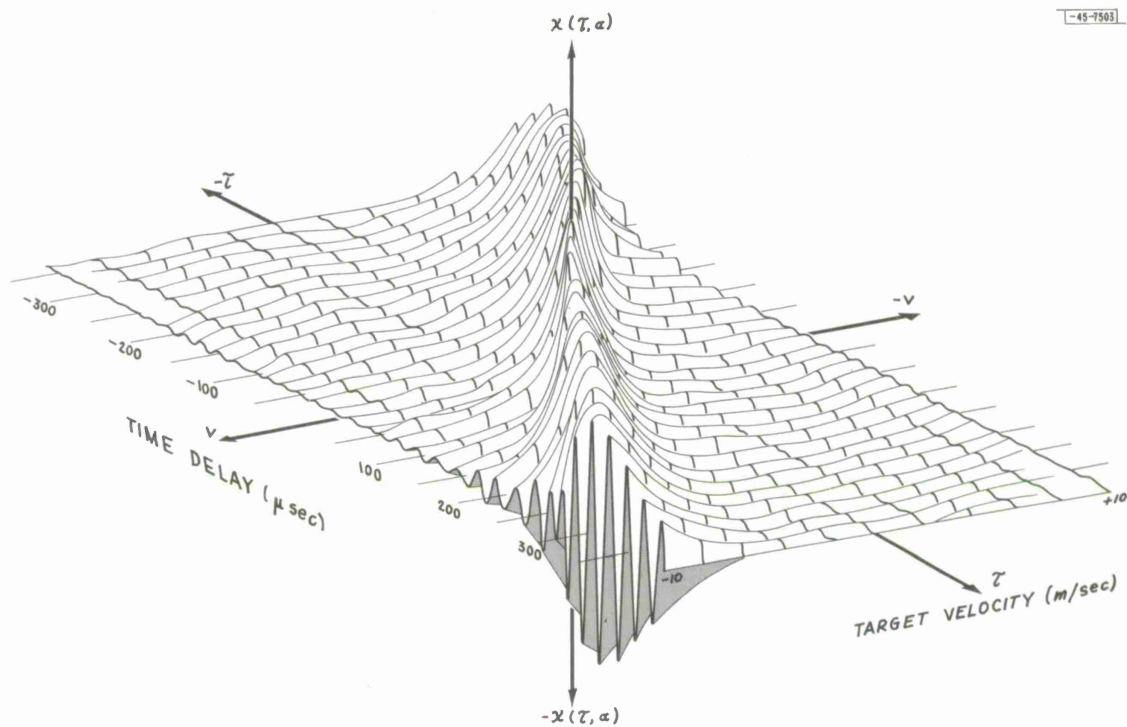
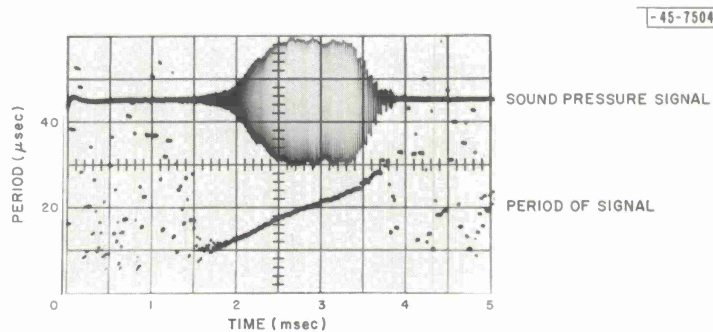


Fig. 33. Cruising-pulse ambiguity diagram for Myotis lucifugus (pulse 2).

Fig. 34. Myotis lucifugus locating pulse (pulse 3).



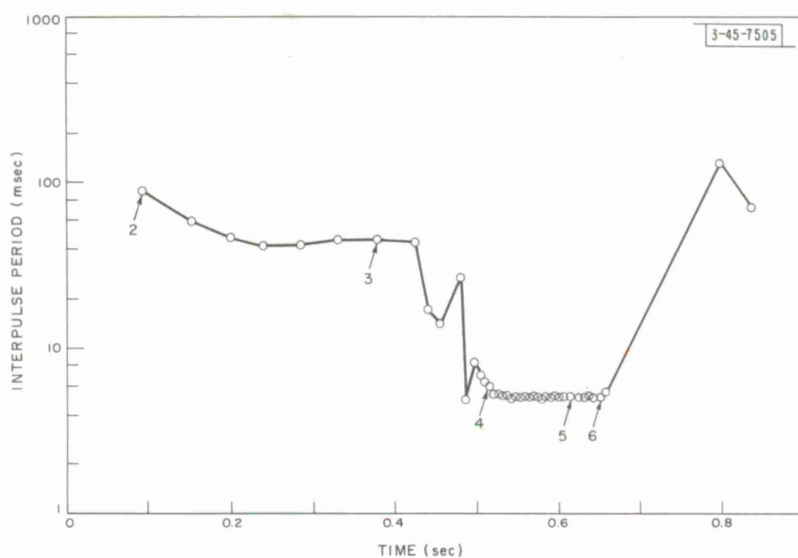


Fig. 35. Time interval between a pulse and preceding pulse for record shown in Fig. 31. Small numbers inside circles correspond to numbers assigned to individual pulses.

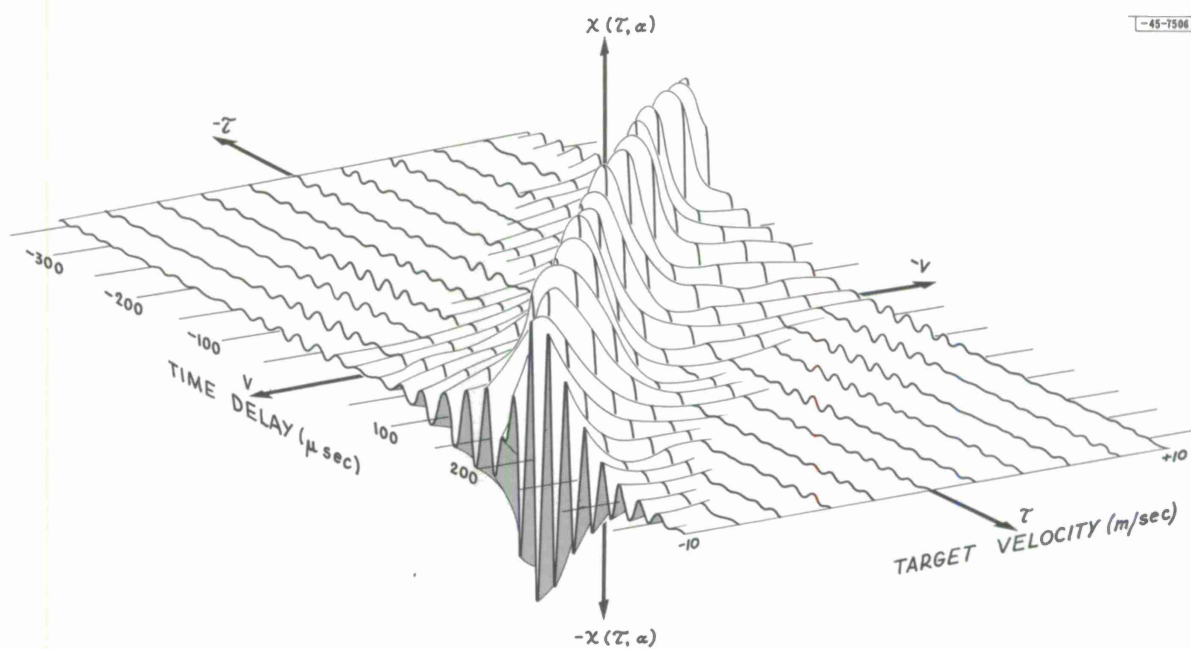


Fig. 36. Locating-pulse ambiguity diagram for *Myotis lucifugus* (pulse 3).

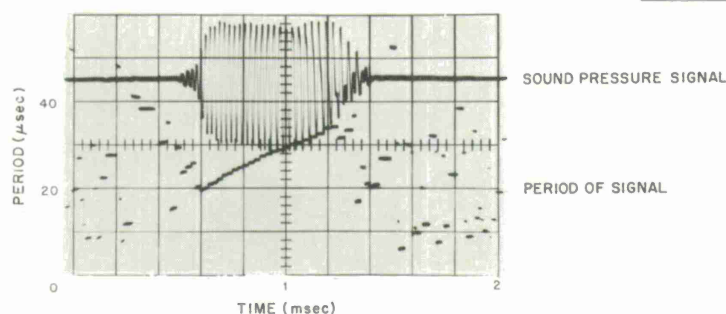


Fig. 37. *Myotis lucifugus* pursuit pulse (pulse 4).

Pulse 4 is emitted after the bat has located the target. A photograph of pulse 4 is shown in Fig. 37. The upper frequency of pulse 4 is about one-half of what it was for pulses 2 and 3, and the duration has decreased from 3.2 msec in pulse 2 and 2.2 msec in pulse 3 to 0.8 msec in pulse 4. A three-dimensional drawing of the ambiguity diagram for pulse 4 is illustrated in Fig. 38. The width of the  $v = 0$  slice of the surface is  $85 \mu\text{sec}$ ; the width of the  $v = 10 \text{ m/sec}$  slice is  $110 \mu\text{sec}$ ; the quantity  $1/\beta$  is equal to  $-1.6 \text{ msec}$ . This ambiguity diagram illustrates the general trend that, as the bat approaches the target, he uses a pulse that gives him a smaller amount of range error for a given velocity error. Although the ambiguity diagram for pulse 2 has nearly 30 maxima (for the amount of diagram illustrated) and the ambiguity diagram for pulse 3 has 15 maxima, the ambiguity diagram for pulse 4 has only 7 maxima.

Pulses 5 and 6 are emitted when the bat is very close to the target. He knows where the target is and is keeping tabs on it to make sure that it doesn't change course. These two pulses are illustrated in Fig. 39(a-b), respectively. The instantaneous frequency of these pulses is no longer defined in the relatively simple way that the instantaneous frequency of the three former pulses has been defined. The signals are no longer sinusoidal in shape, but contain a large amount of second harmonic. If the instantaneous frequency of these signals is defined as the inverse of the time between the zero crossings of the fundamental waveform, upper and lower frequency bounds can be defined. The frequency range for pulse 5 is 40 kcps down to 20 kcps; the duration is 0.4 msec. The frequency range for the fundamental of pulse 6 is 50 kcps down to 17 kcps; the duration is 0.3 msec. Three-dimensional drawings of the ambiguity diagrams for pulses 5 and 6 are illustrated in Fig. 40(a-b), respectively.

The ambiguity diagram of pulse 5 has only 3 maxima. The width of the  $v = 0$  slice of the surface is  $100 \mu\text{sec}$ ; the width of the envelope of the  $v = 10 \text{ m/sec}$  slice of the surface is  $100 \mu\text{sec}$ ; the quantity  $1/\beta$  is equal to  $-0.5 \text{ msec}$ . The ambiguity diagram of pulse 6 has only one maximum. The width of the  $v = 0$  slice of this surface is  $125 \mu\text{sec}$ ; the width of the  $v = 10 \text{ m/sec}$  slice of this surface is  $125 \mu\text{sec}$ ; the quantity  $1/\beta$  is equal to  $-0.4 \text{ msec}$ .

### 5.2.3 Discussion

A summary of the parameters of the pulses and of the ambiguity diagrams is contained in Table IV. It is interesting that the one-Napier width of the envelope of the waveform in the  $v = 0$  slice of the ambiguity diagram remains relatively constant for the various pulses. This means that the amount of resolution that the bat has is relatively independent of the particular signal that he uses, out of the class of signals that are available to him.

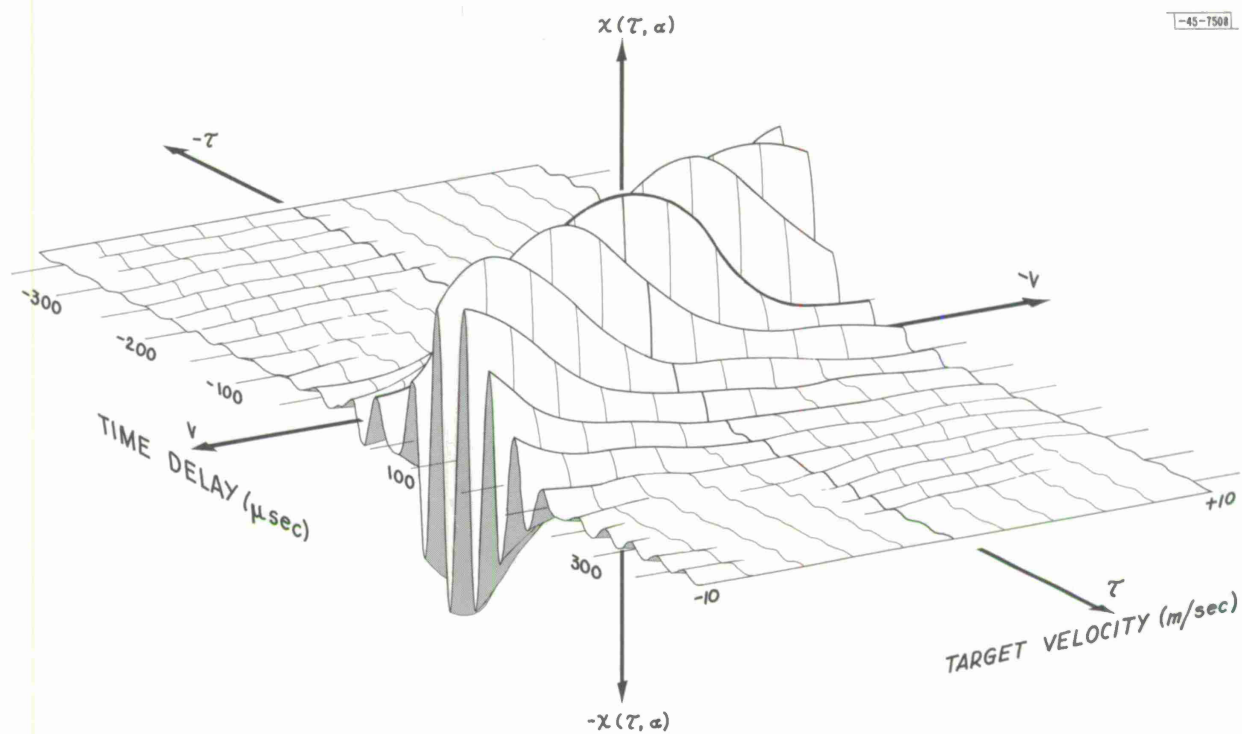


Fig. 38. Pursuit-pulse ambiguity diagram for Myotis lucifugus (pulse 4).

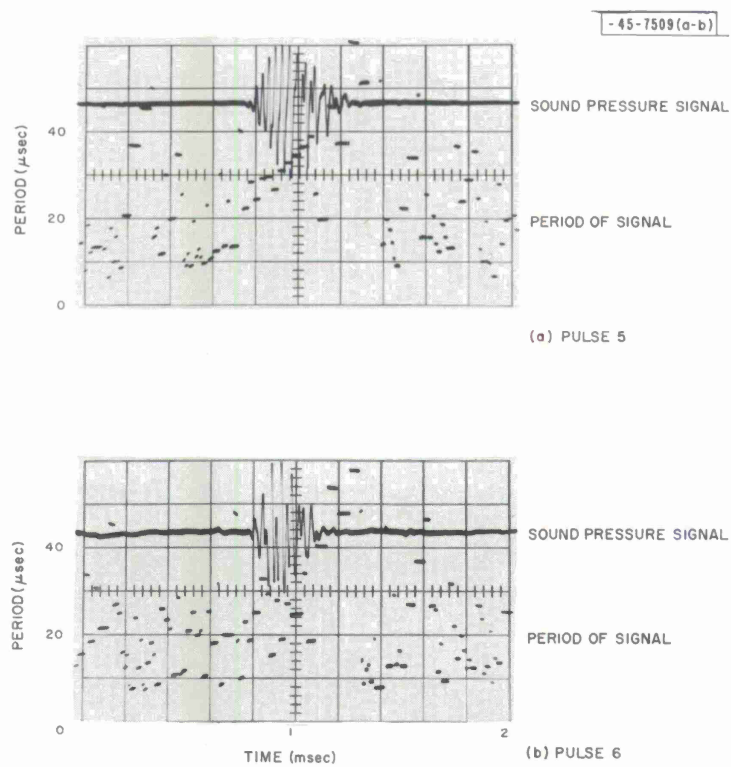


Fig. 39. Myotis lucifugus pursuit pulse.

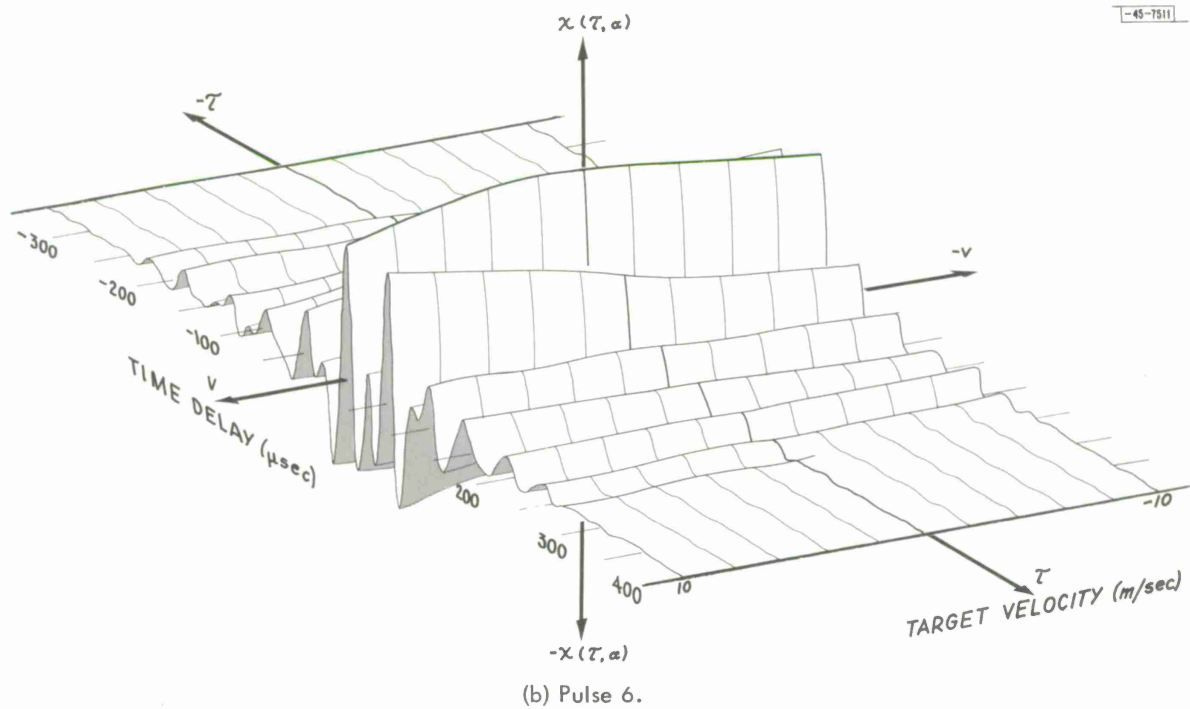
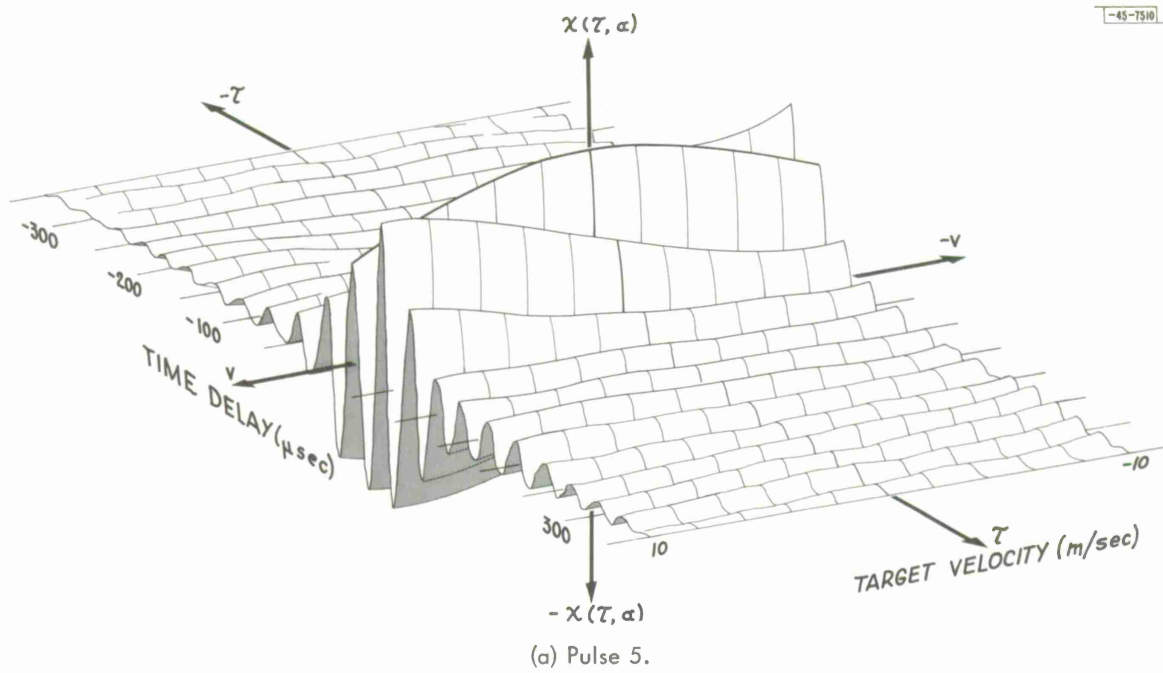


Fig. 40. Pursuit-pulse ambiguity diagram for Myotis lucifugus.

TABLE IV SUMMARY OF THE PARAMETERS OF BAT PULSES AND AMBIGUITY DIAGRAMS							
Pulse Number	BAT PULSE			AMBIGUITY DIAGRAM			
	Duration (msec)	Start f (kcps)	Stop f (kcps)	v = 0 width (μsec)	v = 10 width (μsec)	1/β (msec)	Maxima
<u>Myotis lucifugus</u>							
2	3.2	100	40	85	110	-5.3	30
3	2.2	100	35	70	100	-3.5	15
4	0.8	50	30	85	110	-1.6	7
5	0.4	40	22	100	100	-0.5	3
6	0.3	(50)	(17)	125	125	-0.4	1
<u>Lasiurus borealis</u>							
7	9.6	60	35	380	500	-70	300

Another interesting observation can be made about how the quantity  $1/\beta$  behaves. For the cruising pulse, pulse 2,  $1/\beta$  is equal to -5.3 msec. After the bat detects the target and closes in on it, the magnitude of  $1/\beta$  decreases until  $1/\beta$  is less than -0.5 msec for pulses 5 and 6. The meaning that was associated with the quantity  $1/\beta$  in Sec. 2.3.3 is that this is the time for which the position of the target is determined, relative to the time that the echo bounces off the target.

If it is hypothesized that the magnitude of  $1/\beta$  is equal to the time that it takes for the bat's emitted pulse to travel through the air to the target, it then follows that the time at which the pulse is emitted is the time for which the position of the target is determined. This means that the position of the target, for the time at which the pulse is emitted, is given at the output of the ideal receiver, independent of the velocity of the target.

In order to check this hypothesis, the values given in Table IV for  $1/\beta$  can be examined to determine if they correspond to a reasonable bat-to-target distance. Multiplying the values of  $1/\beta$  by the velocity of sound in air, 346 m/sec, the distance for the cruising pulse is 1.8 m; for the detecting pulse, 1.2 m; and for the last pursuit pulse, it is 0.14 m. These values seem to be a little high, but further work is needed to determine whether or not they are actually inconsistent with the above hypothesis.

Since the power of the echo decreases as the inverse fourth power of the distance from the bat to the target, it seems logical that the bat would be willing to accept some loss in range resolution during cruising in order to be able to use a more powerful signal. Suppose, for example, that the bat can detect a target at a distance of 1 m. If a pulse that has the same energy is used, when he is 0.1 m from the target, the echo energy is  $10^4$  greater!

For the particular pulse train that has been analyzed, the duration of the cruising pulse is more than ten times the duration of the final pursuit pulse and the amplitude of the cruising pulse is about three times the amplitude of the pursuit pulse. Using these figures, the energy contained in the cruising pulse is 100 times the energy contained in the pursuit pulse. This

means that if the bat had a signal-energy-to-noise-power-density ratio of one during cruising, he would have a ratio of  $10^2$  when he is on the final leg of the pursuit. Referring back to the ambiguity diagram for pulse 6, Fig. 40(b), the type of pulse used in the final leg of the pursuit, it can be seen that with this very high signal-to-noise ratio, the position of the target is determined only by the very top of the central spike of this surface. This should lead to extremely good range accuracy.

### 5.3 LASIURUS BOREALIS

#### 5.3.1 Introduction

The bat Lasiurus borealis, commonly known as the red bat, grows to have a wingspread of about 18 inches, and weighs between 10 and 30 grams.

The particular bat whose signals appear in this report was trained by Dr. A. E. Treat and his family to catch moths thrown in the air. The tape recordings were made at Dr. Treat's summer home, at Tyringham, Massachusetts, during an evening when the bat was being thrown moths by several different people.

A microphone was situated in a fixed position near the house, pointing in the general direction of the bat's flight path. The same troubles with signal-to-noise ratio that were encountered with the signals from the Myotis were encountered with the signals from the Lasiurus, with the exception that since the signals were recorded in the free-space outdoors, there were no multipath-echo problems. The signal shown was chosen on the basis of having a good signal-to-noise ratio and is typical of the Lasiurus pulses.

#### 5.3.2 Ambiguity Diagrams

The signal that is analyzed is shown in Fig. 41 and is designated as pulse 7. This is a cruising pulse. That is, it was emitted while the Lasiurus was in search of a target but had not yet detected it. This Lasiurus pulse is very different from any of the Myotis pulses. The

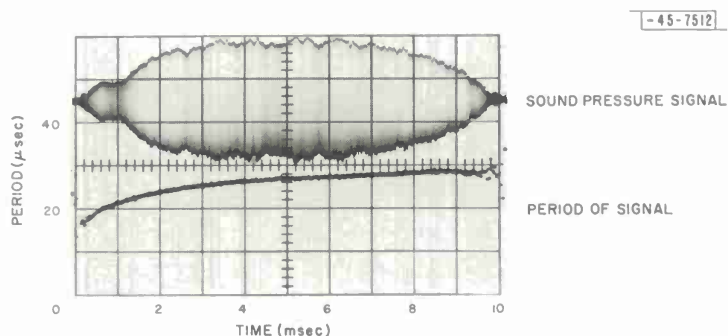


Fig. 41. Lasiurus borealis cruising pulse (pulse 7).

frequency starts at about 60 and sweeps to 35 kcps. The sweep is very nonlinear and exhibits an almost-constant-frequency portion at the end of the pulse. The pulse has an extremely long duration, 9.6 msec, more than twice the duration of the longest Myotis pulse. The autocorrelation function for this signal is shown in Fig. 42. Only half the function is plotted, since the function is symmetrical around  $\tau = 0$ . This autocorrelation function has more than four times the width of the autocorrelation function of the Myotis cruising pulse. The large number of peaks and valleys seem to indicate that this bat cannot make use of the fine structure information

indicated in this autocorrelation function. This is not an exact statement, since, with a high enough signal-to-noise ratio, the position of the target will be determined by the position of the very highest peak of the ambiguity diagram. A drawing of the ambiguity diagram is illustrated in Fig. 43.

Since the fine structure differs so greatly from that of the Myotis slices, a different way of representing the ambiguity diagram for pulse 7 was devised. For the Myotis, the entire ambiguity surface was shown, represented as an opaque surface, with the connections between the individual slices filled in.

For the Lasiurus, however, only the envelopes of the individual slices are represented, with the area inside these envelopes filled in with vertical lines representing the oscillations of the waveforms of the individual slices. The connections between the slices have been omitted because of the difficulty in drawing these lines and because there really isn't enough information to do an intelligent job of filling in the blank volume. Drawn in this way, some of the lower surface is also revealed, and one may observe the shape of the small sections that split off beyond the Doppler-equal-to-zero slice, which would otherwise be hidden by the "mountain range" of peaks.

The distribution of the area of ambiguity is so different from that of the Myotis, that different scales are used on both the time-delay and the Doppler axis of the ambiguity diagram. The relatively restricted range for the Doppler scale,  $-5$  to  $+5$  m/sec, was used because of the time-delay limitations of the ambiguity diagram computer and not because the Lasiurus flies slower or catches slower targets than the Myotis does. On the contrary, the Lasiurus usually flies about twice as fast as the Myotis.

Rather than exhibiting the relatively smooth behavior that the Myotis ambiguity diagrams exhibited, this ambiguity diagram splits into several sections off the Doppler-equal-to-zero slice. This is probably due to the fact that the signal does not have linear frequency modulation but has a very nonlinear type of frequency modulation. The ambiguity diagram consists of the sum of the contributions of the various parts of the signal, as indicated by Eq. (2-27). When the signal is shifted from the  $\tau = 0$  point, each portion of the signal is multiplied by a portion of the signal in its near vicinity. Therefore, the portion of the signal in the near vicinity of any portion is the only part that has a major effect on this portion's contribution to the area of ambiguity.

The width of the zero Doppler slice of this surface is  $380 \mu\text{sec}$ ; the width of the  $-5$ -m/sec slice is  $500 \mu\text{sec}$  (the  $1/e$  width); the quantity  $1/\beta$  is equal to  $70$  msec. The range accuracy corresponding to a time-delay accuracy of  $380 \mu\text{sec}$  is  $6.6$  cm. Since this long pulse is used only for long-range detection, it is not inconsistent that the bat does not have the excellent range measurement accuracy that the Myotis had.

The nature of the Lasiurus pulses changes greatly as the bat closes in on his target. Similar to the Myotis, the Lasiurus shortens his pulses until they are only  $1$  msec in duration when he is in the final leg of his pursuit. The Lasiurus, however, does not decrease the frequency of his signals as the Myotis does. He sweeps over approximately the same frequency range in the shorter length of time. The pursuit signals of the Lasiurus are not included here because ambiguity diagrams have not yet been computed for them.

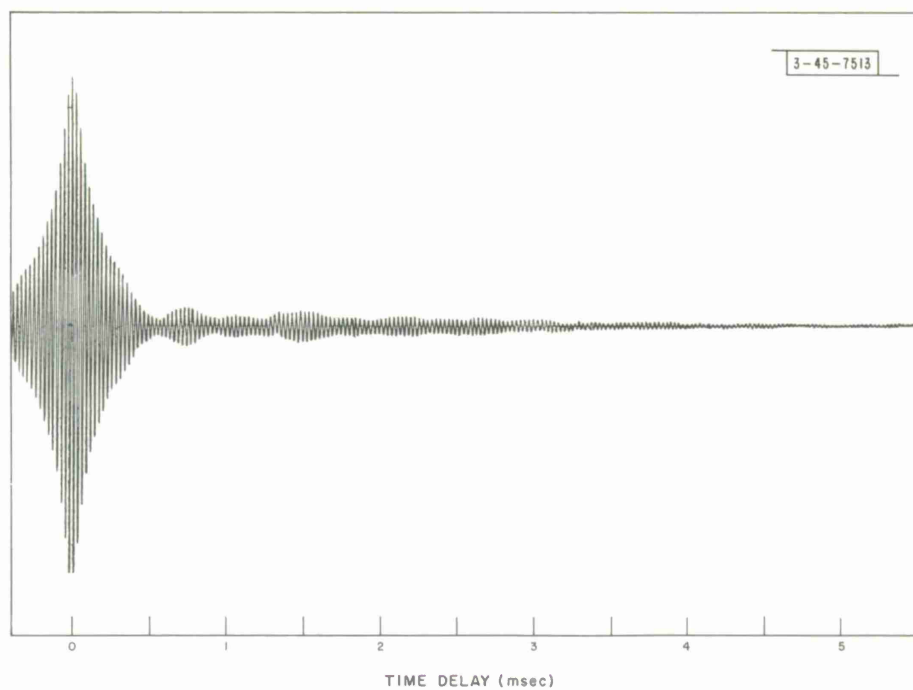


Fig. 42. Cruising-pulse autocorrelation function for Lasiurus borealis (pulse 7).

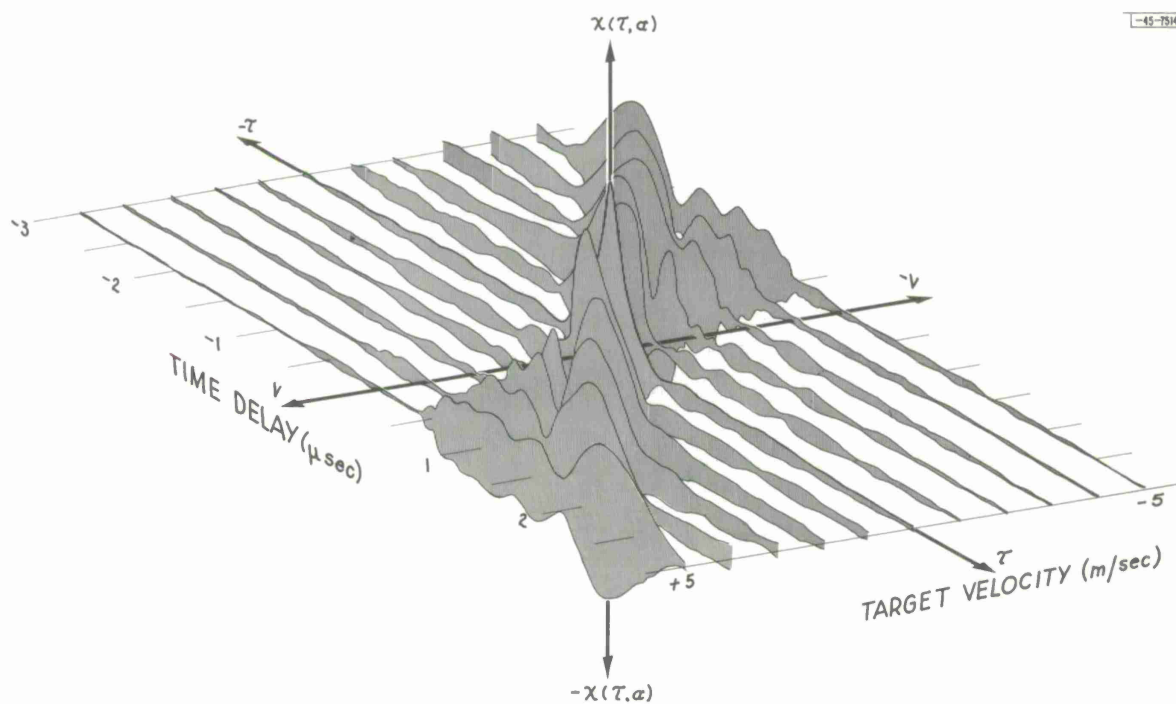


Fig. 43. Slices of cruising-pulse ambiguity diagram for Lasiurus borealis (pulse 7).

## 6. CONCLUSIONS

### 6.1 SUMMARY

It has been the purpose of this study to determine the range and range-rate measurement capabilities of various bat sonar signals. The results indicate that:

- (a) It is possible to derive a wide-band echolocation theory that predicts, on the basis of the a posteriori model, the range and range-rate accuracy of a given signal.
- (b) Accurate angular measurements can be made with the use of wide-band signals and gain-dispersive antennas.
- (c) An analog ambiguity diagram computer that calculates the signal function characterizing the operation of the a posteriori model can be built and operated satisfactorily.
- (d) The effective area of ambiguity of this signal function is dependent on the bandwidth of the transmitted signal and is given approximately by the relation

$$\int_{-\infty}^{\infty} \int_0^{\infty} |\chi(\tau, \alpha)|^2 \frac{\omega_0 d\alpha}{2\pi} d\tau = \frac{1}{2} \left[ 1 + \left( \frac{\beta}{2\omega_0} \right)^2 - \dots \right] \quad [(2-56)]$$

- (e) The signals that are used by the bats Myotis lucifugus and Lasiurus borealis, pulse by pulse, have almost no Doppler information, but have extremely good range-resolution capabilities.

Although bats may not use the principles of the a posteriori model in a manner directly analogous to the one presented, it can be stated that a bat cannot do better than the "ideal receiver" under the conditions of additive Gaussian noise that are stated in Chapter 2. This derivation places a limit on the capabilities of any man-made or biological echolocation system.

In particular, this ideal-receiver approach demonstrates that the signals used by Myotis and Lasiurus are well suited for pulse compression. The 3.2-msec-long cruising pulse of the Myotis, corresponding to a pulse length in air of 1.1 m, compresses when passed through the ideal receiver to a width of 85  $\mu$ sec, which in turn corresponds to a resolution of 1.5 cm.

The nature of the ambiguity diagrams that were computed for the Myotis pulses demonstrate that this bat cannot do much, if any, Doppler discrimination on a single-pulse basis. The height of the surface of ambiguity is nearly as high for the maximum a priori velocity as it is for zero velocity. This indicates that velocity determination on a single-pulse basis is only possible under very high signal-to-noise-ratio conditions. However, the bat does not use only a single pulse but in fact uses a train of pulses. If on each pulse he has good range information, the train of pulses will give him both range and velocity information.

On the other hand, the ambiguity diagram computed for the Lasiurus cruising pulse demonstrates that this bat has some range and some velocity resolution. The 380- $\mu$ sec width of the ambiguity diagram corresponds to a range resolution of 6.5 cm. The peak of the target-velocity-equal-to-zero slice is substantially higher than any of the other peaks of this ambiguity diagram, indicating that under favorable signal-to-noise-ratio conditions, the bat signal is capable of being used to measure velocity. The ambiguity diagram for this particular signal is similar to the circularly symmetrical ambiguity diagram proposed by Klauder,<sup>22</sup> in that this ambiguity diagram breaks into several minor ridges off the target-velocity-equal-to-zero slice.

A complete treatment of the bat sonar problem would include the treatment of the problem of simultaneously determining range, range rate, azimuth, elevation, angular velocity, and

type of target. Since this problem seems to be very complex, if not impossible to handle, the simpler problem of simultaneously determining range and elevation is treated. The results of this treatment indicate that it is possible to determine the elevation of a target from the spectrum of the received signal if a gain-dispersive antenna is used as the receiving aperture. The two simple examples treated serve to illustrate the technique and the possibilities of this type of system. The results show that signals with equivalent power density spectrum give identical performance. As in all a posteriori models, the signal-to-noise ratio affects the operation of the system greatly.

An analog ambiguity diagram computer was designed and built to calculate the signal function defined in Chapter 2. The maximum error introduced by this computer is: height, 5.4 percent; time delay, 0.54 percent; position of a Doppler shift slice, 4.4 percent.

## 6.2 SUGGESTIONS FOR FURTHER INVESTIGATION

### 6.2.1 Equipment Improvements

The weakest link in the ambiguity diagram computer is the input tape reproducer. The amount of flutter introduced by this machine limits the resolution in the Doppler direction and restricts the use of the ambiguity diagram computer. It is doubtful if the addition of a servo system on the present tape reproducer could reduce the flutter by an appreciable amount. Since the operation of this particular tape reproducer is already commensurate with the state of the art of commercial tape reproducers, it is not reasonable to assume that a different commercial tape reproducer would operate significantly better. One possible solution would be to record the signal onto another magnetic drum and then re-record it onto the Goff drum with the Doppler shift. Another solution would be to record the Doppler-shifted signal onto the Goff drum by recording the signal with the movable head, moving at a relatively high rate, while at the same time the non-Doppler-shifted signal is being recorded with a stationary head. A special drive mechanism would have to be designed in order to move the movable head at the high rates necessary to provide the Doppler shift. By recording the two signals at the same time, errors introduced by flutter would cancel each other out.

A digital computer could be used to calculate the ambiguity diagrams. This would introduce a versatility not enjoyed by the analog computer. Using the presently available digital computers, the accuracy of the ambiguity diagram would probably be much better than the accuracy obtained with the analog computer. The entire error would probably be introduced by the first conversion from the analog to the digital form of input signal. Calculation of an ambiguity diagram by a digital computer is a very time-consuming operation, however, and would probably be much more expensive than with the analog computer.

The 60-cps hum in the Goff magnetic-drum reproduce amplifiers affects the operation of zero setting the output of the multiplier as described in Chapter 4. Elimination of this hum, while the multiplier zero is being set, would eliminate this problem. The 120-cps hum, resulting from the squaring of the 60-cps hum signals, can be eliminated by grounding the two multiplier inputs during the time that the zero is being set. These inputs could very easily be grounded with relays connected to the integrate one-shot multiplier. The multiplier inputs would then be grounded until the actual integration was to occur. The inputs, of course, would be connected to the reproduce amplifier outputs while the signal is being multiplied and integrated.

Some signals, for which it is desirable to obtain ambiguity diagrams, cannot be analyzed with this ambiguity diagram computer because their entire ambiguity diagram lies very near

the target-velocity-equal-to-zero axis. An example of such a pulse is the echolocation pulse of the bat Rhinolophus ferrum-equinum. This pulse has a long constant-frequency section, as well as a short FM section at the end of the pulse. A typical center frequency for this pulse is 85 kcps; a typical duration is 20 msec. With this signal, the entire ambiguity diagram is contained between plus and minus 0.1 m/sec, way out of the range of this ambiguity diagram computer. Such a signal could be analyzed if this relatively narrow-band signal were played at normal speed on a tape reproducer, beat down in frequency so that it would become a wide-band signal in another frequency range, and re-recorded on a tape recorder. This beating down could probably be accomplished with the aid of an oscillator, the multiplier that is used in this computer, and a band-pass filter.

### 6.2.2 Field Measurements of the Capabilities of Bat Sonar Systems

This research project has built up the theoretical basis for the comparison of the performance of the sonar system of individual bats to the performance of an ideal receiver. Further measurements of the capabilities of bats are needed in order to determine if their performance is indeed comparable to that of the ideal receiver.

Some experiments that might be undertaken are: a determination of the resolution of targets in the presence of Gaussian jamming noise, the range accuracy of the bat's system, and the angular accuracy of the bat's system. Such experiments might be relatively difficult to devise and carry out.

Simultaneous high-speed motion-picture photography and tape recording can be used to great advantage in studying the bats. As an example of its application, one could use this technique to check whether or not the quantity  $c/\beta$  is equal to the distance between the bat and his target as is hypothesized in Chapter 5.

### 6.2.3 Ambiguity Diagrams of Various Bat Signals

There are many species of bats that use many different echolocating signals. Each bat may have a special reason for using the particular signal that he uses. It would be very interesting to know what kind of ambiguity diagrams result from the pursuit pulses of the Lasiurus. The fishing bat, Noctilio, seems to switch back and forth between CW pulses and FM pulses. This bat uses these signals to locate fish swimming in the water. The long-eared bats, Plecotus townsendii, emit pulses that are much lower in frequency than the signals of the Myotis. These signals are very rich in harmonic content and may produce a very different type of ambiguity diagram. The number of different species of bats is very large. It would be interesting indeed to obtain the ambiguity diagrams of all of them, for each of their different uses, but time is not available to pursue all of them.



## ACKNOWLEDGMENTS

I am grateful to many people for their help and guidance during the period of research and preparation of this report. It would be impossible to list all the people who have helped.

Dr. J. J. G. McCue, my supervisor, has provided many helpful suggestions. Frederic Webster made his "Bat Flight Facility" available to me for recording, training, and photographing the bats. The facilities of the Research Laboratory of Electronics were made available for my use. In particular, I should like to acknowledge the fine work that Kenneth W. Goff did in building his magnetic-drum delay unit and to thank Prof. Kenneth Stevens for allowing me to use the Goff drum as the time delay and storage element in my analog ambiguity diagram computer. I am grateful to Prof. Harold E. Edgerton who made his equipment available to me, as well as providing many helpful suggestions and moral support. Last but surely not least, I should like to express deep gratitude to the members of my family for their help during the preparation of this report.

## BIBLIOGRAPHY

### ANTENNAS

1. RUZE, J., "Physical Limitations on Antennas," Sc. D. Thesis, Electrical Engineering Department, M.I.T. (1952).

### BATS

2. FREEDMAN, J., "On the Other Hand," *Contemp. Psychol.* 4, 327-373 (November 1959).
3. GRIFFIN, D. R., *Listening in the Dark* (Yale University Press, New Haven, 1958).
4. \_\_\_\_\_, "Measurements of the Ultrasonic Cries of Bats," *J. Acoust. Soc. Am.* 22, 247-55 (March 1950).
5. \_\_\_\_\_, "More about Bat 'Radar'," *Sci. Am.* 199, 40-44 (July 1958).
6. \_\_\_\_\_, "The Navigation of Bats," *Sci. Am.* 185, 52-55 (August 1952).
7. GRIFFIN, D. R., D. C. DUNNING, D. A. CAHLANDER, and F. A. WEBSTER, "Correlated Orientation Sounds and Ear Movements of Horseshoe Bats," *Nature* 196, 1185-1188 (22 December 1962).
8. GRIFFIN, D. R., J. J. G. MCCUE, and A. D. GRINNELL, "The Resistance of Bats to Jamming," TR-285, Lincoln Laboratory, M.I.T. (23 October 1962), DDC 296493; and *J. Exp. Zool.* 152, 229-250 (April 1963).
9. GRIFFIN, D. R., F. A. WEBSTER, and C. R. MICHAEL, "The Echolocation of Flying Insects by Bats," *Animal Behavior*, 8, 141-154 (July - October 1960).
10. LICKLIDER, J. C. R., "Nature as a Sonar Engineer," *Contemp. Psychol.* 4, 1-4 (January 1959).
11. MCCUE, J. J. G., "How Bats Hunt with Sound," *National Geographic*, 119, 570-578 (April 1961).
12. ROEDER, K. D. and A. E. TREAT, "The Detection and Evasion of Bats by Moths," *Am. Sci.* 49, 135-148 (June 1961).

### CORRELATORS

13. BARLOW, J. S. and R. M. BROWN, "An Analog Correlator System for Brain Potentials," Technical Report No. 300, Research Laboratory of Electronics, M.I.T. (1955).
14. GOFF, K. W., "Analog Electronic Correlator for Acoustic Measurements," *J. Acoust. Soc. Am.* 27, 223-236 (1955).
15. \_\_\_\_\_, "The Application of Correlation Techniques to Some Acoustic Measurements," Sc D. Thesis, Electrical Engineering Department, M.I.T. (1954).
16. \_\_\_\_\_, "Development of a Variable Time Delay," S.M. Thesis, Electrical Engineering Department, M.I.T. (1952).
17. \_\_\_\_\_, "Instruction Manual for Analog Correlator," Acoustics Laboratory, M.I.T. (August 1954).
18. HOLMES, J. N. and J. M. C. DUKES, "A Speech-Waveform Correlator with Magnetic-Tape Delay and Electronic Multiplication," *J. Inst. Elec. Engrs. (London)* 101, 225-237 (July 1954).

### DETECTION THEORY

19. COOK, C. E., "Pulse Compression-Key to More Efficient Radar Transmission," *Proc. IRE* 48, 310-316 (March 1960).
20. FELLER, W., *An Introduction to Probability Theory and Its Applications* (Wiley, New York, 1957).
21. HELSTROM, C. W., *Statistical Theory of Signal Detection* (Pergamon Press, New York, 1960).
22. KLAUDER, J. R., "The Design of Radar Signals Having Both High Range Resolution and High Velocity Resolution," *Bell System Tech. J.* 39, 809-820 (July 1960).
23. KLAUDER, J. R., A. C. PRICE, S. DARLINGTON, and W. J. ALBERSHEIM, "The Theory and Design of Chirp Radars," *Bell System Tech. J.* 39, 745-808 (July 1960).
24. MARCUM, J. I., "A Statistical Theory of Target Detection by Pulsed Radar," *Trans. IRE, PGIT-6*, 59-268 (1960).

25. SIEBERT, W. M., "Some Applications of Detection Theory to Radar," IRE National Convention Record, Part 4, pp. 5-14 (1958).
26. \_\_\_\_\_, "Statistical Theories of Radar Synthesis," Proc. National Elect. Conf. 12, 401-410 (1956).
27. WOODWARD, P. M., Probability and Information Theory, with Applications to Radar (McGraw-Hill, New York, 1957).

#### ELECTRONICS

28. BRUBAKER, T. A., "Precision Analog Memory Has Extended Frequency Response," Electronics 34, 141-143 (29 September 1961).
29. CAHLANDER, D. A., "A Direct-Coupled Multiplier for Acoustic Sonar," S.M. Thesis, Electrical Engineering Department, M.I.T. (1960).
30. COX, L. G., "A Wide-Range Wow and Flutter Indicator," J. SMPTE 71, 9-12 (January 1962).
31. DAVIES, G. L., Magnetic Tape Instrumentation (McGraw-Hill, New York, 1961).

#### HUMAN HEARING

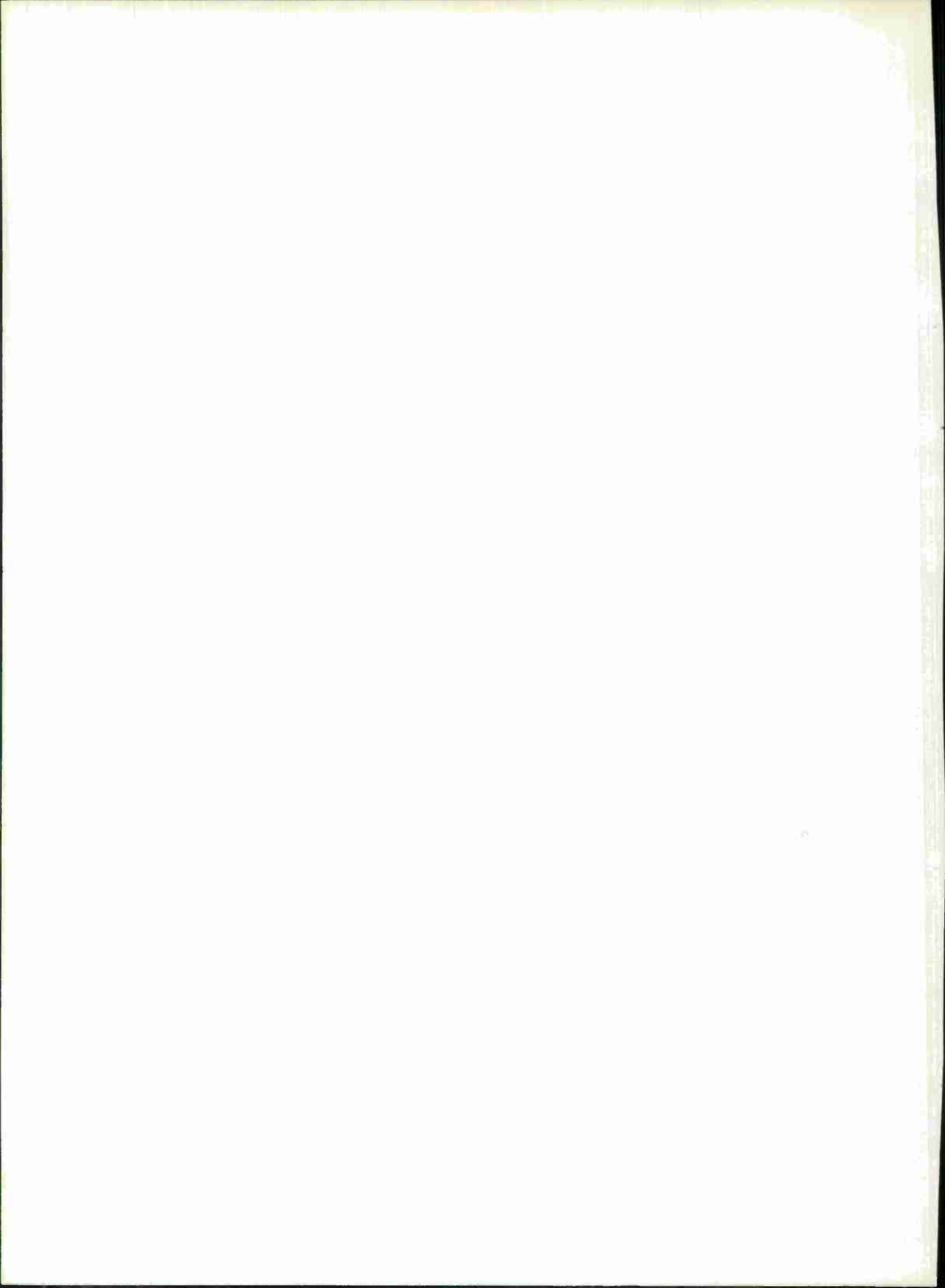
32. JONGKEES, L. B. W. and R. A. v. D. VEER, "On Directional Sound Localization in Unilateral Deafness and Its Explanation," Acta Oto-Laryngol. 49, 119-131 (March - April 1958).
33. MILLS, A. W., "On the Minimum Audible Angle," J. Acoust. Soc. Am. 30, 237-246 (April 1958).
34. MOUZON, J. C., "Stereophonic Hearing with One Earphone," J. Acoust. Soc. Am. 27, 381 (1955).
35. PIERCE, J. R., "Some Work on Hearing," Am. Sci. 48, 40-45 (March 1960).

#### MICROPHONES

36. KUHLE, W., G. R. SCHODDER, and F. K. SCHRÖDER, "Condenser Transmitters and Microphones with Solid Dielectric for Airborne Ultrasonics," Acustica 4, 519-532 (1954).
37. MATSUZAWA, K., "Condenser Microphones with Plastic Diaphragms for Airborne Ultrasonics," Part I: J. Phys. Soc. Japan 13, 1533-1543 (December 1958); Part II: J. Phys. Soc. Japan 15, 167-174 (January 1960).

#### PHOTOGRAPHY

38. CAHLANDER, D. A., "Precision Speed Control of a High-Speed Camera," Proceedings of the 5th International Congress on High-Speed Photography (Mack Printing Co., Easton, Penn. 1962), pp. 473-477.
39. HARDY, A. C. and F. H. PERRIN, The Principles of Optics (McGraw-Hill, New York, 1932).



~~UNCLASSIFIED~~

Security Classification

DOCUMENT CONTROL DATA - R&D

(Security classification of title, body of abstract and indexing annotation must be entered when the overall report is classified)

1. ORIGINATING ACTIVITY (Corporate author)		2a. REPORT SECURITY CLASSIFICATION	
Lincoln Labs., Lexington, Mass.		UNCLASSIFIED	
		2b. GROUP	
		N/A	
3. REPORT TITLE			
Echolocation with Wide-Band Waveforms: Bat Sonar Signals			
4. DESCRIPTIVE NOTES (Type of report and inclusive dates)			
Technical Report			
5. AUTHOR(S) (Last name, first name, initial)			
Cahlander, D.A.			
6. REPORT DATE		7a. TOTAL NO. OF PAGES	7b. NO. OF REFS
May 64		74	0
8a. CONTRACT OR GRANT NO.		9a. ORIGINATOR'S REPORT NUMBER(S)	
AF19(628)500		TR-271	
b. PROJECT NO.		9b. OTHER REPORT NO(S) (Any other numbers that may be assigned this report)	
		ESD-TDR-64-60	
10. AVAILABILITY/LIMITATION NOTICES			
Qualified Requesters May Obtain Copies From DDC.			
11. SUPPLEMENTARY NOTES		12. SPONSORING MILITARY ACTIVITY	
		ESD, L.G. Hanscom Field, Bedford, Mass.	
13. ABSTRACT			
<p>The wide-band, echolocating sonar signals of bats are investigated with reference to statistical estimation theory to ascertain the implications of this class of signals. The work is divided into four major sections: (1) The concept of an receiver for the simultaneous measurement of range and velocity of a target is extended to cover wide-band signals; (2) angular localization of a target by means of a fixed, gain-dispersive antenna in the presence of additive Gaussian noise is studied; (3) an ambiguity diagram computer is designed and built which calculates the signal function, defined in Chapter 2, of an arbitrary waveform; and (4) ambiguity diagrams are calculated for several types of bat sonar signals emitted by the bat <u>Myotis lucifugus</u> and one cruising signal emitted by the bat <u>Lasiurus borealis</u>.</p>			

## KEY WORDS

**LINK A**

LINK B

**LINK C**

ROLE

WT

ROLE

WT

ROLE

WT



